


5-2018

DEVELOPMENT OF 3D-PRINTED PATIENT SPECIFIC BOLUS FOR CLINICAL USE IN TOTAL SCALP IRRADIATION

Garrett Baltz

Follow this and additional works at: https://digitalcommons.library.tmc.edu/utgsbs_dissertations

 Part of the [Medical Biophysics Commons](#), [Oncology Commons](#), [Other Physics Commons](#), and the [Radiology Commons](#)

Recommended Citation

Baltz, Garrett, "DEVELOPMENT OF 3D-PRINTED PATIENT SPECIFIC BOLUS FOR CLINICAL USE IN TOTAL SCALP IRRADIATION" (2018). *The University of Texas MD Anderson Cancer Center UTHealth Graduate School of Biomedical Sciences Dissertations and Theses (Open Access)*. 850.
https://digitalcommons.library.tmc.edu/utgsbs_dissertations/850

This Thesis (MS) is brought to you for free and open access by the The University of Texas MD Anderson Cancer Center UTHealth Graduate School of Biomedical Sciences at DigitalCommons@TMC. It has been accepted for inclusion in The University of Texas MD Anderson Cancer Center UTHealth Graduate School of Biomedical Sciences Dissertations and Theses (Open Access) by an authorized administrator of DigitalCommons@TMC. For more information, please contact digitalcommons@library.tmc.edu.

DEVELOPMENT OF 3D-PRINTED PATIENT SPECIFIC BOLUS FOR CLINICAL
USE IN TOTAL SCALP IRRADIATION

by

Garrett Christopher Baltz, B.S.

APPROVED:



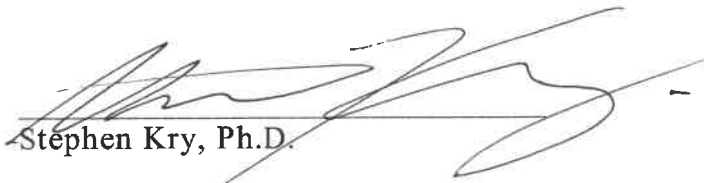
Rebecca M. Howell, Ph.D.
Advisory Professor



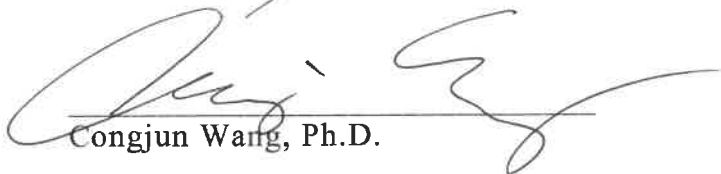
Pai-Chun Melinda Chi, Ph.D.



Adam S. Garden, M.D.



Stephen Kry, Ph.D.



Congjun Wang, Ph.D.

APPROVED:

Dean, The University of Texas
MD Anderson Cancer Center UTHHealth Graduate School of Biomedical Sciences

DEVELOPMENT OF 3D-PRINTED PATIENT SPECIFIC BOLUS FOR CLINICAL
USE IN TOTAL SCALP IRRADIATION

A
THESIS

Presented to the Faculty of
The University of Texas
MD Anderson Cancer Center UTHealth
Graduate School of Biomedical Sciences
in Partial Fulfillment
of the Requirements
for the Degree of

MASTER OF SCIENCE

by
Garrett Christopher Baltz, B.S.
Houston, Texas
May, 2018

Copyright © 2018 Garrett Baltz. All rights reserved.

Dedication

To my brother, Connor, who has selflessly volunteered to serve his country in the US Army

Acknowledgements

I would like to first and foremost thank my advisor, Dr. Rebecca Howell. Beyond guiding me on this project, she has been a great mentor and I am very appreciative of the guidance and opportunities she has provided to set me up for a successful future career in medical physics.

Thank you to my advisory committee members, Dr. Melinda Chi, Dr. Stephen Kry, Dr. Adam Garden, and Dr. Chester Wang. Their input, help, and guidance contributed greatly to the success of this project and the development of something ready to enter the clinic.

Thank you to Pei-Fong Wong for his help with measurements, treatment planning and providing guidance on the project. Thank you to Stacy Lin for the extensive time she spent teaching me how to treatment plan in RayStation.

Thank you to my lab mates, Daniel Craft and Mary Peters, for your help with afterhours measurements and everything 3D-printing related. Special thank you to Daniel Craft! I greatly appreciate all the time you spent to get me up to speed on 3D-printing and it helped greatly in getting my project going.

Finally, thank you to my Mom and Dad. Your guidance, love, and support has allowed me to follow my passions, achieve my goals, and get to where I am today.

Abstract

DEVELOPMENT OF 3D-PRINTED PATIENT SPECIFIC BOLUS FOR CLINICAL USE IN TOTAL SCALP IRRADIATION

Garrett Christopher Baltz, B.S.

Advisory Professor: Rebecca M. Howell, Ph.D.

Total scalp irradiation (TSI) is a specialized radiation therapy technique that aims to deliver a uniform dose to the entire scalp. Original electron-based TSI techniques had limited homogeneity due to hot and cold spots created at field junctions due to the multiple matched fields that were required to treat the entire scalp. The transition to photon volumetric-modulated arc therapy based TSI techniques has improved homogeneity, to the point where non-conformal bolus is now a limiting factor. Bolus is required to build-up full dose to the scalp surface in total scalp irradiation. Creating bolus that is conformal to the scalp is technically challenging due to the convex curvature of the scalp, and most methods in the literature are laborious yet produce bolus with limited conformality and setup reproducibility. The purpose of this study was to develop and validate the use of patient-specific 3D-printed bolus caps for TSI. 3D-printing materials were studied to find materials suitable for use as a bolus cap. Clinical workflows were developed to 3D-print two bolus caps for an anthropomorphic head phantom: one printed using an in-house 3D printer, and the other using a commercial vendor. CT simulation scans were used to assess bolus cap scalp conformality, and to generate radiation treatment plans. The planned treatment was delivered to the head phantom for both bolus caps, and dosimetric validation was performed using thermoluminescent dosimeters (TLD). The resulting 3D-printed bolus caps had excellent conformality to the phantom scalp, with air gaps of less than 4 mm. Dosimetric measurements demonstrated the bolus caps can generate full build-up to the scalp surface and that measured doses agreed with predicted doses to within 2.4% on average. In conclusion, this study has developed a novel technique to 3D-print highly conformal patient-specific bolus caps that satisfy clinical and dosimetric requirements for total scalp irradiation.

Table of Contents

Dedication	iv
Acknowledgements	v
Abstract	vi
List of Illustrations	x
List of Tables	xiv
1 Introduction	1
1.1 Total Scalp Irradiation.....	1
1.2 Statement of Problem	7
1.3 3D-Printing.....	9
1.3.1 Applications in Radiation Oncology.....	13
1.4 Hypothesis	14
1.5 Specific Aims	15
1.6 Organization of Thesis	15
2 Specific Aim 1: Determination of Suitable 3D-Printing Materials for the Bolus Cap.....	16
2.1 Introduction	16
2.2 Methods and Materials	18
2.2.1 Materials for a Fused Deposition Modeling 3D Printer.....	18
2.2.2 Materials for a PolyJet 3D Printer	19
2.3 Results	24
2.3.1 NinjaFlex Properties and Suitability for use as 3D-Printed Bolus Cap	24

2.3.2	PolyJet Material Properties and Suitability for use as 3D-Printed Bolus Cap.....	25
3	Specific Aims 2 and 3: Generation, Fabrication and Assessment of Bolus Cap Designs	34
3.1	Introduction	34
3.2	Methods and Materials	36
3.2.1	Generating the Bolus Cap 3D-Model	37
3.2.2	NinjaFlex Bolus Cap Design	40
3.2.3	Agilus Bolus Cap Design.....	47
3.2.4	CT Simulation	50
3.3	Results	53
3.3.1	3D-Printed Bolus Cap Designs	53
3.3.2	CT Simulation Measurements.....	54
4	Specific Aim 4: Demonstrate 3D-Printed Bolus Caps can Reproducibly Generate a Homogenous Dose to the Scalp	58
4.1	Introduction	58
4.2	Methods and Materials	61
4.2.1	Treatment Planning.....	61
4.2.2	Dosimetric Validation	66
4.2.3	Reproducibility Study	69
4.3	Results	70
4.3.1	Treatment Planning.....	70
4.3.2	Dosimetric Validation	73

4.3.3	Reproducibility Study	75
5	Specific Aim 5: Development of a Clinical Workflow for Fabrication	78
5.1	Introduction	78
5.2	Methods and Materials	78
5.3	Results	81
6	Discussion.....	82
6.1	General Review	82
6.2	Comparison of In-house and External Fabrication Methods	83
6.3	Clinical Implications	84
6.4	Limitations and Future Research.....	86
6.5	Conclusion.....	87
7	Appendix	88
7.1	RayStation Bolus Contour Creation Script	88
7.2	BAT Script to Open 3DSlicer	91
7.3	3DSlicer DICOM Contour to .STL Conversion Script.....	91
8	Bibliography	93
	Vita.....	100

List of Illustrations

Figure 1-1: 12 field electron total scalp irradiation technique. ⁵ The plots show the hot and cold spots at field junctions. Used with permission Able CM, Mills MD, McNeese MD, Hogstrom KR. Evaluation of a total scalp electron irradiation technique. Int J Radiat Oncol Biol Phys. 1991;21(4):1063-1072.	3
Figure 1-2: (a) Vertical lines show lateral electron fields, horizontal lines show photon fields. (b) axial view showing overlap between electron and photon fields. ⁸ Used with permission Tung SS, Shiu AS, Starkschall G, Morrison WH, Hogstrom KR. Dosimetric evaluation of total scalp irradiation using a lateral electron-photon technique. Int J Radiat Oncol Biol Phys. 1993;27(1):153-160.	4
Figure 1-3: Dose-volume histograms for the treatment plans generated by lateral-electron photon technique (red line), tomotherapy (blue line), and VMAT (green line). ¹¹ Used with permission Song JH, Jung JY, Park HW, et al. Dosimetric comparison of three different treatment modalities for total scalp irradiation: The conventional lateral photon-electron technique, helical tomotherapy, and volumetric-modulated arc therapy. J Radiat Res. 2015;56(4):717-726.	6
Figure 1-4: Percent depth dose curves for 11 MeV electrons (blue line) and 6 MV photons (orange line). The dose at the surface for the photon beam is only 50%, and 83% for the electron beam.	7
Figure 1-5: CT slices showing the air gaps that can form between the bolus and the scalp for the MD Anderson scalp bolus technique	9
Figure 1-6: Schematic of an extruder head gantry for a typical FDM 3D-printer. ¹⁸ Used with permission N. Turner B, Strong R, A. Gold S. A review of melt extrusion additive manufacturing processes: I. Process design and modeling. Rapid Prototyp J. 2014;20(3):192-204.....	11

Figure 1-7: Schematic of the extruder head gantry for a typical PolyJet 3D printer. Taken from: http://ss.whiteclouds.com/3dpedia-index/light-polymerized-3d-printing	12
Figure 2-1: 3D-printed sample composition cubes for Agilus (top row, labeled A27- A100) and Tango (bottom row, labeled T27-T100). The materials are labeled with their Shore value. The softest and most flexible materials are at the left (A27 and T27) and they gradually get firmer as the Shore value increases to the firmest materials on the right (A100 and T100).....	20
Figure 2-2: (left) Blocks printed for the PDD measurements. (right) close up showing the location of the holes for the ionization chamber.....	22
Figure 2-3: (left) PDD measurement setup showing the surface of the blocks at 100 cm source to surface distance. (right) Close-up of the PDD blocks setup.	23
Figure 2-4: The PDD measurement setup in RayStation. The yellow circles show locations for point dose calculations that correspond to the measurement locations.	24
Figure 2-5: (left) 3D-printed 5 mm thick NinjaFlex strip. (right) Picture showing the NinjaFlex material is still flexible when 5 mm thick.....	25
Figure 2-6: Plot of the measured density and HU for each material cube sample and the CT calibration curve.....	28
Figure 2-7: Plot of the measured density and HU for each Agilus strip sample and the CT calibration curve.....	29
Figure 2-8: Picture demonstrating the difference in flexibility and deformability between the Agilus-27 strip (clear an in the foreground) and the Agilus-60 strip (purple and in the background). The Agilus-27 strip is highly deformed under its own weight, unlike the Agilus-60 strip.	30
Figure 2-9: Plot of percent depth dose measurements in Agilus-60 material (squares). The blue line is the commissioning PDD curve in water. Also plotted is the treatment planning system calculated dose for no density override (star) and density of blocks overridden (triangle).....	31

Figure 3-1: Picture showing a typical case where support material is needed in 3D-printing. The T on the left has no support and the object had defects at the overhangs. The T on the right was printed with support and was printed correctly. Taken from:

<https://www.3dhubs.com/knowledge-base/supports-3d-printing-technology-overview> 35

Figure 3-2: CIRS ATOM anthropomorphic head phantom..... 37

Figure 3-3: Process for creating a bolus cap contour from a CT scan in RayStation. 39

Figure 3-4: Rendering of the 3D-model of the bolus cap after exporting from 3DSlicer 40

Figure 3-5: Rendering of the first iteration design for the NinjaFlex bolus cap 41

Figure 3-6: Picture of the 3D-printed top piece with support. 42

Figure 3-7: Pictures showing the first iteration of NinjaFlex bolus cap design. (left) The bottom and top pieces separate. (right) The two bolus pieces together on the head phantom. 43

Figure 3-8: Rendering of the second iteration design for the NinjaFlex bolus cap. 44

Figure 3-9: Pictures showing the second iteration of NinjaFlex bolus cap design. The picture of the cap on the phantom shows how the pieces did not align and interlock correctly. 45

Figure 3-10: Renderings of the 3D-model for the third iteration design. The overlapping lips on each side are 2.5 mm thick so when they join, they are 5 mm thick. 46

Figure 3-11: The halves were printed on their side with the use of support material..... 46

Figure 3-12: Pictures showing the third iteration of the NinjaFlex bolus cap design. (left) the two halves taped together on the phantom head. (right) Left half of the bolus cap on the phantom. Shown clearly is the overlapping lip. The right half has the complementary lip. 47

Figure 3-13: Picture of first Agilus-27 bolus cap design. (left) demonstration of how deformable the Agilus-27 material is. (right) Agilus-27 bolus cap on phantom head with back piece taped to top piece. 48

Figure 3-14: Picture of second Agilus bolus cap design using the Agilus-60 compound. (left) The bolus cap is slightly flexible, but can hold up under its own weight. (right) The bolus cap fit well on the phantom and was easy to get on in one piece.	49
Figure 3-15: Picture of the CT simulation setup, (left) setup shown without the immobilization mask, (right) setup with the immobilization mask in place.	51
Figure 3-16: Picture showing the locations of the measurement positions for measuring the gap between the bolus and the scalp.....	52
Figure 3-17: CT slices from the NinjaFlex bolus cap CT simulation.....	54
Figure 3-18: CT slices from the Agilus-60 bolus cap CT simulation.....	55
Figure 4-1: Diagram of the thermoluminescent process in TLD.....	59
Figure 4-2: Picture showing the marked isocenter (red) and the defined treatment isocenter (blue).	63
Figure 4-3: Picture of the collimator field sizes and angles used for both arcs. Also shown are the contours for the brain (brown), CTV (blue), and external contour (green).	64
Figure 4-4: Picture of flat-pack TLD taped to the phantom scalp surface.....	66
Figure 4-5: Pictures of the TLD locations on the phantom scalp marked with BBs	68
Figure 4-6: Isodose distributions for NinjaFlex bolus cap plan.....	70
Figure 4-7: Isodose distributions for Agilus bolus cap plan.	71
Figure 4-8: DVH for the NinjaFlex plan (dotted lines) and the Agilus plan (solid line).....	72
Figure 4-9: Fusion of the original CT simulation used for treatment planning (white) and the therapist scan 1 (pink)	76
Figure 5-1: Automated workflow to create patient-specific bolus cap 3D-model.....	80

List of Tables

Table 2-1: Density and CT data for Tango and Agilus material samples.....	26
Table 2-2: Comparison of measured density and density predicted by CT calibration curve	27
Table 2-3: Physical data for 5 mm Agilus strips.....	29
Table 2-4: Agilus-60 PDD Data	32
Table 3-1: Fabrication related data for each tested bolus cap design	53
Table 3-2: Gap measurements for both tested bolus caps.....	56
Table 4-1: MCO planning objectives and constraints.....	65
Table 4-2: Objectives used to manually optimize VMAT treatment plans	65
Table 4-3: Correction factors used to convert TLD reading to dose	69
Table 4-4: Dose statistics for bolus cap treatment plans.....	72
Table 4-5: TLD results compared to TPS	74
Table 4-6: Bolus and scalp gap measurements for therapist reproducibility setups.....	75
Table 6-1: Comparison of in-house and external fabrication methods.....	83

1 Introduction

1.1 Total Scalp Irradiation

Total scalp irradiation (TSI) is a specialized radiation therapy technique that aims to deliver a uniform dose to the entire scalp. This technique is used to treat malignancies of the superficial scalp, which include: basal cell carcinoma, Merkel cell carcinoma, squamous cell carcinoma, cutaneous lymphoma and angiosarcoma.¹ As with most cancers, a multi-modality approach combining surgery, chemotherapy, immunotherapy, and radiation therapy is used to treat these diseases. However, radiation therapy through total scalp irradiation is often the primary or secondary treatment modality for malignancies of the scalp as multi-focal lesions and sub-clinical disease spread are difficult to treat with surgery or chemotherapy alone.

Total scalp irradiation is particularly important for treatment of angiosarcoma. Angiosarcoma is a rare form of soft tissue sarcoma that is a malignant tumor of the vascular endothelial cells. The incidence rate of soft tissue sarcoma is 3.1 per 100,000.² While angiosarcoma accounts for only 5% of all soft tissue sarcomas, 60% of the cases occur in the head and neck region.³ This cancer is very aggressive and spreads widely through the skin, meaning it often presents as multifocal lesions. Angiosarcoma also metastasizes early through hematogenous spread, with the lung being the most common site of metastasis.⁴ These combined factors make the disease very difficult to control and mean patients with this disease have a poor prognosis, with the 5-year survival rate ranging from only 10-15%.³ Traditionally, surgery has been the primary treatment for this disease, but local recurrence rates after surgical resection alone are high due to missed sub-clinical disease. Radiation therapy was only performed in cases where the tumor was too widely spread to be surgically resected. Recent studies have shown that a combination of surgery and radiation therapy offers a better treatment.

A retrospective study from Japan showed patients with angiosarcoma treated with a combination of surgery and radiation therapy had higher 2-year overall survival rates (45.8%) compared to patients treated with surgery or radiation therapy alone (11.1%).⁴ A similar retrospective study from The Mayo Clinic found that the use of radiation therapy was associated with higher 5-year locoregional control (20% vs 12%) and higher recurrence-free survival (19% vs 12%).³ The results of these studies have led to a combination of surgery and total scalp irradiation being the recommend treatment strategy for scalp angiosarcoma.

There are several factors that must be considered for effective total scalp irradiation. The first factor is the scalp is extremely superficial and techniques must be able to effectively deliver dose to the scalp surface. The second is the scalp is superficial to the brain, which serves as a large adjacent organ that the dose delivered to must be minimized. Finally, the scalp is a relatively large and convex target that proves to be difficult to uniformly irradiate. The technique used for total scalp irradiation has evolved and improved with advancements in radiation therapy.

Traditionally, 5-7 MeV electron beams were used to irradiate the scalp. Electrons were used because they are able to deliver a high surface dose, and electrons have a finite range, meaning they are ideal to limit incidental dose to the brain.⁵ Because electron beams must be tightly collimated and delivered normal to the surface, electron based techniques required multiple fields to treat the entire scalp. One technique shown in Figure 1-1 used 12 different stationary fields to cover the entire scalp. The limitations of this technique are mainly associated with the large number of fields, which not only made treatment setup and delivery lengthy, but led to non-uniform irradiation due to hot and cold spots created at field junctions, shown in the dose profiles in Figure 1-1. Other electron based TSI techniques in the literature include a

reduced 4 field technique,⁶ and a technique using a single setup point with concentric blocking and several different energy electron beams to treat the entire scalp.⁷

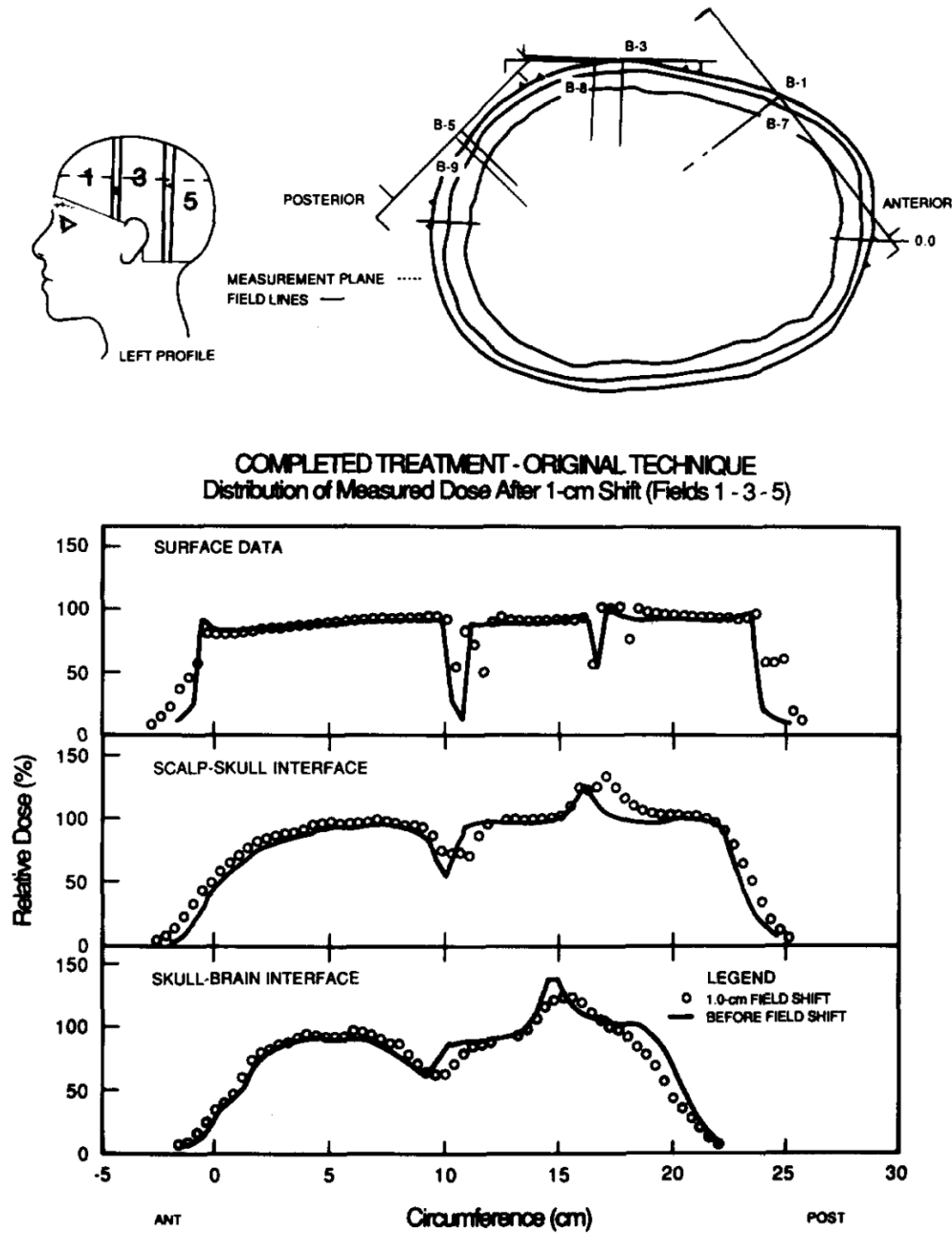


Figure 1-1: 12 field electron total scalp irradiation technique.⁵ The plots show the hot and cold spots at field junctions. Used with permission
Able CM, Mills MD, McNeese MD, Hogstrom KR. Evaluation of a total scalp electron irradiation technique. Int J Radiat Oncol Biol Phys. 1991;21(4):1063-1072.

Due to field matching related issues with electron based techniques, TSI techniques using a combination of photon and electron beams gained popularity. The most common technique was a lateral- electron photon technique.⁸ This technique used four fields: two 6 MeV electron fields that irradiated the lateral portions of the scalp, and two opposed 6 MV photon fields that irradiated the rind in the medial part of the scalp. The fields are shown in Figure 1-2. This technique reduced the amount of fields needed compared to electron only techniques, which correspondingly reduced treatment times. However, hot and cold spots of up to 18% were still present at the field junctions.

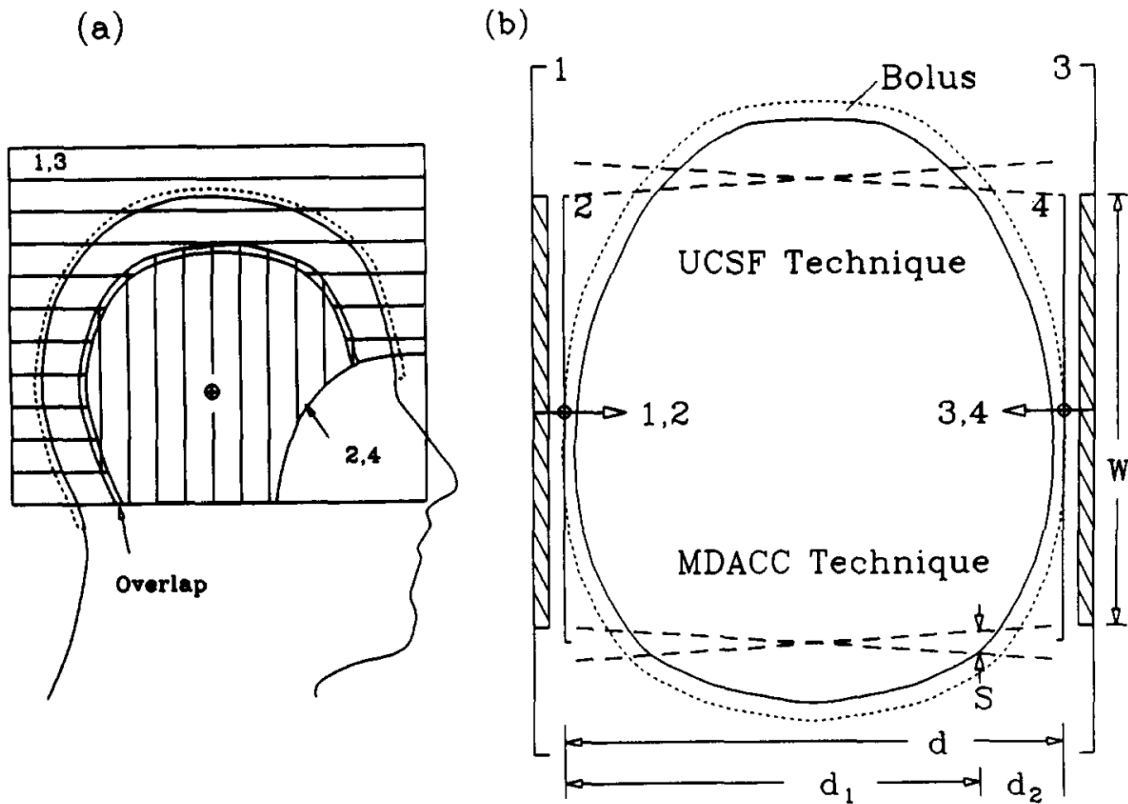


Figure 1-2: (a) Vertical lines show lateral electron fields, horizontal lines show photon fields. (b) axial view showing overlap between electron and photon fields.⁸ Used with permission
Tung SS, Shiu AS, Starkschall G, Morrison WH, Hogstrom KR. Dosimetric evaluation of total scalp irradiation using a lateral electron-photon technique. Int J Radiat Oncol Biol Phys. 1993;27(1):153-160.

Advancements in dose shaping with photon beams that can be achieved with intensity-modulated radiation therapy (IMRT) and volumetric modulated arc therapy (VMAT) techniques allowed for the use of photon only TSI techniques. IMRT made it possible to deliver highly conformal dose distributions by splitting each beam into multiple segments, each with different intensities and field apertures.⁹ Each IMRT segment aperture is created using a multi-leaf collimator (MLC), which uses many tungsten leaves to shape the field. This can be used in TSI to conform the dose to the desired scalp treatment volume while minimizing the dose delivered to the brain. Orton *et al.* demonstrated that helical IMRT tomotherapy using 6 MV photons could be used for total scalp irradiation.¹⁰ VMAT is a further advancement upon IMRT, which is an arc based treatment delivery technique in which the gantry speed, dose rate, and MLC can all be modulated while the beam is on.⁹ Song *et al.* conducted a dosimetric study comparing the dose distributions for TSI that could be delivered by the conventional lateral- electron photon (LEP) technique, 6MV photon tomotherapy IMRT, and linac based 6 MV photon VMAT.¹¹ The dose-volume histograms for each treatment technique they studied are presented in Figure 1-3. The VMAT plan was found to have similar dose homogeneity and better conformity index compared to the LEP plan. The VMAT plan also had a lower maximum dose to the brain than the LEP plan, but delivered dose to a larger volume of the brain compared to the tomotherapy plan. The primary benefit of VMAT TSI plans is they do not require the use of multiple matched fields, which reduces the occurrence of hot and cold spots, offers improved dose homogeneity, and reduces treatment delivery time. It is for these reasons that VMAT based TSI has become one of the more popular techniques in use currently.

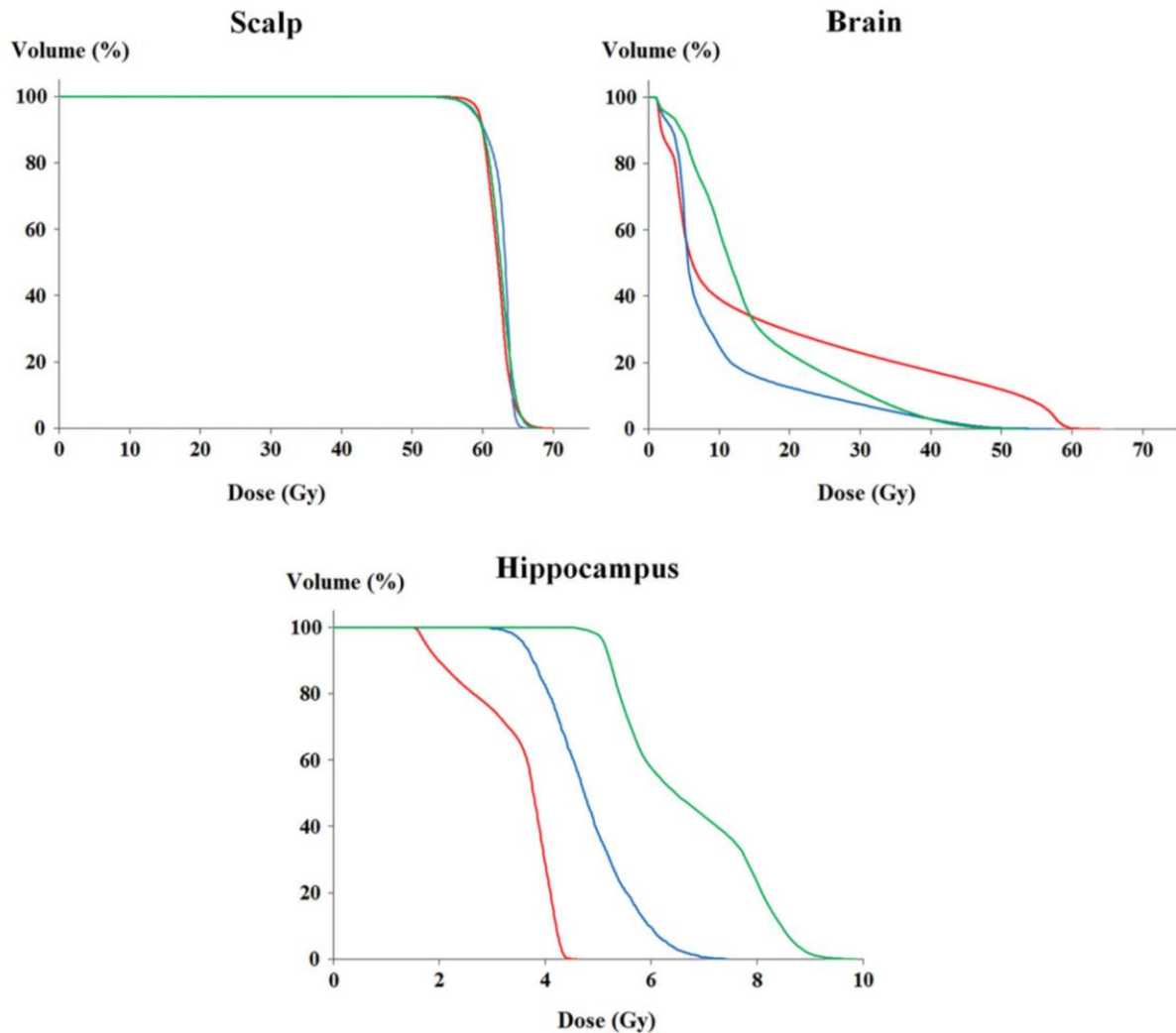


Figure 1-3: Dose-volume histograms for the treatment plans generated by lateral-electron photon technique (red line), tomotherapy (blue line), and VMAT (green line).¹¹ Used with permission Song JH, Jung JY, Park HW, et al. Dosimetric comparison of three different treatment modalities for total scalp irradiation: The conventional lateral photon-electron technique, helical tomotherapy, and volumetric-modulated arc therapy. *J Radiat Res.* 2015;56(4):717-726.

Although the type of radiation and technique used for TSI has evolved, the use of bolus on the scalp has been required for all techniques. Shown in Figure 1-4 are plots of the percent depth dose (PDD) for electron and photon beams. This plot shows that for both types of radiation, the dose at the surface is low, as build-up of electrons is required to achieve electronic equilibrium before maximum dose is achieved.¹² The implication of this for TSI is that the low surface dose of both electrons and photons will cause the scalp skin to be under-dosed. Low

surface dose is usually remedied with the use of bolus. Bolus is water or tissue equivalent material that is placed on the skin to provide build-up of dose inside the bolus so that full dose can be delivered to the surface of the treatment area. For the use of bolus in TSI, dosimetric studies have demonstrated that 0.5 cm of bolus material on the scalp is sufficient to deliver adequate surface dose to the superficial scalp.¹³

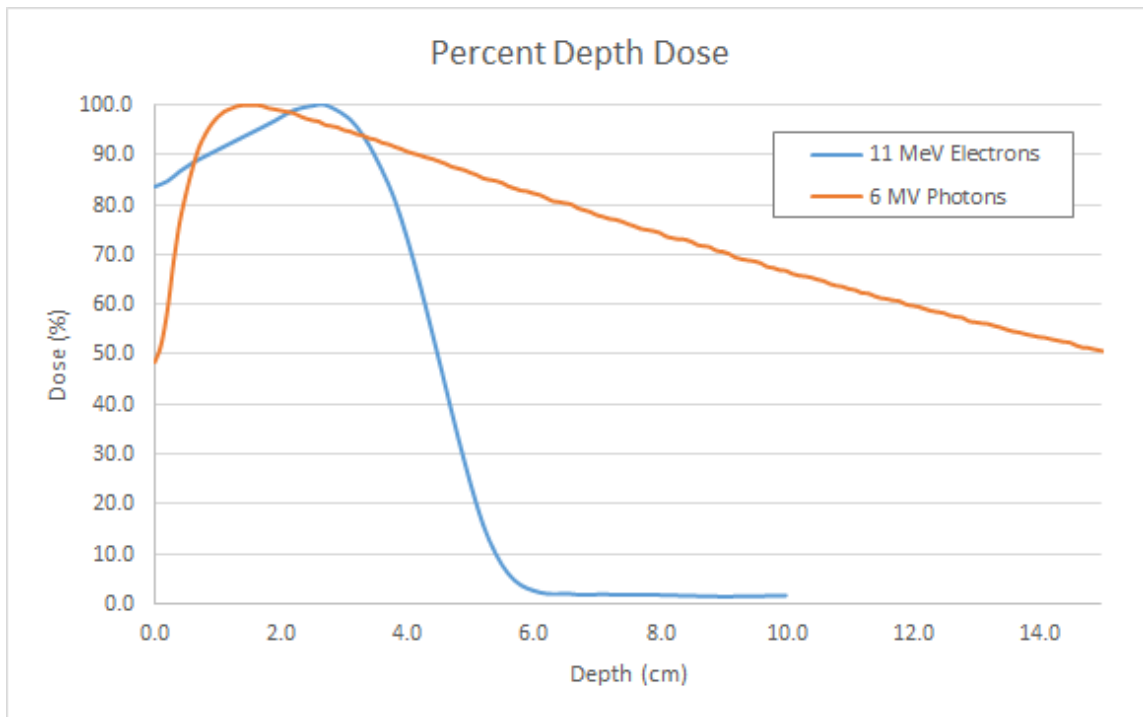


Figure 1-4: Percent depth dose curves for 11 MeV electrons (blue line) and 6 MV photons (orange line). The dose at the surface for the photon beam is only 50%, and 83% for the electron beam.

1.2 Statement of Problem

The use of bolus has proved to be one of the main technical challenges of total scalp irradiation. Because the scalp is a large, convex treatment surface, it is very difficult to apply bolus that is uniformly conformal to the scalp. The consequence of non-conformal bolus is that air gaps can form between the bolus and the scalp, which will negatively affect the build-up

dose effect provided by the bolus. One study found air gaps between the bolus and scalp surface can cause the delivered dose to the scalp to differ up to 12% compared to the planned dose.¹³

Many techniques for applying bolus to the scalp for TSI have been presented in the literature, but each have had limitations. Bedford *et al.* used an immobilization shell with 1 cm of wax built up on the interior surface.¹³ This method suffered from large air gaps between the wax bolus and scalp surface, which led to large differences in delivered and planned doses. Lin *et al.* used a thermoplastic mesh mask formed to the posterior of the patient's head and then glued 0.5-cm bolus slabs to the surface of the mask.¹⁴ This method had good daily setup reproducibility but still had air gaps as large as 1.5 cm and required the construction of a custom head rest and immobilization device. Most other TSI studies described in the literature have used 0.5- to 1.0-cm thick solid sheets of thermoplastic material that are heated and formed to the patient's medial scalp, with sheets of soft bolus material taped on to cover the lateral portions of the scalp.^{1,15,16} Although these methods have demonstrated good conformality, they still require manual fabrication and are prone to reproducibility issues.

The technique used at MD Anderson Cancer Center differs from any presented in the literature. Sheets of 0.5 cm thick flexible commercial bolus material are cut into smaller pieces and formed to the patient's head and then taped together. A swim cap is then stretched over the taped together bolus material to hold it tight to the scalp. This method to fabricate bolus is laborious and time consuming, taking up to 40 minutes to fabricate the bolus while the patient is in the CT Simulation suite. Additionally, the final fabricated bolus cap is prone to deforming under the swim cap and creating air gaps, as shown in Figure 1-5. Because the bolus is very deformable, it also has limited reproducibility meaning dosimetric cold spots due to air gaps cannot be compensated for during treatment planning as the air gaps are not consistent.

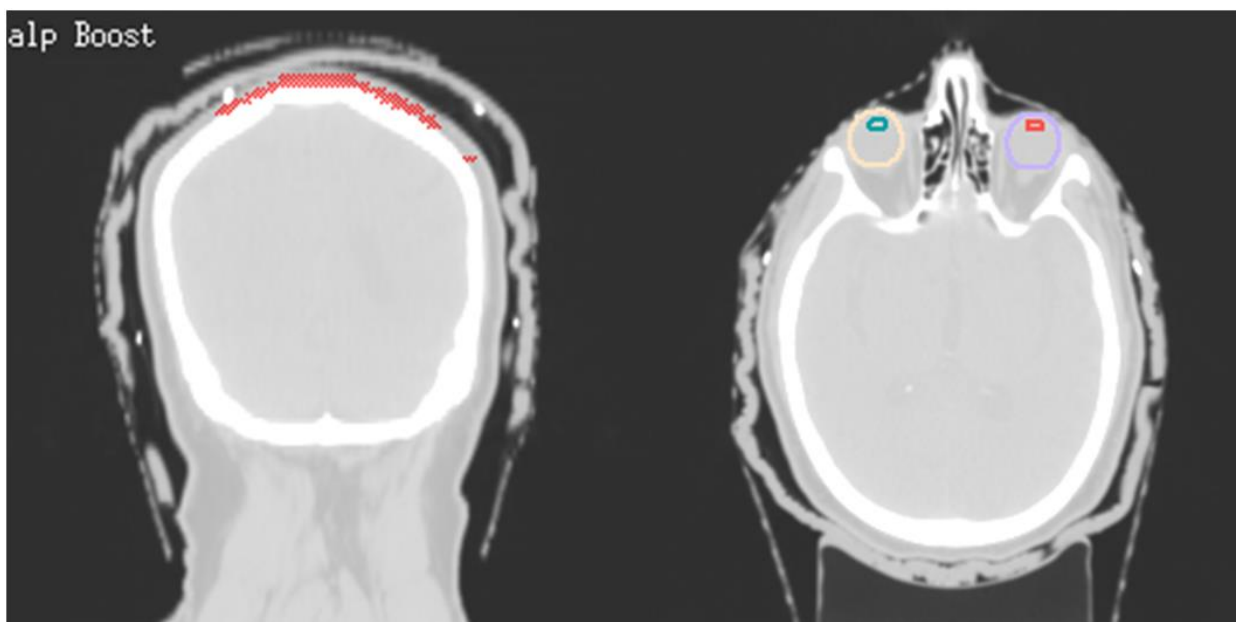


Figure 1-5: CT slices showing the air gaps that can form between the bolus and the scalp with the MD Anderson scalp bolus technique

Although newer treatment techniques have improved the dose homogeneity in TSI, non-conformality of the bolus now serves as a primary limiting factor of dose homogeneity. This project sought to solve the problems of laborious fabrication, air gaps, and limited reproducibility present in current bolus techniques through the development of 3D-printed patient specific bolus caps for total scalp irradiation.

1.3 3D-Printing

3D printers allow for the rapid fabrication of custom objects through the additive manufacturing process. Additive manufacturing processes build objects by successively depositing thin layers of material and building up an object layer by layer. The generalized additive manufacturing process begins by using computer-aided design (CAD) software to generate a 3D model of the object to be manufactured. The CAD model is then converted into a Standard Tessellation Language (.STL) file, which converts the continuous geometry CAD data into a triplet list of x, y, and z coordinates of normal vectors.¹⁷ The .STL file contains the data a

3D printer uses to fabricate an object via the computer control of an additive manufacturing device. This process is identical for all 3D-printers, however, there are several different additive manufacturing technologies that are used in commercially available 3D printers.

The most common additive manufacturing technology used in 3D printers is Fused Deposition Modeling (FDM).¹⁸ A schematic of the extruder head gantry for an FDM 3D printer is presented in Figure 1-6. This process uses thermoplastic material, such as polylactic acid (PLA) or acrylonitrile butadiene styrene (ABS), to additively manufacture objects. A long rolled filament of the thermoplastic material is placed in-between rollers that feed the filament into a heated liquefier, which melts the material into a liquid. The liquefier ends in a small nozzle and is attached to a computer control gantry, called the extruder head. The 3D printer moves the gantry in the x-y plane and the melted thermoplastic material is continuously extruded through the nozzle and deposited in a layer on to a build surface. FDM printers extrude molten material in a layer ranging from 0.1 - 0.3 mm thick. Once the molten material has been extruded, it quickly solidifies. After the gantry has extruded all the material for a layer, the build surface lowers in the z-axis and the gantry begins extruding for the next layer, repeating this process until the object has been completely fabricated.

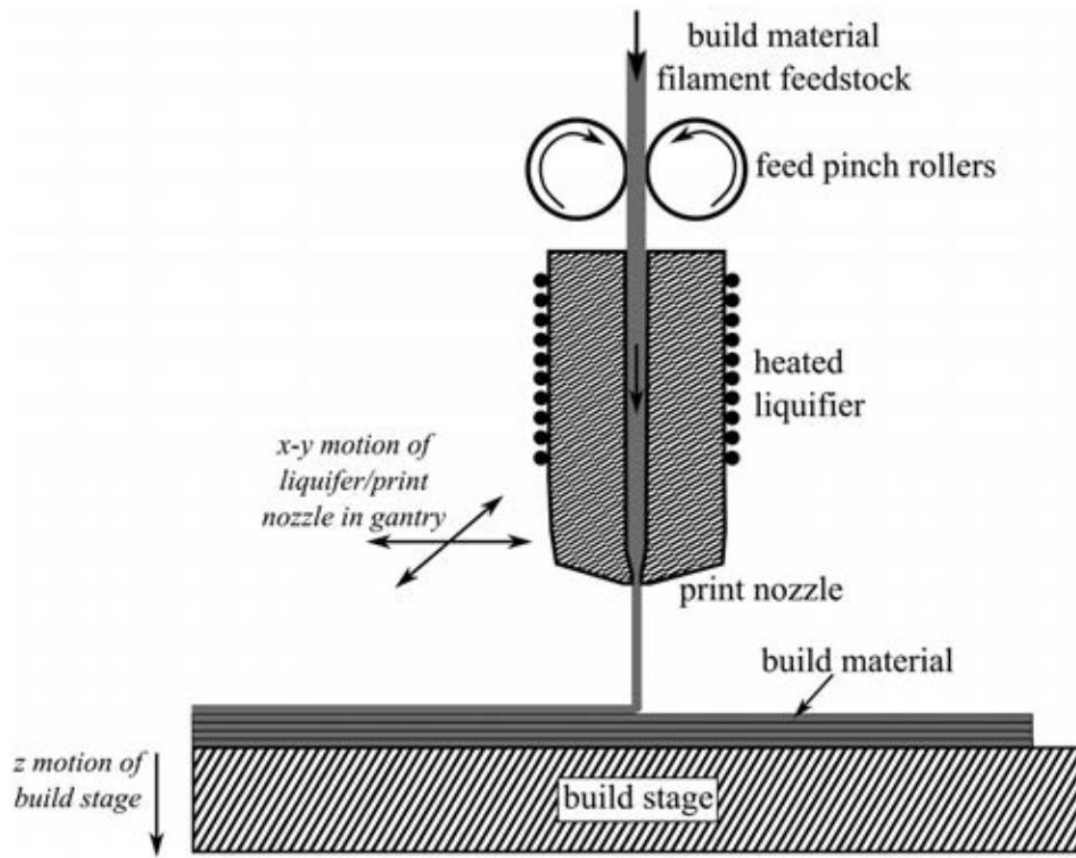


Figure 1-6: Schematic of an extruder head gantry for a typical FDM 3D-printer.¹⁸ Used with permission N. Turner B, Strong R, A. Gold S. A review of melt extrusion additive manufacturing processes: I. Process design and modeling. Rapid Prototyp J. 2014;20(3):192-204.

Another type of additive manufacturing process that is gaining popularity is PolyJet 3D printing. A diagram of the PolyJet process is presented in Figure 1-7. This process uses a liquid acrylic-based photopolymer resin to build objects.¹⁹ The extruding gantry for a PolyJet 3D printer uses a conventional inkjet print head to selectively jet drops of the photopolymer resin into a 16 μm thick layer onto a build surface. The jetted layer of the photopolymer material on the build surface is immediately cured by UV light that is emitted by an ultraviolet lamp attached to the extruding gantry.

PolyJet 3D printers are typically more expensive than FDM printers due to their ability to fabricate objects very high resolution, and their ability to print digital materials. A digital

material is a manufactured composite material with predetermined mechanical properties.

PolyJet 3D printers are able to fabricate digital materials due to the inkjet print head being able to simultaneously jet an elastic polymer and a rigid polymer. By controlling the proportion of each polymer jetted, different material compounds can be created. PolyJet printers can print digital materials with predetermined elasticity, density, and firmness that can range from a very soft, elastic rubber-like material to a very rigid, plastic-like material. This makes PolyJet 3D printers very versatile and unique in their capability to print a material that exactly meets desired characteristics and mechanical specifications.

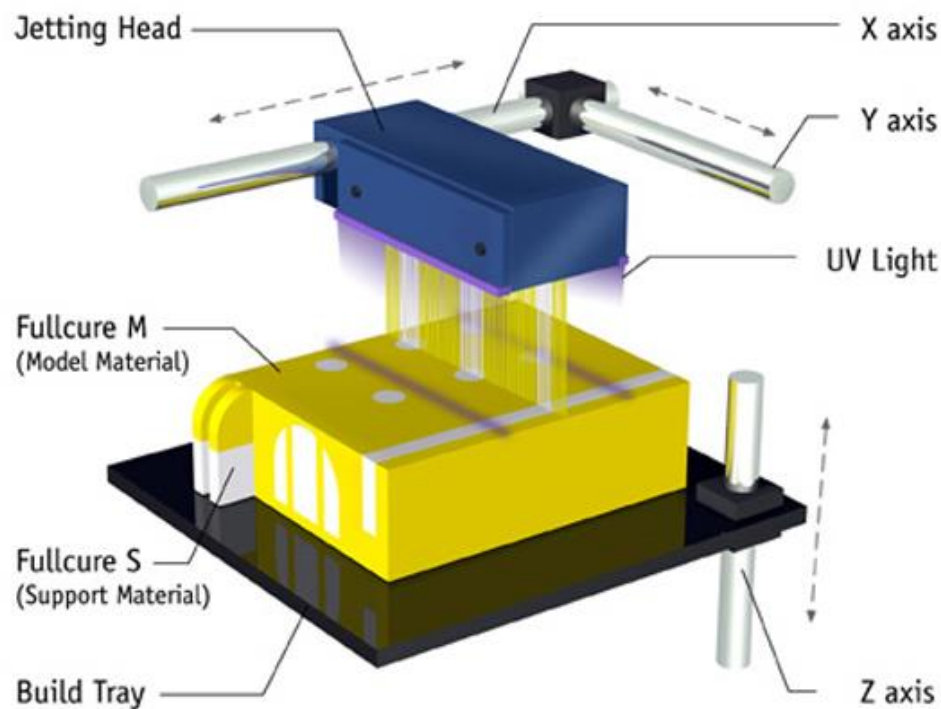


Figure 1-7: Schematic of the extruder head gantry for a typical PolyJet 3D printer. Taken from: <http://ss.whiteclouds.com/3dpedia-index/light-polymerized-3d-printing>

1.3.1 Applications in Radiation Oncology

A growing area of research in radiation oncology physics has been exploring the capability of 3D printers to fabricate many of the treatment accessories that are used in radiation therapy. 3D printers are well suited for fast and minimally labor-intensive fabrication of custom objects. This has naturally led to researching the ability of 3D printers to print many of the custom patient specific treatment accessories used in radiation therapy.

The primary area of research for 3D-printing in radiation oncology has been in the fabrication of bolus. As previously discussed for total scalp irradiation, in order to create the desired surface dose using a bolus, the bolus must be adhered directly to the treatment surface and be conformal to minimize air gaps that can negatively affect the surface dose. Typically commercially available sheets of bolus material can be used for most treatments where the surface is smooth and relatively flat. However, conventional bolus materials are difficult to adhere to very curved and non-smooth treatment areas, such as the ear, nose, and some extremities. For these treatment sites, bolus that is exactly conformal to the curved or irregular surface can be 3D-printed. A patient's Computed Tomography (CT) scan can be imported as a 3D-model of the patient's anatomy into CAD software and a 3D model for a conformal bolus can be created. This technique has been demonstrated in the literature to create bolus for the foot surface,²⁰ nose,²¹ eye canthi,²² and ear²³. These studies have demonstrated that CT data sets can be used to create 3D-models for patient-specific bolus and that the resulting 3D-printed bolus has good conformality to the desired treatment area.

The use of 3D-printers to fabricate compensators has also been a topic of research. A compensator is a treatment device that is placed in the path of the treatment beam to filter or alter the beam. Compensators are made of dense material and are specially fabricated such that

they “compensate” for changes in tissue density within the patient or changes in patient thickness, i.e. the neck, by spatially attenuating the beam to create uniform irradiation.¹² One use case for compensators is in total body irradiation. Park *et al.* presented a novel method for using 3D-printers to assist in the fabrication of a compensator for total body irradiation.²⁴ Their method used an optical scanner to acquire a 3D-model of a phantom that was imported into CAD software. The phantom 3D-model and a dose calculation algorithm were used to create a model for a compensator that would selectively attenuate the beam to create a uniform total body irradiation. A mold for the developed compensator was 3D-printed and filled with molten cerrobend to cast the compensator.

Prior research has demonstrated the efficacy of using 3D-printers to create bolus and compensators for radiation therapy, which provided the inspiration to research the potential of 3D-printed patient specific bolus caps to solve the issues with current bolus techniques used for total scalp irradiation.

1.4 Hypothesis

The hypothesis for this work was that for total scalp irradiation, a 3D-printed bolus cap can reproducibly generate a homogeneous dose distribution over the scalp within $\pm 5\%$ of the prescribed dose.

1.5 Specific Aims

The following five specific aims were established to develop a 3D-printed bolus cap for use in total scalp irradiation and test the hypothesis:

1. Determine a suitable 3D-printing material for the bolus cap.
2. Generate a standard bolus cap design that satisfies clinical requirements and can be readily 3D-Printed.
3. Fabricate 3D-printed bolus caps using in-house and out-sourced fabrication methods.
4. Demonstrate 3D-printed bolus caps can reproducibly generate homogenous dose distribution over scalp.
5. To develop a clinical workflow for both methods of fabrication, draft proposals for the New Protocol Review Committee.

1.6 Organization of Thesis

A chapter is dedicated to each specific aim detailing the motivation and relevant background information, methods and materials, and results. Specific Aims 2 and 3 are combined into one chapter for the purpose of clarity. Final discussion and conclusions are presented in Chapter 6.

2 Specific Aim 1: Determination of Suitable 3D-Printing Materials for the Bolus Cap

2.1 Introduction

There were several factors that had to be considered when selecting what 3D-printing material to use for the scalp bolus cap.

First, the material has to be suitable for use as a bolus. This generally means the material should be water or tissue equivalent. This is so both electronic and dosimetric equivalence can be maintained at the bolus-skin surface interface, and because most treatment planning systems are optimized to calculate dose in water and tissue like materials.¹² Previous studies have identified 3D-printing materials that have similar density to water, however, their exotic chemical composition causes radiation to interact much differently in the material than in water.²¹ For this reason it is necessary to verify the material's physical properties for water equivalence and also measure its radiological properties.

One method the radiological properties of a material can be determined is by measuring the material's Hounsfield Unit (HU) from a CT scan. The HU is defined by Equation 1, where μ is the linear attenuation coefficient for a given voxel in a CT study, and μ_w is the linear attenuation coefficient of water.²⁵ HU is defined as 0 for water and -1000 for air.

Equation 1

$$HU = 1000 \times \frac{\mu - \mu_w}{\mu_w}$$

The HU information from CT scans is used in radiation therapy treatment planning to convert HU to density, which allows for the density of tissue at any location in the patient to be known. The dominant interaction of radiation in soft tissue is the Compton interaction, for

which the interaction rate is proportional to the tissue's density.²⁵ This allows for dose calculation algorithms to use a CT scan to derive voxel based density information to account for tissue inhomogeneities when calculating dose. Typical HU values for adipose tissue range from -80 to -30, and most organ parenchyma ranges from 30 to 220.²⁵ This means most tissue in the human body has HU in the range of -80 to 220. If a material has an HU in this range with an appropriate physical density, it can be considered tissue equivalent. CT scans of material samples were used in this section to determine radiological tissue equivalence.

The second factor considered for selecting a material is the final 3D-printed bolus should be comfortable enough for the patient to wear while the patient is in the immobilization mask during treatment delivery. This was an important consideration as previous techniques in the literature for TSI bolus have noted patients can experience pain when having to put on the bolus due to radiation-induced acute skin toxicity causing the scalp to be very sensitive in the latter stages of their treatment course.²⁶ Thus far most 3D-printed boluses presented in the literature have been made out of hard plastic materials, such as PLA and ABS. These materials would not be suitable for use as a scalp bolus as a rigid, highly conformal bolus would be very difficult to fit onto a patient's head, and it would be uncomfortable for the patient to wear while in the immobilization setup.

As discussed in Section 1.3, there are several types of commercially available 3D-printers capable of printing different types of materials. For this specific aim, material samples produced by two different types of 3D printers were analyzed to find a suitable material to use to 3D-print a scalp bolus using each 3D printer. The first material to be analyzed was a potential bolus material identified by previous research that can be printed by a fused deposition modeling 3D printer. FDM printers represent the majority of 3D printers currently in the consumer market

and are the most likely type of 3D printer a radiation oncology department would have access to. If a material that can be printed by an FDM printer is found suitable for use as a scalp bolus, many departments that already own an FDM 3D printer could start using it to produce 3D-printed bolus caps for their TSI patients. This would serve as a method for the in-house fabrication of a 3D-printed bolus cap.

Materials produced by a PolyJet 3D printer were the second to be analyzed. As previously discussed, PolyJet printers are capable of printing materials with varying elasticity and hardness. Even though PolyJet 3D printers are much more expensive, they are capable of printing materials that very closely mimic traditional commercial bolus material, which would be an ideal material for the 3D-printed bolus cap in regards to patient comfort. Radiologic properties of PolyJet 3D print materials have not yet been presented in literature and thus the majority of the tests conducted in this section were devoted to analyzing the properties of PolyJet materials. Due to the prohibitive cost, most radiation oncology departments would not own a PolyJet printer, but this method would allow for departments to contract out the fabrication of the bolus cap to a commercial vendor if they did not have any 3D-printing resources in-house.

2.2 Methods and Materials

2.2.1 Materials for a Fused Deposition Modeling 3D Printer

NinjaFlex (NinjaTek; Manheim, PA, USA) is a thermoplastic polyurethane (TPU) based material that has been previously identified for potential use as 3D-printed bolus.²⁷ NinjaFlex is unique among FDM materials as if it is printed thin enough, it is very flexible. If the material could still be flexible when printed 5 mm thick for the bolus cap, it would make it ideal for a 3D-printed bolus cap as the flexibility would make the bolus easier to fit onto the patient's head. To test the flexibility, a 20 mm x 200 mm x 5 mm thick strip of NinjaFlex was 3D printed using

a Gigabot 3 3D-printer (re:3D; Houston, TX, USA). The material was printed at 100% infill with an extruder nozzle temperature of 235 °C and heated bed temperature of 40 °C with no additional tape or adhesive.

2.2.2 Materials for a PolyJet 3D Printer

This section details analysis of materials that can be printed by a Stratasys PolyJet J750 3D Printer (Stratasys; Eden Prairie, MN, USA). This included the photopolymer materials Tango and Agilus. Both of these soft, rubber-like materials can be blended in different concentrations with a rigid photopolymer material called Rigur during printing to produce digital materials with varying softness or hardness, ranging from a very soft rubber-like material to a solid plastic material. The specific mixture and resulting final material is characterized by its Shore durometer value, which is a value that characterizes the hardness of rubber and plastic materials by the relative indentation of a probe.²⁸ Shore value ranges from 0 for the full indentation of 2.50 mm to 100 for no indentation. The Tango and Agilus materials can be printed to have a specific Shore value, ranging from 27 to 100 in increments of 5. Agilus-27, for example, has a Shore value of 27 and is the softest material that can be printed, Agilus-100 is the firmest material.

To determine if the Tango or Agilus material would be best for use as a bolus, 3 cm × 3 cm × 3 cm 100% infill cubes of Tango and Agilus were 3D-printed using a Stratasys PolyJet J750. Ten cubes each were printed for Tango and Agilus, with shore values of 27, 30, 35, 40, 50, 60, 70, 85, 95, and 100. The printed cubes are shown in Figure 2-1.

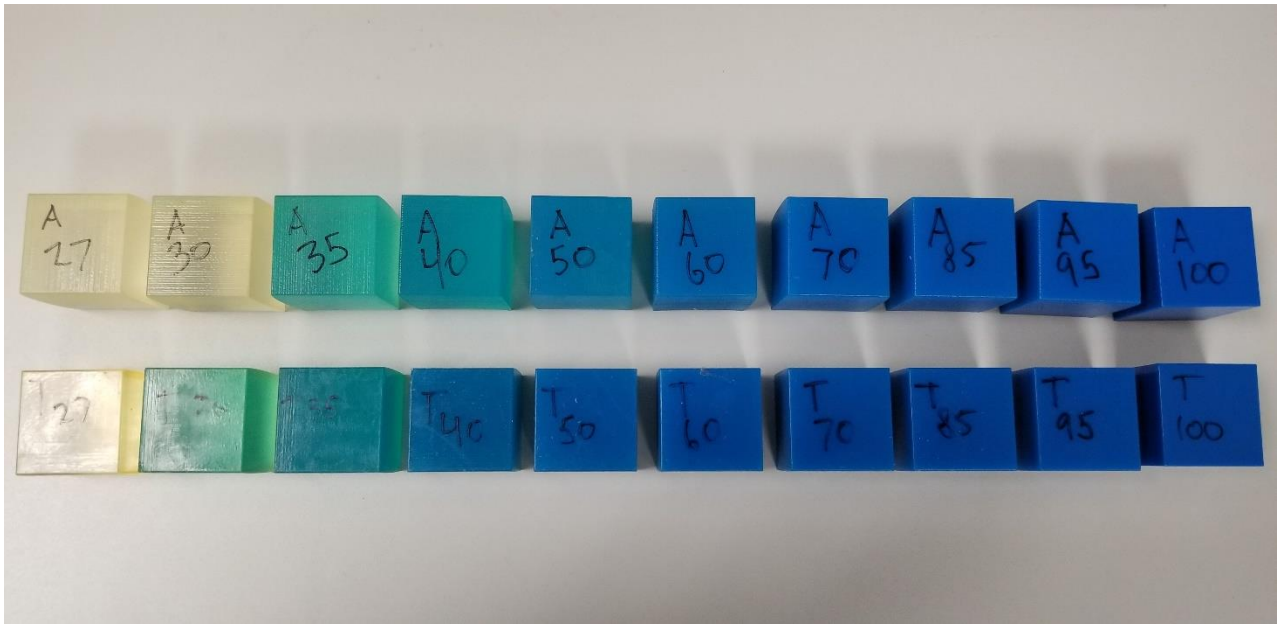


Figure 2-1: 3D-printed sample composition cubes for Agilus (top row, labeled A27- A100) and Tango (bottom row, labeled T27-T100). The materials are labeled with their Shore value. The softest and most flexible materials are at the left (A27 and T27) and they gradually get firmer as the Shore value increases to the firmest materials on the right (A100 and T100).

The first material test was a Computed Tomography (CT) analysis to see how well the sample material's density was predicted by the treatment planning system's CT calibration curve. The CT calibration curve is used by the treatment planning system to convert CT Hounsfield units (HU) to physical density for dose calculations. The accuracy of this conversion is important to assure dose calculations are accurate.²¹ A CT of the cubes was acquired using a Philips Brilliance Big Bore Scanner (Philips Healthcare, Andover, MA, USA). The physical density of each cube was calculated using the cube's weight measured with a high accuracy balance, and the cube's dimensions measured with calipers. The average HU of each cube was measured using the DICOM imaging software OsiriX (Pixmeo, Bernex, Switzerland). Each cube's density and HU was plotted against the CT calibration curve, and the percent error between the cube's physical density ($\rho_{measured}$) and CT calibration curve predicted density (ρ_{CT}) was calculated using Equation 2.

Equation 2

$$\% \text{ Error} = \frac{|\rho_{measured} - \rho_{CT}|}{\rho_{measured}}$$

The second material test was to assess the flexibility and deformability of different Shore values to determine which Shore value would be most appropriate for the bolus cap. The results of the initial CT analysis demonstrated the Agilus material was better predicted by the CT calibration curve, suggesting it was more tissue equivalent than the Tango material. Five sample 20 mm × 200 mm × 5 mm thick test strips were printed, with Shore values 27, 40, 50, 60, and 70. These strips allowed for an assessment of the material's flexibility and deformability when 5 mm thick like the bolus. An additional CT analysis was conducted to determine the fidelity of the HU-to-density conversion when the material is only 5 mm thick. A CT study of the strips was acquired and the same procedure to calculate the physical density, measure HU number, and compare to the CT calibration curve was repeated.

The second CT analysis demonstrated Agilus with a Shore value of 60 to be most suitable for a 3D-printed bolus cap. To further verify the accuracy of calculating dose in this material, Percent Depth Dose (PDD) measurements were conducted. PDD measurements would allow for the comparison of measured doses and doses calculated by the treatment planning system at depth. The PDD measurements were conducted using a method presented by Craft *et al.* and summarized here.²⁹ Five blocks of the Agilus-60 material were printed: one 20 cm × 10 cm × 2.5 cm, two 20 cm × 5 cm × 2.5 cm, one 20 cm × 2.5 cm × 0.5 cm, and one 20 cm × 2.5 cm × 0.3 cm. The blocks are presented in Figure 2-2. As shown in Figure 2-2, the blocks larger than 2.5 cm thick were printed with holes at 1.4 cm, 2.3 cm, and 5 cm deep in the material, with the hole diameter just large enough to accommodate an ionization chamber.

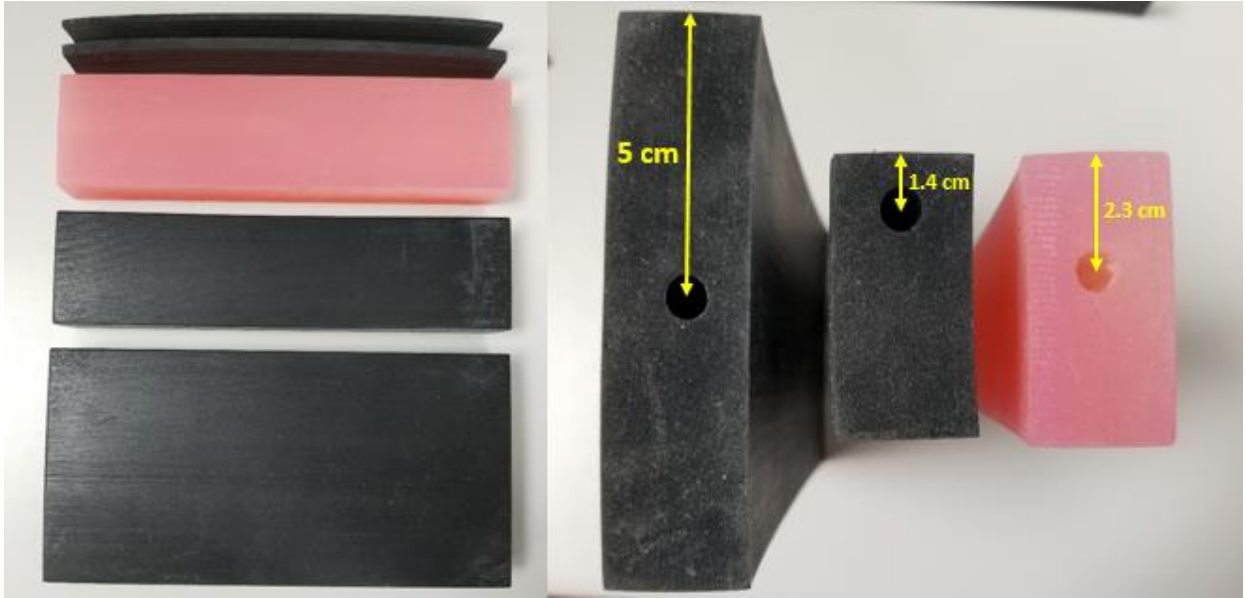


Figure 2-2: (left) Blocks printed for the PDD measurements. (right) close up showing the location of the holes for the ionization chamber.

The setup used to obtain the PDD measurements is shown in Figure 2-3. The blocks were stacked vertically in between blocks of acrylic, which was used to maintain electronic equilibrium on both sides. An Exradin A1SL small volume ionization chamber (Standard Imaging Inc., Middleton, WI, USA) was placed in the fabricated holes in the blocks and connected to a Radiation Products Design Model 206 Electrometer (Radiation Products Design Inc., Albertville, MN, USA). Ionization measurements in 1 cm increments at depths ranging from 1 cm - 19 cm in the material were acquired by stacking the blocks in different configurations and placing the ionization chamber into the appropriate hole. Additionally, the 0.5 and 0.3 cm thick strip were selectively placed on top of the blocks to obtain finer measurements proximal and distal to the depth of maximum dose. Ionization measurements were acquired by delivering 200 monitor units of a 6 MV beam with a $10\text{ cm} \times 10\text{ cm}$ field size produced by a Varian Truebeam linear accelerator (Varian Medical Systems, Palo Alto, CA, USA). The surface of the PDD block setup was placed at a distance of 100 cm from the

radiation source. Ionization measurements were normalized to the depth of maximum dose (d_{max}), which was 1.5 cm. Because the factors for converting ionization measurements to dose do not change as a function of depth,³⁰ normalizing ionization measurements is equivalent to normalizing dose measurements.

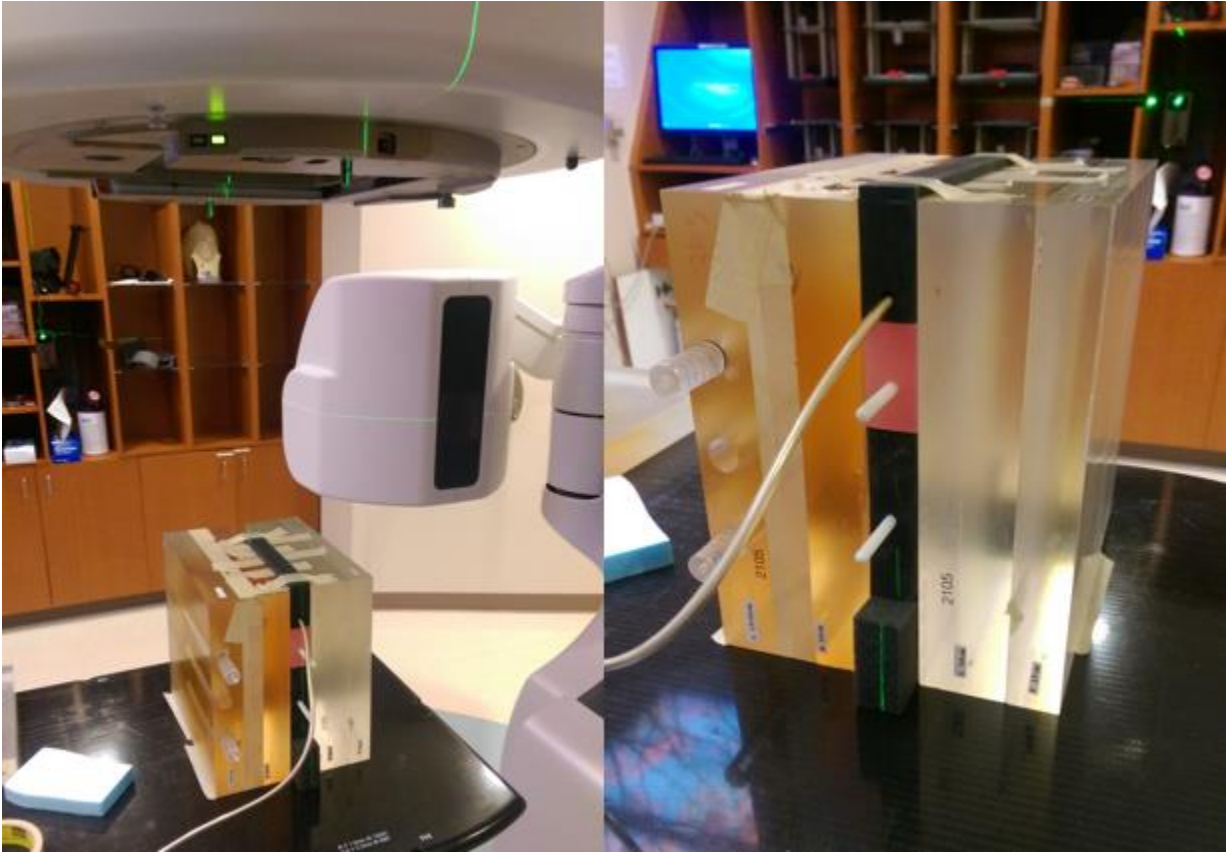


Figure 2-3: (left) PDD measurement setup showing the surface of the blocks at 100 cm source to surface distance. (right) Close-up of the PDD blocks setup.

A CT of the PDD measurement setup was acquired using a Philips Brilliance Big Bore scanner. The CT study was imported into the RayStation 5.0.2 treatment planning system (TPS) (RaySearch Laboratories, Stockholm, Sweden). The irradiation and setup conditions were reproduced in the treatment planning system and doses were calculated at the measurement points, shown in Figure 2-4. Dose was calculated under two conditions, one with the density of the blocks overridden with an acrylic based material with density of 1.14 g/cm^3 (the

manufacturer given density³¹⁾) and one with the density of the blocks derived from the CT calibration curve. This was to determine which method would produce calculated doses that agreed best with measured doses. PDD data were also compared to the water commissioning PDD curve to compare how radiation behaves in the Agilus material compared to water.

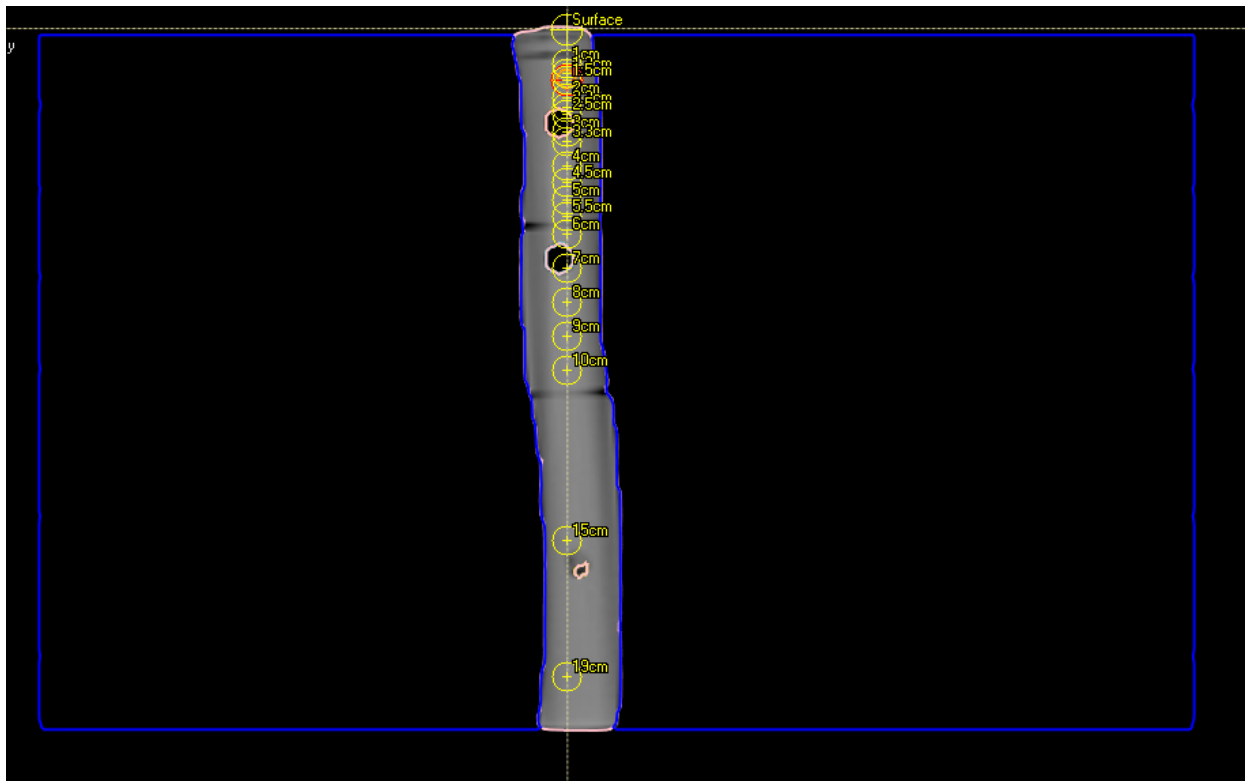


Figure 2-4: The PDD measurement setup in RayStation. The yellow circles show locations for point dose calculations that correspond to the measurement locations.

2.3 Results

2.3.1 NinjaFlex Properties and Suitability for use as 3D-Printed Bolus Cap

The 3D-printed NinjaFlex test strip was found to have a physical density of 1.04 g/cm^3 and average Hounsfield Unit of -45 ± 43 . These properties mean NinjaFlex is a tissue equivalent material and suitable for use as bolus. Additionally, percent depth dose (PDD) measurements conducted in a previous study demonstrated measured doses agreed with treatment planning system calculated doses to within 3 mm.²⁷

Shown in Figure 2-5 is the 5 mm thick 3D-printed NinjaFlex strip. Even when printed 5 mm thick, the strip is still flexible enough to be deformed, yet will return to its original shape. This means the material would be suitable for use in a bolus cap for total scalp irradiation, as the flexibility would make the bolus cap more comfortable to wear while the patient lies down during treatment, yet the cap will maintain its original printed shape to remain conformal to the patient's scalp.

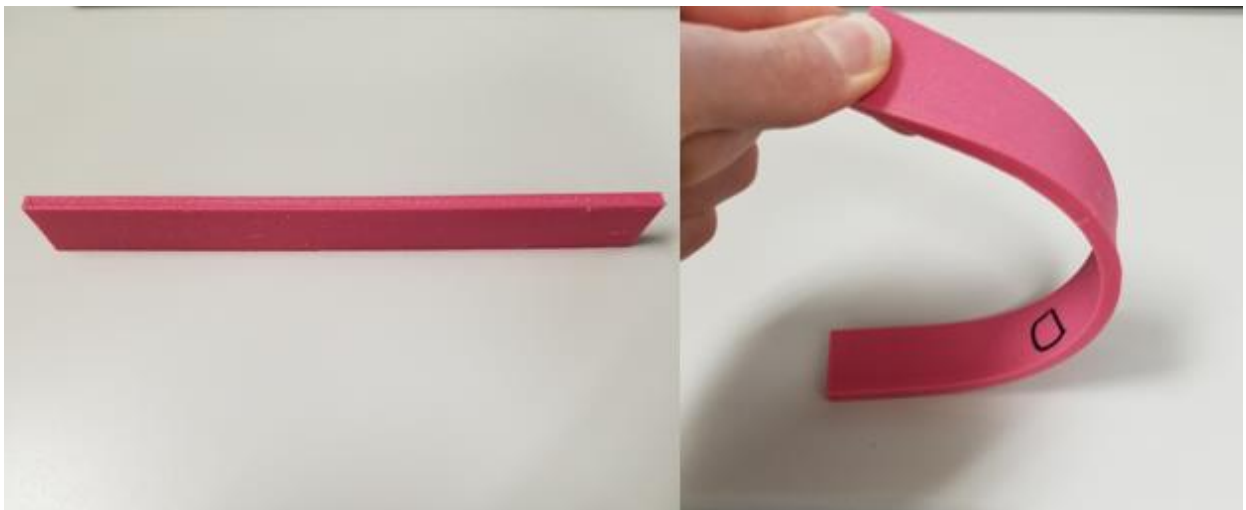


Figure 2-5: (left) 3D-printed 5 mm thick NinjaFlex strip. (right) Picture showing the NinjaFlex material is still flexible when 5 mm thick.

2.3.2 PolyJet Material Properties and Suitability for use as 3D-Printed Bolus Cap

Table 2-1 presents the measured weight, dimensions, average HU and standard deviation for all the Agilus and Tango material sample cubes. The Tango material samples had a density ranging from 1.12 to 1.18 g/cm³. The Agilus material samples had a density ranging from 1.11 to 1.18 g/cm³. In general, the Tango material density was greater than the Agilus material density for the same Shore value. For both materials, the density generally increased with increasing Shore values.

Table 2-1: Density and CT data for Tango and Agilus material samples

Material	X (cm)	Y (cm)	Z (cm)	Mass (g)	Density (g/cm³)	Average HU	HU Standard Deviation
T27	3.02	3.01	2.60	26.619	1.126	61.76	29.04
T30	2.62	3.00	3.02	26.587	1.120	54.82	39.9
T35	2.61	3.03	3.04	27.027	1.124	43.46	44.41
T40	2.61	3.00	3.00	26.459	1.126	36.92	56.42
T50	2.62	3.00	2.99	26.427	1.124	36.32	47.08
T60	2.61	3.00	3.00	26.606	1.133	39.19	51.56
T70	2.62	3.00	3.00	26.635	1.130	44.03	53.07
T85	2.62	3.01	3.01	26.858	1.131	55.97	50.35
T95	2.62	3.00	3.01	27.012	1.142	74.67	43.79
T100	2.61	3.00	3.00	27.744	1.181	111.34	36.36
A27	3.06	3.02	3.03	30.933	1.105	77.59	39.86
A30	3.03	3.01	3.04	30.918	1.115	74.92	38.64
A35	3.04	3.03	3.00	30.855	1.117	64.73	47.98
A40	3.07	3.01	3.00	30.878	1.114	60.44	43.32
A50	3.04	3.01	3.00	30.848	1.124	57.8	46.46
A60	3.06	3.00	3.01	30.798	1.115	58.53	49.41
A70	3.04	3.01	3.00	30.910	1.126	66.66	47.39
A85	3.08	3.04	3.02	31.272	1.106	69.27	59.91
A95	3.05	3.02	3.01	31.270	1.128	87.81	43.61
A100	3.00	3.00	3.01	31.992	1.181	119.64	28.64

The results of the HU measurements from the CT studies provided some insight into the materials' radiological properties. The HU for the Tango material ranged from 36 to 111, and 57 to 119 for the Agilus material. Interestingly and potentially of concern, the HU did not linearly correlate with density for either material. The HU for the lowest Shore value was 61.76 for Tango and 77.59 for Agilus. The HU value decreased to a minimum value of 36.32 for Tango and 57.8 for Agilus both at a Shore value of 50. The HU then increases as Shore value increases above 50, as the proportion of the flexible material decreases. This suggests the way the flexible and rigid materials are blended when printed affects the polymerization and subsequently the electron density of the printed material. This is a potential issue as it is important for tissue

equivalence that the HU can be used to accurately predict the material's physical density for accurate dose calculations.

This was analyzed by using the CT calibration curve to convert HU to density and see how the predicted density compared to the measured density. Table 2-2 shows the results of this analysis for both Tango and Agilus. Figure 2-6 shows a visual representation of the measured density and HU for each sample cube plotted against the CT calibration curve.

Table 2-2: Comparison of measured density and density predicted by CT calibration curve

Material	Measured Density (g/cm³)	CT Calibration Curve Predicted Density (g/cm³)	% Error
T27	1.126	1.077	4.4
T30	1.120	1.069	4.5
T35	1.124	1.058	5.9
T40	1.126	1.051	6.7
T50	1.124	1.050	6.6
T60	1.133	1.053	7.0
T70	1.130	1.058	6.3
T85	1.131	1.071	5.4
T95	1.142	1.090	4.5
T100	1.181	1.111	6.0
Average			5.6
A27	1.105	1.093	1.1
A30	1.115	1.090	2.2
A35	1.117	1.080	3.3
A40	1.114	1.075	3.5
A50	1.124	1.073	4.6
A60	1.115	1.073	3.7
A70	1.126	1.082	3.9
A85	1.106	1.084	2.0
A95	1.128	1.103	2.2
A100	1.181	1.113	5.8
Average			3.0

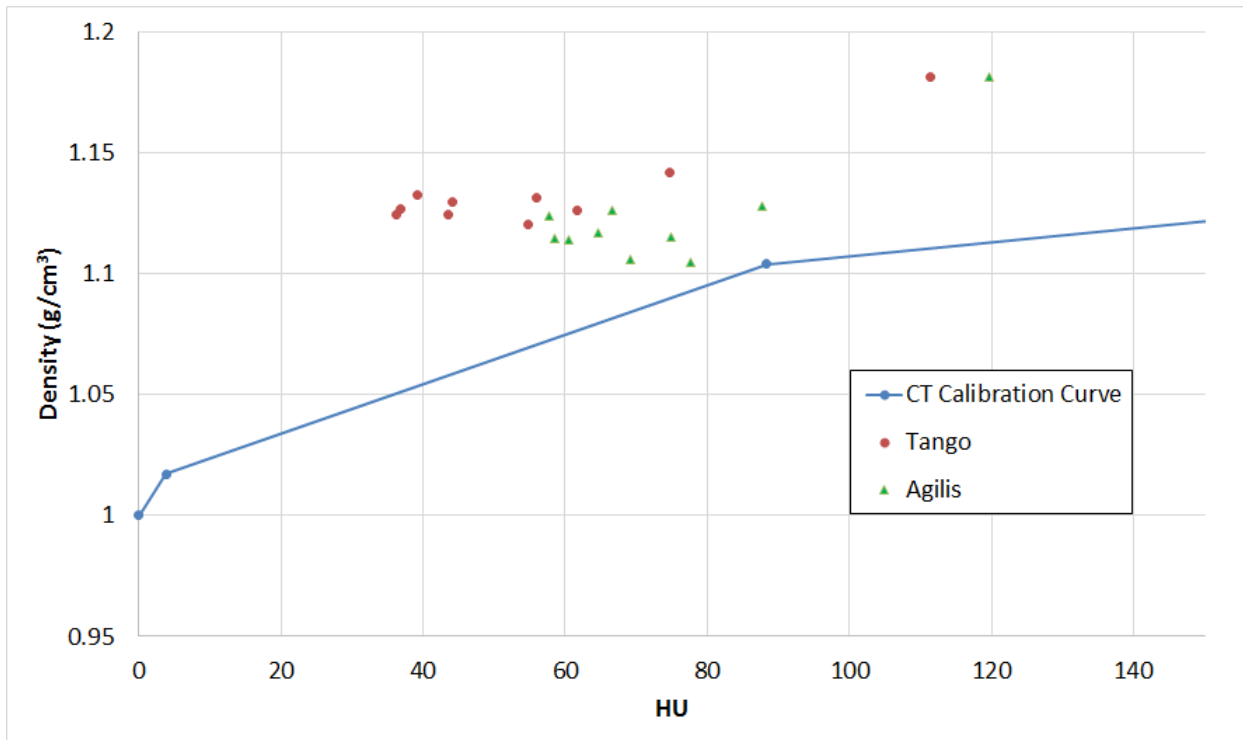


Figure 2-6: Plot of the measured density and HU for each material cube sample and the CT calibration curve.

Table 2-2 shows that the average percent error between the measured density and predicted density was 5.6% for the Tango material samples and 3.0% for the Agilus material samples. This is also shown visually in Figure 2-6, as most of the Agilus sample points are closer to the CT calibration curve than the Tango points. This suggests the Agilus material is a better tissue equivalent material than the Tango material, as it is better modeled by the CT calibration curve. The Agilus material was selected for further research to determine what Shore value composition would be best to use for the bolus cap.

The measured weight, dimensions, average HU, and CT calibration curve predicted density for the Agilus 5 mm thick strips printed to determine what Shore value to use is presented in Table 2-3. A visual representation of the measured density and HU for each strip plotted against the CT calibration curve is presented in Figure 2-7.

Table 2-3: Physical data for 5 mm Agilus strips

Material	X (mm)	Y (mm)	Z (mm)	Mass (g)	Average HU	Density (g/cm ³)	CT Calibration Curve Density (g/cm ³)	Error
A27	20.7	4.95	1.10	121	67.65	1.074	1.083	0.85%
A40	20.5	2.50	0.51	28.422	52.75	1.087	1.067	1.84%
A50	20.5	2.49	0.55	28.255	48.24	1.006	1.063	5.59%
A60	20.55	2.50	0.51	28.342	52.13	1.082	1.067	1.39%
A70	20.51	2.45	0.55	28.536	45.37	1.033	1.060	2.64%

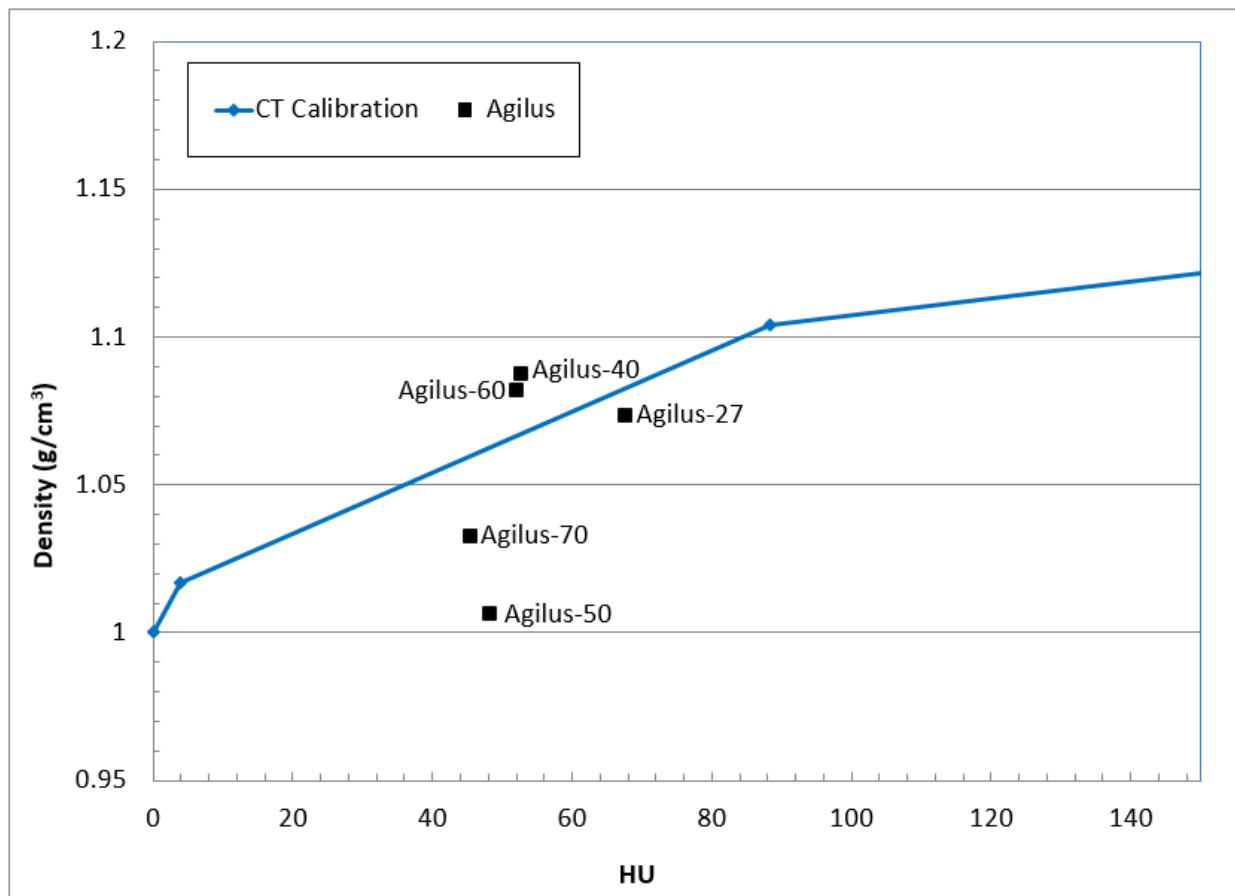


Figure 2-7: Plot of the measured density and HU for each Agilus strip sample and the CT calibration curve.

From Figure 2-7, the Agilus-27 strip appears to be the best predicted by the CT calibration curve, and this was confirmed by the percent error between the measured and predicted density being only 0.85%. However, the Agilus-27 strip was very flexible, to the point of not being elastic. This suggested a bolus cap printed in Agilus-27 might not be able to remain conformal to the scalp under its own weight. The composition next best predicted by the CT calibration curve was the Agilus-60 strip, with a 1.39% error between the measured and predicted density. Additionally, the 60 Shore value strip was less deformable compared to the Agilus-27 strip, while still remaining soft to the touch, shown in Figure 2-8. It was for these reasons Agilus-60 was selected as the PolyJet material to use for further study for the bolus cap.



Figure 2-8: Picture demonstrating the difference in flexibility and deformability between the Agilus-27 strip (clear in the foreground) and the Agilus-60 strip (purple and in the background). The Agilus-27 strip is highly deformed under its own weight, unlike the Agilus-60 strip.

The results of the PDD measurements are presented in Figure 2-9. In general the measured PDD values fall close to the commissioning water curve. This demonstrates that Agilus material behaves very similarly to water, which is good for maintaining electronic equilibrium at the surface of the skin, and for dose calculation purposes.

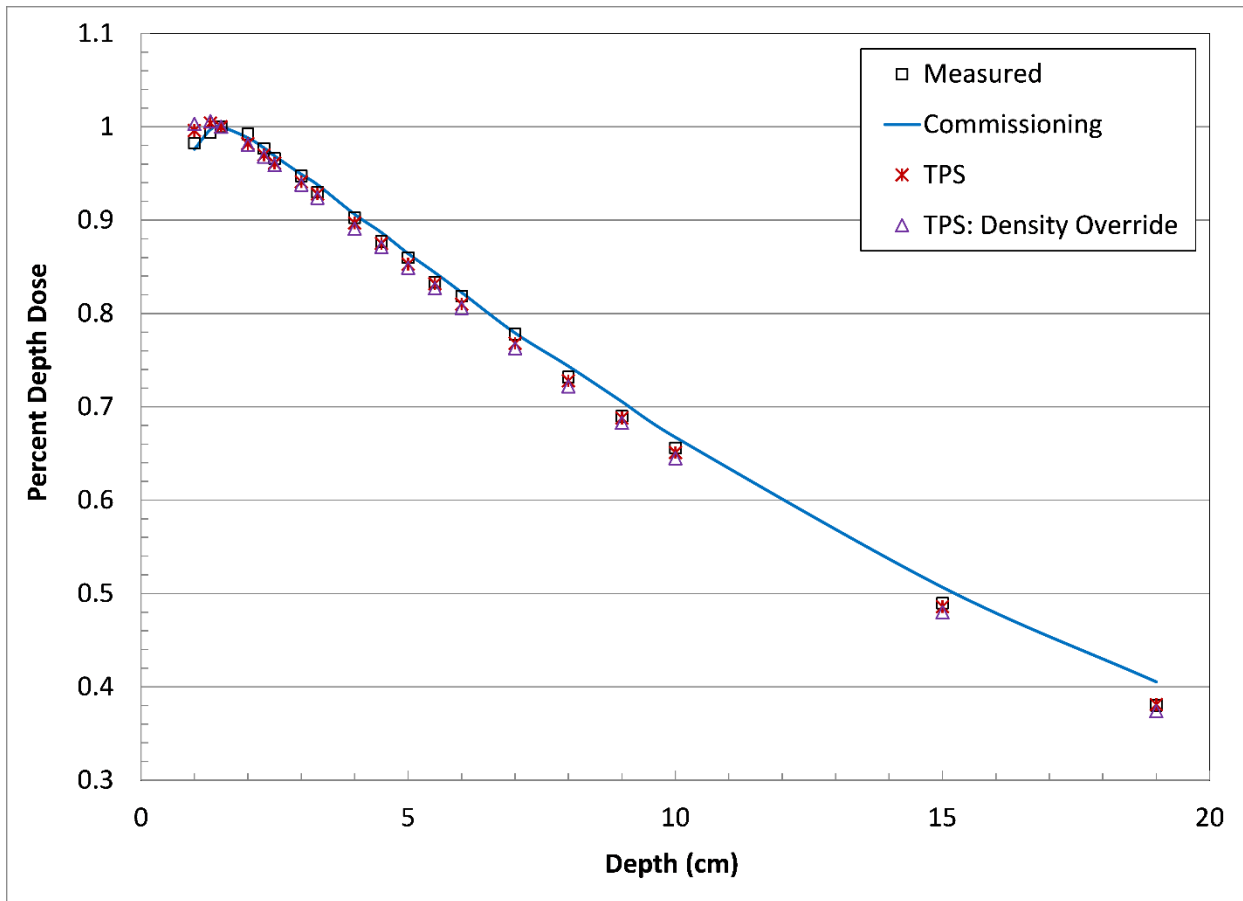


Figure 2-9: Plot of percent depth dose measurements in Agilus-60 material (squares). The blue line is the commissioning PDD curve in water. Also plotted is the treatment planning system calculated dose for no density override (star) and density of blocks overridden (triangle).

Additionally, the treatment planning system calculated doses were in good agreement with the measured doses. Table 2-4 provides the data for the measured PDD, the commissioning PDD, and the treatment planning system calculated PDD for both no density override and density override cases. The coefficient of determination was calculated for the data with respect to the measured PDD values.

Table 2-4: Agilus-60 PDD Data

Depth (cm)	Measured PDD	Water Commissioning PDD Curve	TPS: No Override	TPS: Density Override
1.0	0.982	0.9760	0.996	1.003
1.3	0.994	0.9971	1.004	1.006
1.5	1.000	0.9998	1.000	1.000
2.0	0.992	0.9882	0.982	0.981
2.3	0.977	0.9774	0.970	0.968
2.5	0.966	0.9688	0.961	0.959
3.0	0.947	0.9491	0.941	0.938
3.3	0.930	0.9381	0.928	0.924
4.0	0.903	0.9062	0.897	0.891
4.5	0.877	0.8867	0.875	0.871
5.0	0.860	0.8641	0.853	0.849
5.5	0.833	0.8438	0.832	0.827
6.0	0.819	0.8225	0.810	0.806
7.0	0.778	0.7791	0.768	0.763
8.0	0.732	0.7435	0.728	0.722
9.0	0.690	0.7056	0.688	0.683
10.0	0.656	0.6674	0.651	0.645
15.0	0.490	0.5067	0.486	0.480
19.0	0.380	0.4054	0.381	0.374
R^2	1	0.9995	0.9988	0.9979

The coefficient of determination was used as a quantitative measure of the agreement between measured PDD values and the values calculated by the treatment planning system. The water commissioning data had the largest coefficient of determination, followed by the treatment planning system with no density override, and the lowest was the treatment planning system with density override. This suggests that it is better to have the treatment planning system account for the inhomogeneity correction using the CT calibration curve rather than manually override the density. This is most likely due to the fact that the PDD blocks were not perfectly uniform, with the coefficient of variation of the blocks' HU measured to be 39%.

Overriding the density manually will not capture this non-uniformity within the blocks.

Additionally, the coefficient of determination data suggest the water commissioning data was in the best agreement with the measured Agilus PDD data. However, close examination of the PDD values will reveal this is mainly due to the treatment planning system overestimating doses at depths shallower than d_{max} . Recalculating the coefficient of determination and excluding PDD values at depths shallower than d_{max} , the coefficient of determination for the treatment planning system calculated PDD with no density override increases to 0.9997, 0.9996 for the treatment planning system with density override, and 0.9996 for the commissioning curve. This again confirmed that calculating the dose in the treatment planning system with no density override and native inhomogeneity correction leads to the best agreement with measured PDD values.

Although this data is relevant for use cases where the dose at depth in the material must be known accurately, e.g. using the material for a compensator, it is important to point out that for the use case of a 5 mm thick bolus cap, it is not imperative that the treatment planning system can accurately calculate dose at depth in the material. As previously discussed, the purpose of the bolus cap is to just provide a minimally necessary layer of material to allow the dose to build up at the surface of the skin. The relatively thin material layer in the bolus cap will not significantly affect doses deep in the tissues.

The tests and data collected in this section identified Agilus-60 as a suitable material for use in a 3D-printed bolus cap. Agilus-60 is soft, flexible, and has the ability to retain its shape, which are ideal physical properties. Additionally, the material is tissue equivalent and the treatment planning system was able to accurately calculate dose in the material.

3 Specific Aims 2 and 3: Generation, Fabrication and Assessment of Bolus Cap Designs

3.1 Introduction

The basic design for a bolus cap for use in total scalp irradiation is straight-forward: it should be 5 mm thick and be conformal to the entire scalp. However, there were some additional considerations specific to the design of a 3D-printed bolus cap. The first is the bolus cap needs to be able to be fit onto the patient's head with minimal difficulty to minimize discomfort to the patient. As the bolus cap will be very conformal, this meant the bolus cap needs to be flexible enough to deform when put on the patient and then able to return to its original conformal shape, or if the material is not flexible enough, the bolus cap needs to be printed in two pieces and put back together on the patient's head.

The second consideration is that the design needs to be optimized to be 3D-printed. As discussed in the introduction, 3D-printers fabricate an object by building it up layer by layer. This means if an object has large overhangs, such as in the case of a convex object like the bolus cap, support material must be used or else the object will not print correctly. This principle is demonstrated in Figure 3-1. Support material is additional material the 3D-printer prints to later use as a support to print part of the object upon. The most common type of support printed is a thin accordion like lattice that is able to be easily removed from the object after it is finished printing. Although support can be used to print objects with overhangs, it is best to minimize the amount of support material needed. The use of support material increases the print time and amount of material needed, and can increase the likelihood of failure when printing the object or cause defects in the printed part when removing the support material. Thus the design of the bolus cap should minimize the amount of support material required for it to be printed.



Figure 3-1: Picture showing a typical case where support material is needed in 3D-printing. The T on the left has no support and the object had defects at the overhangs. The T on the right was printed with support and was printed correctly. Taken from: <https://www.3dhubs.com/knowledge-base/supports-3d-printing-technology-overview>

Also considered in the fabrication process were the many parameters that need to be adjusted to successfully 3D-print an object with good quality and high fidelity to the 3D-model. For FDM 3D printers, the most important parameter is the temperature of the extruder nozzle. The nozzle melts the thermoplastic material and controls the flow of material onto the print bed. If the extruder temperature is too high, the viscosity of the molten material will be too low and material will leak out of the extruder. Extruder leaking can cause stringing or pooling of material that will cause the object to have defects and may lead to the print failing if too much material leaks out and the gantry gets obstructed. Conversely, if the nozzle temperature is too low, the material may not stick to itself or extrude fast enough to keep up with the motion of the gantry, which will negatively affect the integrity of the object. The temperature of the print surface is another important parameter. Heated print surfaces better allow extruded material to adhere to the surface and keep the object stationary while printing. Heated beds can also

minimizing the amount an object warps, which occurs if extruded material cools too fast.

However, the temperature cannot be too high or the heat will cause the object to warp. Most of these parameters have recommended settings from manufacturers, but it is sometimes necessary to adjust the parameters for specific applications.

The factors discussed above were considered when generating and fabricating bolus cap designs. Designs were researched for both the NinjaFlex and Agilus-60 materials separately, as their properties differed enough that two different designs were required. A CT analysis of the final printed NinjaFlex and Agilus-60 bolus cap designs fitted on the head phantom was conducted to assess the conformality of the bolus caps.

3.2 Methods and Materials

Two different bolus cap designs were developed: one for the NinjaFlex material and one for the Agilus-60 material. A CIRS ATOM anthropomorphic head phantom (CIRS, Norfolk, VA, USA), shown in Figure 3-2, was used to develop and test the bolus cap designs. This head phantom is anatomically correct, making it a good substitute for the development of a bolus cap in lieu of developing designs for a specific patient. Additionally, the head phantom is made of dosimetrically equivalent tissue and bone materials meaning it can later be used with the fabricated bolus caps for dosimetric verification measurements for total scalp irradiation.



Figure 3-2: CIRS ATOM anthropomorphic head phantom

3.2.1 Generating the Bolus Cap 3D-Model

The first step of creating the bolus cap was to generate a 3D-model of the bolus cap. A CT scan of the bare head phantom was acquired using a standard head and neck protocol. The CT scan was imported into RayStation, for which a multi-step process was used to create a contour of a conformal bolus cap. The first step in the process was to create an external body contour using an HU threshold of -250. The second step was to create a contour in the sagittal plane outlining the desired extent of the bolus on the phantom head. The outline contour was edited so the bolus cap would go around the ears, and the same contour was copied and pasted to all sagittal slices. The third step was to create a new contour that was a uniform 5 mm expansion of

the external body contour. Finally, the bolus cap contour was created by using the ROI algebra functions to first subtract the body contour from the expanded body contour, then create the union of the subtracted contour and the outline contour, creating a conformal, uniformly 5 mm thick bolus cap. This process is presented in Figure 3-3. The CT and contours were then exported as DICOM files to perform the conversion of the DICOM data to an .STL 3D-model file.

The exported DICOM data was imported into the open-source DICOM image processing software 3DSlicer 4.8.0³² with the SlicerRT extension³³. This software loads the bolus cap contour as a segmentation. 3DSlicer has a built-in function in the segmentation editor module that was used to export the bolus cap segmentation as an .STL file. Shown in Figure 3-4 is the .STL 3D-model of the phantom specific bolus cap ready to be 3D-printed or further manipulated.

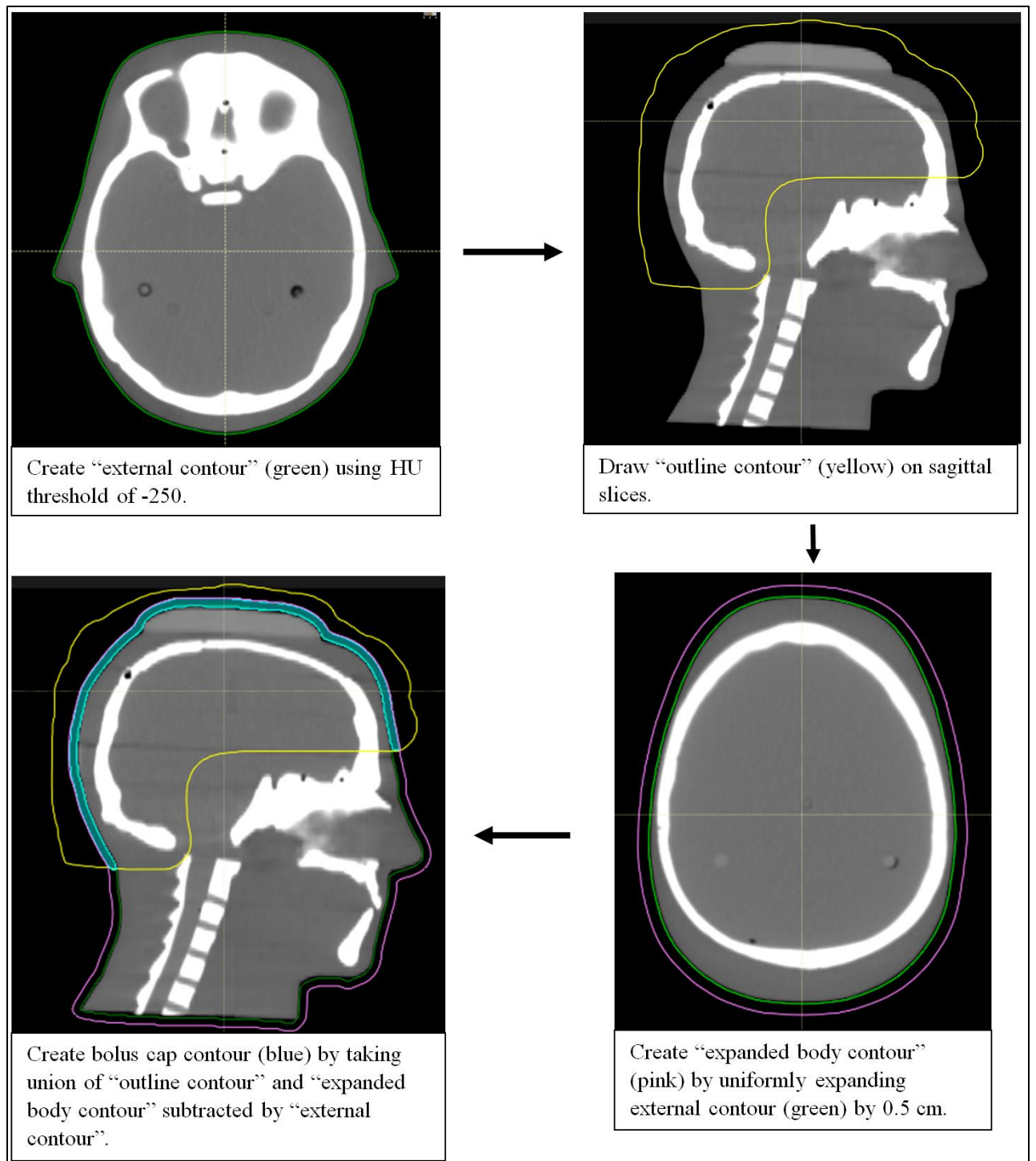


Figure 3-3: Process for creating a bolus cap contour from a CT scan in RayStation.

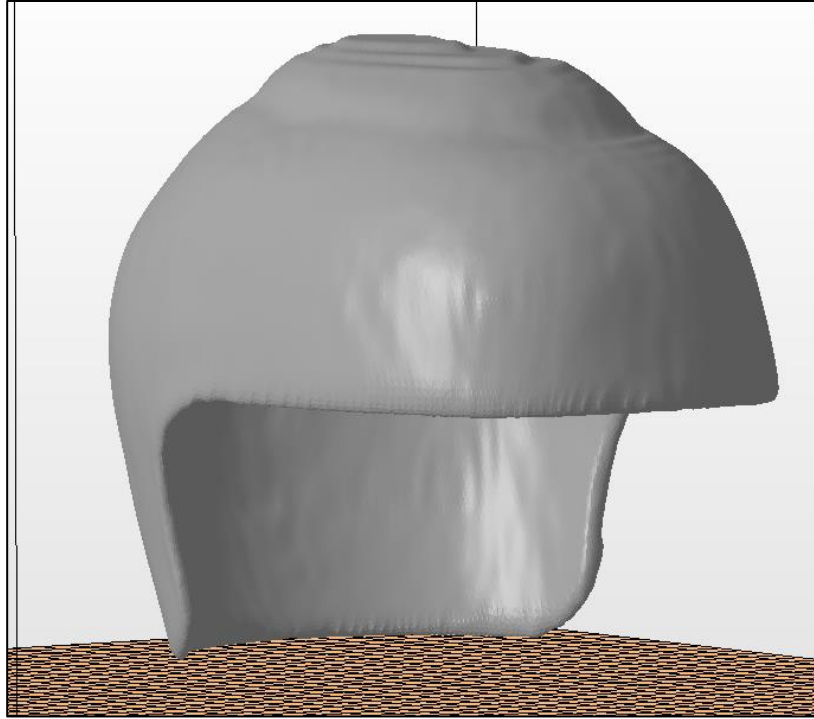


Figure 3-4: Rendering of the 3D-model of the bolus cap after exporting from 3DSlicer

3.2.2 NinjaFlex Bolus Cap Design

Although the NinjaFlex material is flexible, it requires some force to bend it. Because of this, it was decided to develop a two piece bolus cap design for easier fitting onto a patient's head.

In order to create a two piece bolus cap, separate 3D-models needed to be generated for two pieces that would fit together. The bolus cap .STL file was imported into the 3D modeling software Netfabb (Autodesk, San Rafael, CA, USA), which has built-in tools to manipulate 3D-models. A rendering of the first iteration of the two piece design is shown in Figure 3-5, which shows the cap split into a top piece and a back piece. The two pieces join together using dovetail joints, which is a common woodworking technique used to join pieces of wood. The dovetail joint was created by using a Netfabb template 3D-model of a trapezoid with the Boolean operation tool to cut out dovetails in the top piece and complementary cutouts in the bottom

piece, such that the dovetails on the top piece would interlock with the cutouts in the bottom piece and join the two pieces.

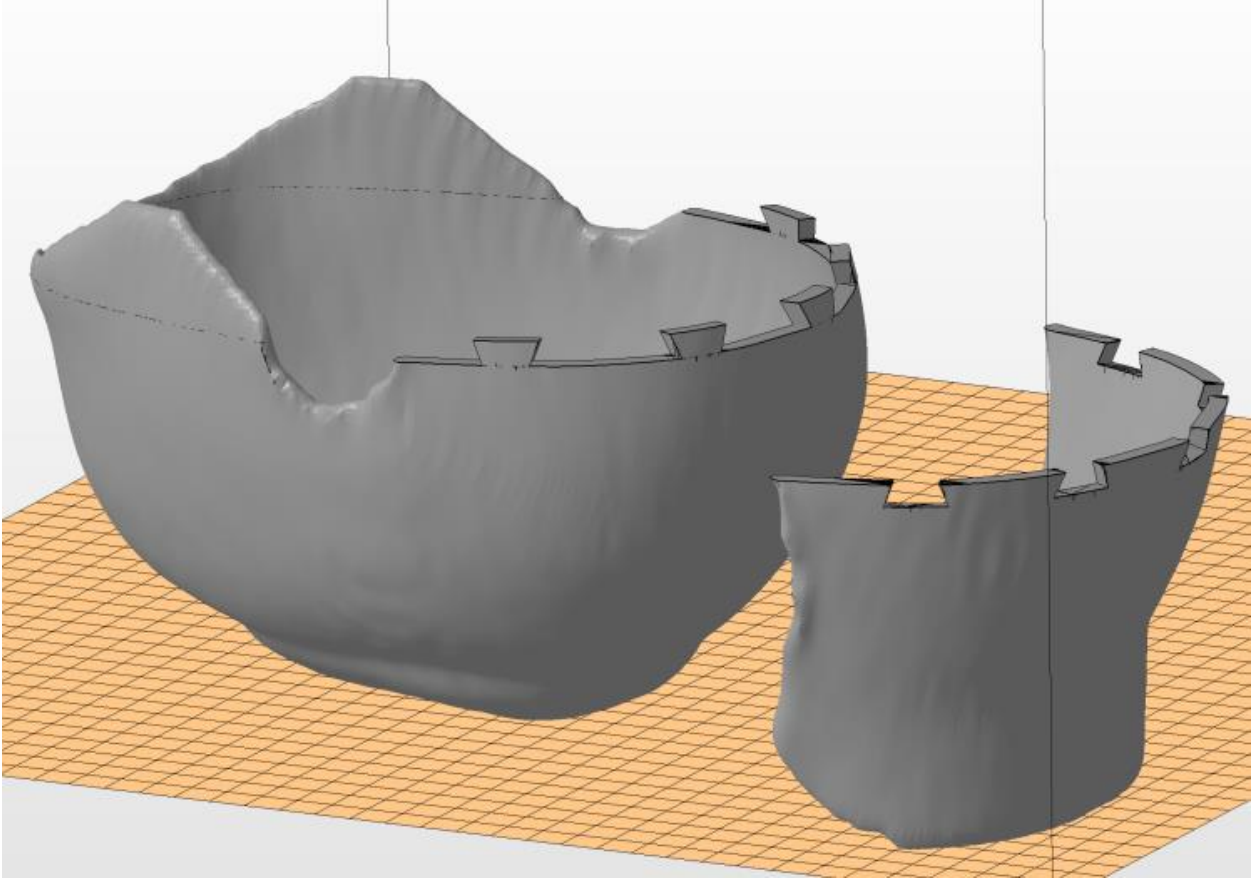


Figure 3-5: Rendering of the first iteration design for the NinjaFlex bolus cap.

To 3D-print this design for testing, the .STL 3D models were converted into gcode files for our 3D printer using Simplify3D software (Simplify3D, Cincinnati, OH, USA). When generating the gcode files, support was generated using the standard settings in Simplify3D. For the back piece gcode file, a raft with a radius of 2 cm was added to be printed to prevent the piece from falling over while printing. The two pieces were printed with NinjaFlex material using a Gigabot 3 3D-printer. Based on NinjaFlex manufacturer recommendations, an extruder temperature of 235 °C and a print surface bed temperature of 40 °C were used.³⁴ The print

orientation of the top piece and the support used is shown in Figure 3-6. Pictures of the two printed bolus cap pieces for the first design are presented in Figure 3-7.

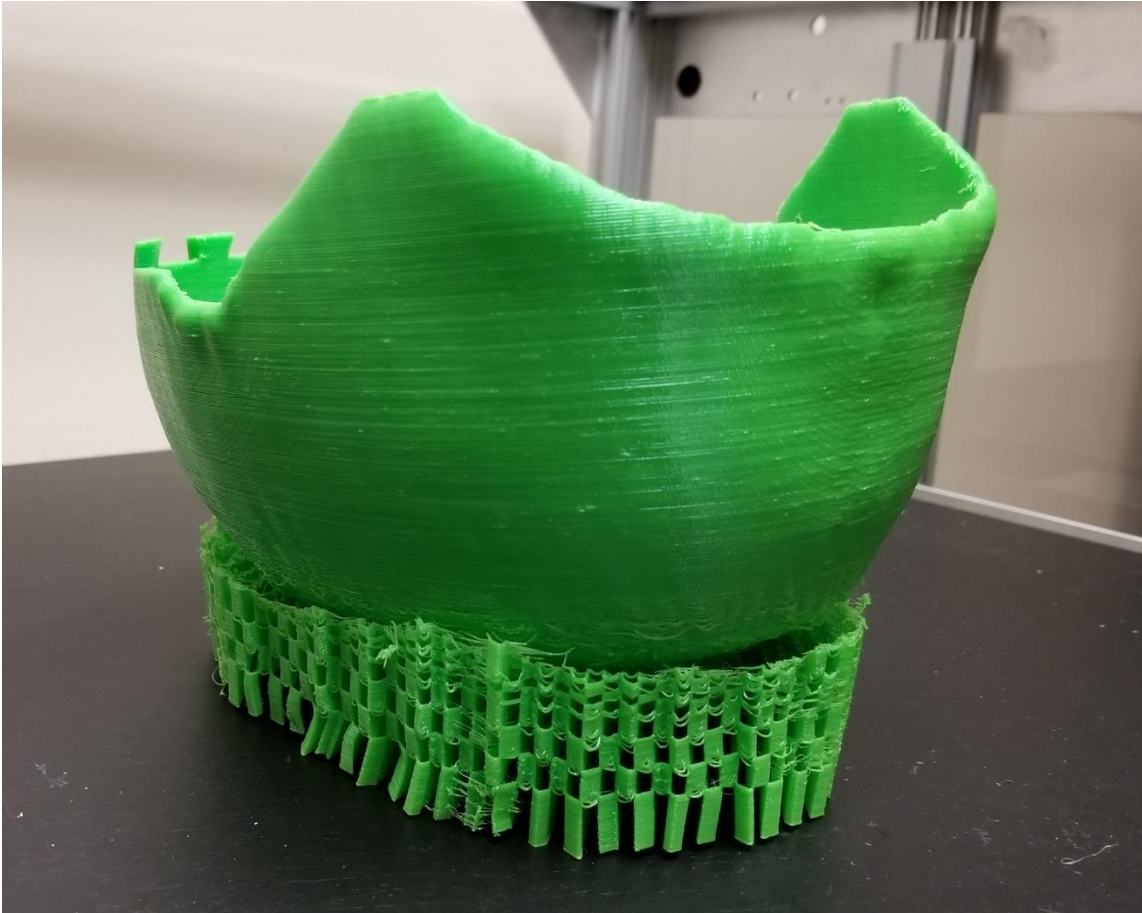


Figure 3-6: Picture of the 3D-printed top piece with support.

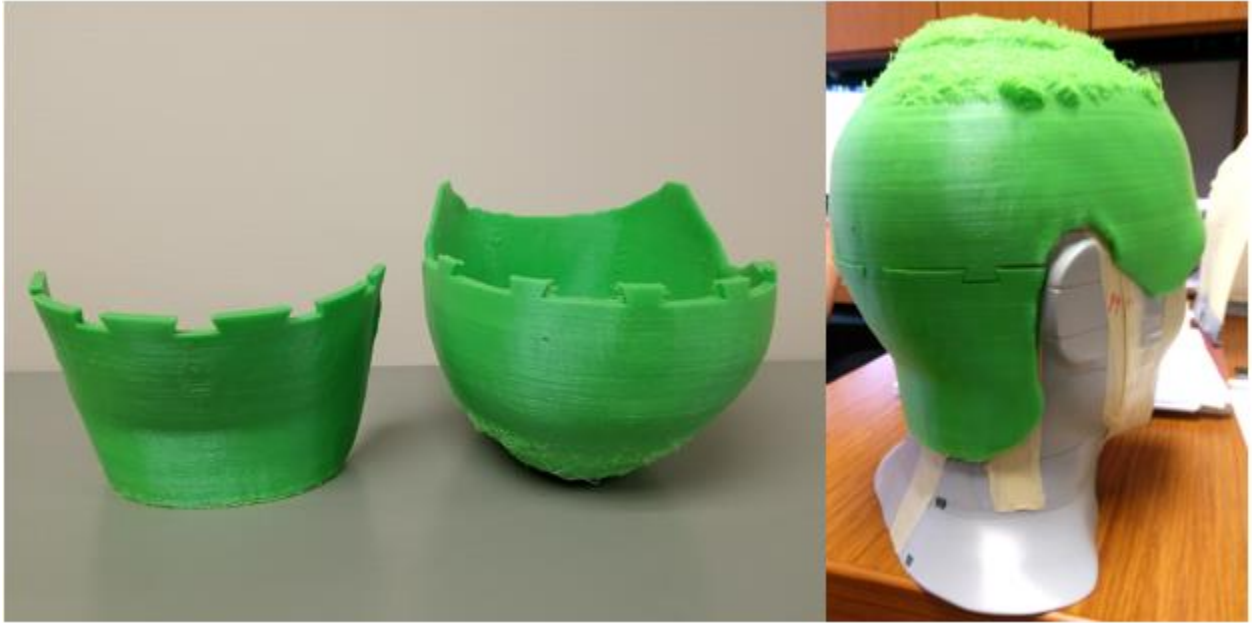


Figure 3-7: Pictures showing the first iteration of NinjaFlex bolus cap design. (left) The bottom and top pieces separate. (right) The two bolus pieces together on the head phantom.

Both pieces of the bolus cap successfully printed and had minimal defects. This suggested that the extruder and bed temperature used are appropriate for printing NinjaFlex bolus caps. The only defects present were the surface stringing and drooping defects that can be seen on the superior of the top piece in Figure 3-7. The defects were most severe where there was no support material and demonstrate why support is needed. Where there was no support material, the molten extruded material simply drooped until it cooled and solidified. The standard support generation settings in Simplify3D generate support for areas where the overhang angle (with respect to the print surface) is 40° or larger. This test print demonstrated that NinjaFlex requires a smaller overhang angle to be used to prevent the stringing and drooping defects. While the first iteration design fit well onto the head phantom, the design did not solve the issue of difficultly fitting the conformal bolus cap onto the head the two piece design sought to remedy. The top piece was very snug, and a lot of force had to be used to press down on the top piece to get it onto the head.

The second iteration of the two piece design sought to make the top piece easier to fit on the head by shifting the joint further superior and at angle. This would allow for the top piece to be “slid” on from the front instead of having to be shoved down from above. A rendering of the second iteration design is presented in Figure 3-8.

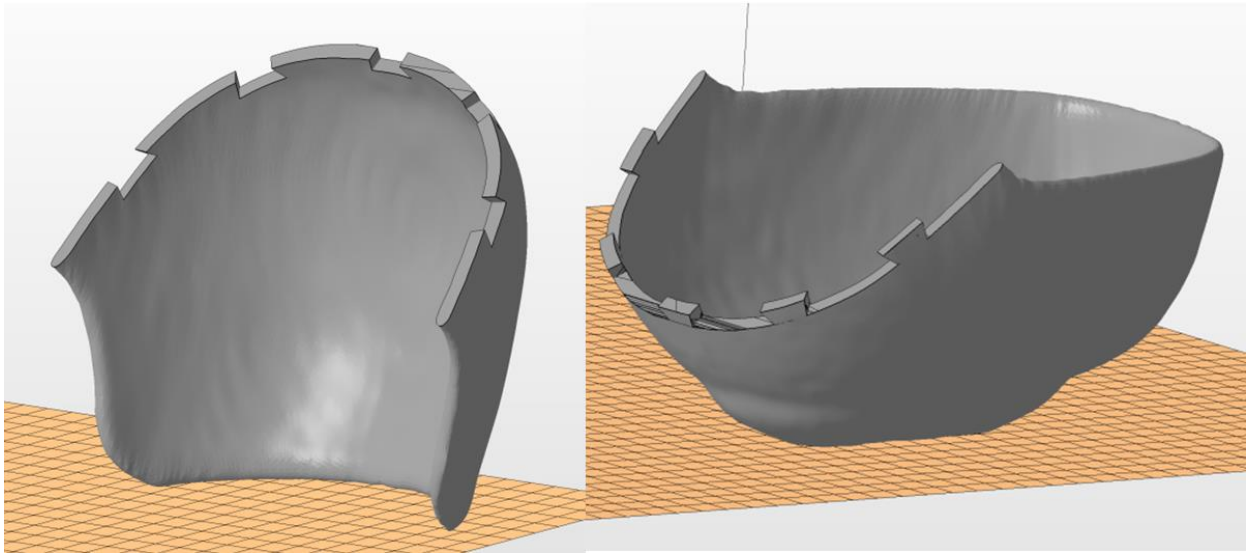


Figure 3-8: Rendering of the second iteration design for the NinjaFlex bolus cap.

When generating the gcode files to print the second iteration design, the support generation settings were changed to create support for areas with overhang angle of 35° or larger. This change sought to increase the support material used to prevent the surface defects that occurred in the prints of the first iteration design.

The two pieces for the second iteration design were printed on the same Gigabot 3 3D-printer with the same extruder temperature of 235°C and print surface bed temperature of 40°C used. Pictures of the two printed bolus cap pieces for the second design are presented in Figure 3-9.

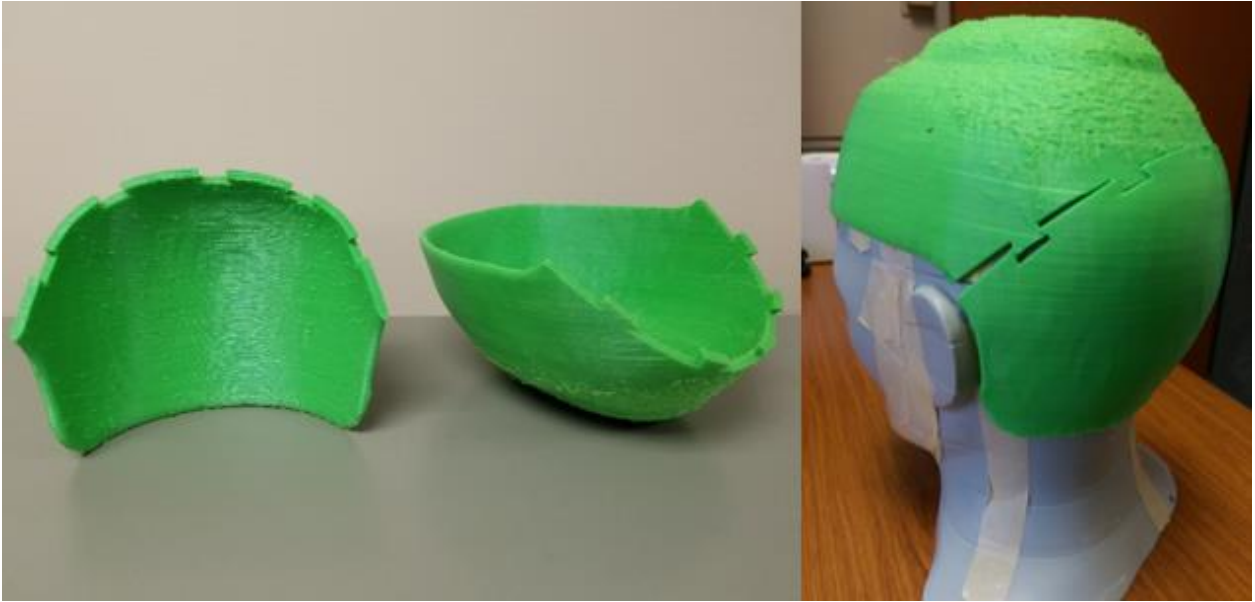


Figure 3-9: Pictures showing the second iteration of NinjaFlex bolus cap design. The picture of the cap on the phantom shows how the pieces did not align and interlock correctly.

Changing the support overhang angle to 35° prevented the stringing and drooping surface defects that occurred on the superior of the top piece in the first iteration design. While the second design had less surface defects, the design introduced more issues than it solved. The angled joint made the two pieces no longer align correctly and it was difficult to interlock the dovetail joints. Additionally, the top piece was still difficult to slide on from the front of the head.

The third iteration, renderings shown in Figure 3-10, significantly altered the design by splitting the cap into two pieces along the sagittal midplane. This design allows for the two halves to be individually placed on the side of the head and then taped together. Additionally, the use of dovetail joints to join the two halves was no longer used. Instead, an overlapping lip was created at the midplane junction of the two halves. A close-up of the overlapping lip joint is shown in Figure 3-10. Because the two halves cannot physically interlock, there is the potential of air gaps forming if the two halves do not meet in the middle flush. The overlapping lip design

allows for there to always be at least 2.5 mm of bolus material to provide some dose buildup in the event of a gap.

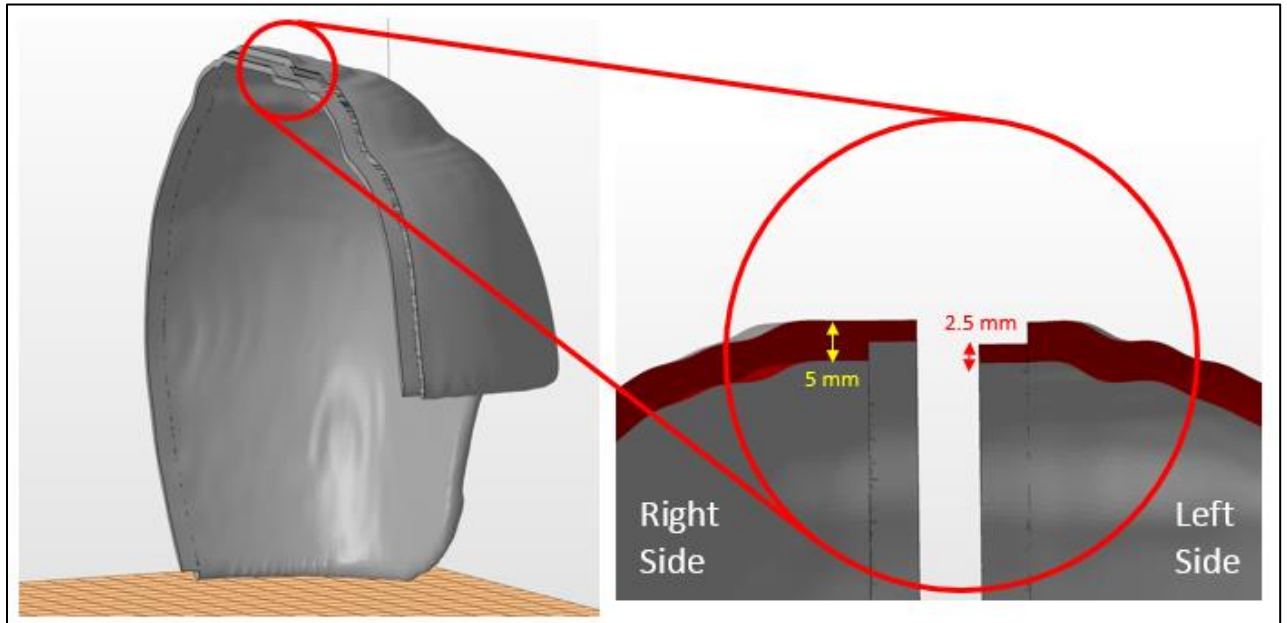


Figure 3-10: Renderings of the 3D-model for the third iteration design. The overlapping lips on each side are 2.5 mm thick so when they join, they are 5 mm thick.

The third iteration design was printed using the same printer and settings used for the second iteration design. Figure 3-11 shows how the halves were oriented to be printed.

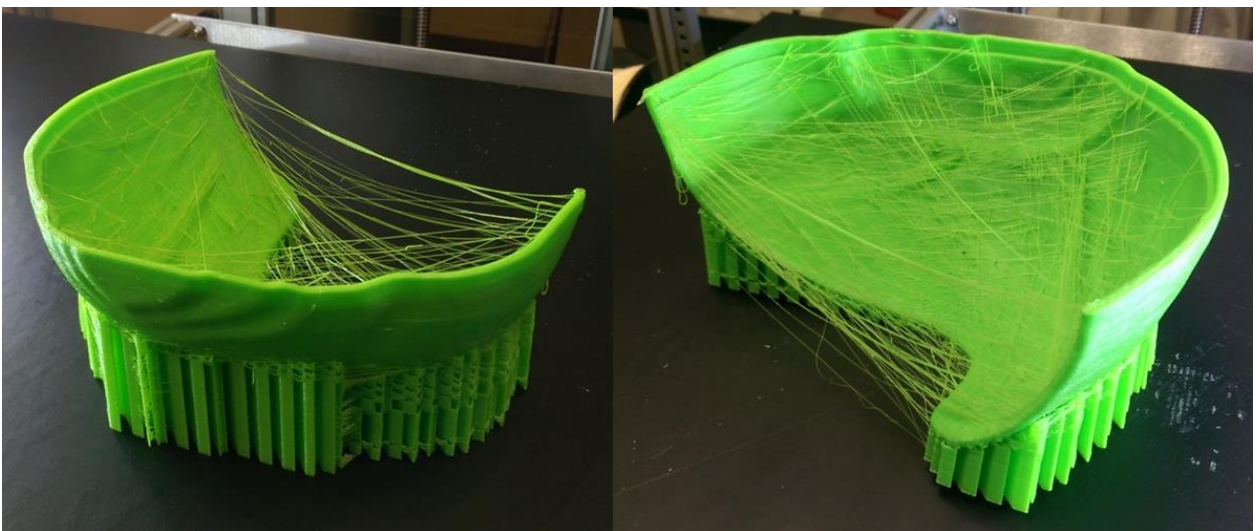


Figure 3-11: The halves were printed on their side with the use of support material.

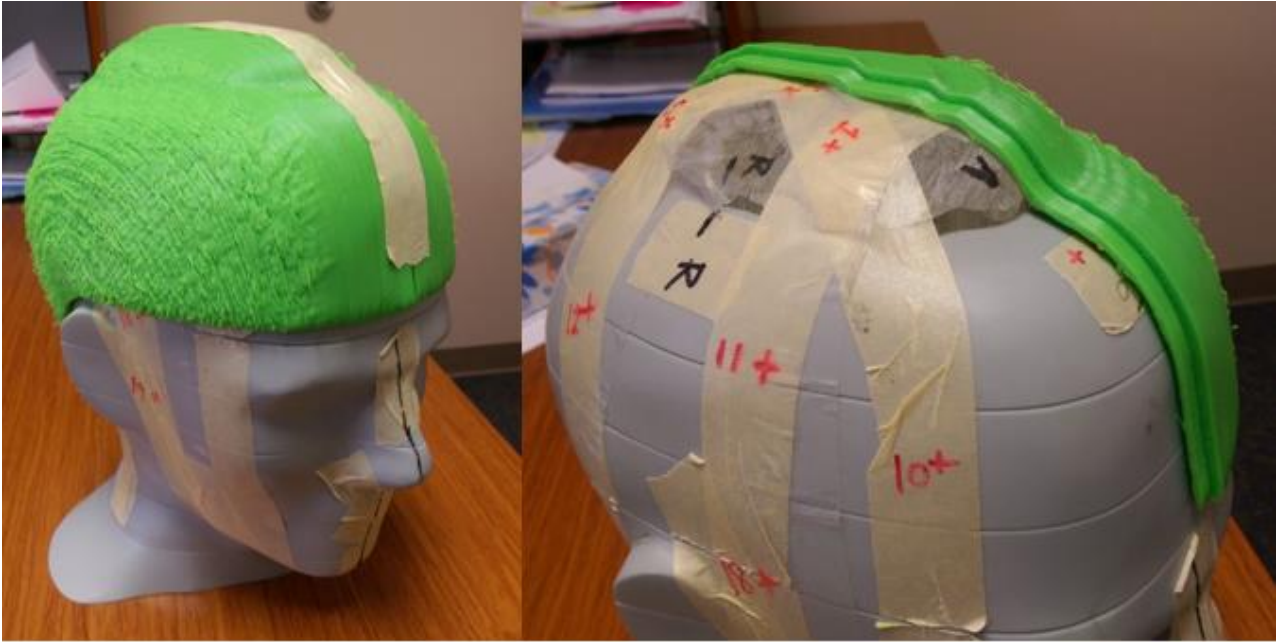


Figure 3-12: Pictures showing the third iteration of the NinjaFlex bolus cap design. (left) the two halves taped together on the phantom head. (right) Left half of the bolus cap on the phantom. Shown clearly is the overlapping lip. The right half has the complementary lip.

The third iteration NinjaFlex design remedied the problems with the previous designs.

The two halves were easy to fit onto the phantom head and tape together. Visually, the two halves fit together well, and unlike in the second iteration, any areas that there were small gaps between the two pieces were covered by the overlapping lips. For these reasons, the third iteration design was chosen as the final design to be used for further testing of the NinjaFlex bolus cap.

3.2.3 Agilus Bolus Cap Design

Development on the bolus cap design for the Agilus material began during the development of the second iteration of the NinjaFlex design. For this reason, the first design tested for the Agilus material used the same 3D-model developed for the NinjaFlex second iteration design shown in Figure 3-8. Additionally, the first Agilus bolus cap was tested with the Agilus-27 material, as the initial material analysis conducted suggested this was the best tissue

equivalent Agilus compound to use. The Agilus bolus cap was printed by a commercial vender using a Stratasys PolyJet J750 3D printer, with 16 μm layer height. The resulting cap is presented in Figure 3-13.



Figure 3-13: Picture of first Agilus-27 bolus cap design. (left) demonstration of the deformability of the Agilus-27 material under its own weight. (right) Agilus-27 bolus cap on phantom head with back piece taped to top piece.

The printed bolus cap fit well on the phantom and was free of defects. However, as shown in Figure 3-13, the Agilus-27 bolus cap ended up being very deformable and could barely maintain its shape under its own weight. Another finding was that although the dovetail joint worked well in the NinjaFlex material, it did not work with the Agilus-27 material. The deformability of the material made it very difficult to align the dovetails with the cutouts, and the material was so deformable that the joints did not stay interlocked and the pieces would naturally fall apart. The only way to connect the two pieces was to tape them together, which defeated the purpose of printing the bolus cap in two pieces and using an interlocking design.

The results of the first Agilus bolus cap design led to several changes being implemented in the second design. First, the material compound was changed from Agilus-27 to Agilus-60. As discussed in Section 2.3.2, Agilus-60 was found to have similar tissue equivalence to Agilus-27, but is slightly more rigid, meaning it shouldn't deform as much as the Agilus-27 bolus cap, while still being soft and flexible. The second change was to print the Agilus bolus cap as one piece. The first Agilus design demonstrated the dovetail joints did not work with the material, and that when the two pieces were taped together the Agilus material was flexible enough to easily fit the cap in one piece onto the phantom's head. Printing the bolus cap in one piece also meant that the original bolus cap 3D-model produced in Section 3.2.1 could be used to print the bolus cap. Figure 3-14 shows the printed Agilus-60 bolus cap.



Figure 3-14: Picture of second Agilus bolus cap design using the Agilus-60 compound. (left) The bolus cap is slightly flexible, but can hold up under its own weight. (right) The bolus cap fit well on the phantom and was easy to get on in one piece.

The Agilus-60 bolus cap design improved on the issues with the first Agilus-27 design. The one piece Agilus-60 cap was rigid enough to maintain its shape, while being flexible and elastic enough to easily fit onto the phantom head in one piece. For these reasons, this design was chosen to be the final design for the Agilus material to further test the bolus cap for use in total scalp irradiation.

3.2.4 CT Simulation

To assess the conformality and suitability of using the 3D-printed bolus caps for total scalp irradiation, CT simulation scans were acquired. CT simulation is the process of setting a patient up in the support and immobilization devices that will be used for treatment and acquiring a CT scan. The CT simulation scan is imported into a treatment planning system and used to virtually localize the treatment fields, contour targets and critical structures, and create and review treatment delivery plans.³⁰ Assessing the conformality of the bolus caps using CT simulation scans allowed for a pragmatic assessment of how the bolus caps might fit on a patient during treatment.

The treatment immobilization setup used for the CT simulation is presented in Figure 3-15, which is based on the standard setup used for total scalp irradiation at MD Anderson Cancer Center. The head phantom was rested on an Orfit regular density head support (Orfit Industries, Wijnegem, Belgium). The locations of the lasers marking the setup isocenter were marked on tape on the head phantom. A three-point thermoplastic immobilization mask was formed to the phantom head with the bolus cap on. The setup isocenter was also marked on the immobilization mask with marker and BBs at the laser cross-hairs. CT simulation scans were acquired with a Philips Brilliance Big Bore scanner. The same immobilization setup was used to acquire scans for both the NinjaFlex and Agilus-60 bolus caps.

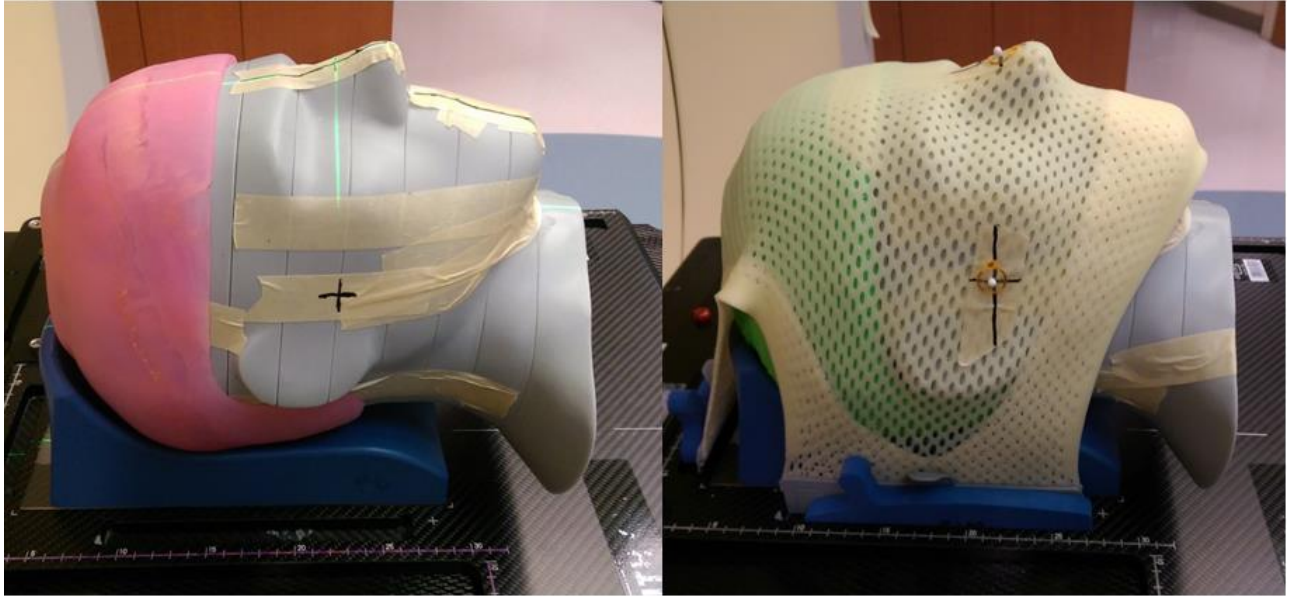


Figure 3-15: Picture of the CT simulation setup, (left) setup shown without the immobilization mask, (right) setup with the immobilization mask in place.

Conformality of the scalp bolus was assessed by measuring the distance of gaps between the bolus cap and the phantom scalp. The CT simulation scans were imported into RayStation, where the ruler tool was used to measure the gap between the bolus and the scalp at four locations on a given slice. The four locations were chosen by centering the cross-hair in the phantom head ($x = 0.03$ cm, $y = -9.12$ cm) and measuring at the anterior (position 1), left (position 2), right (position 3), and posterior (position 4) of the scalp, shown in Figure 3-16. The maximum gap on a given slice was also measured. Measurements were acquired using the lung preset window and level (L: -600, W: 1600), on three different axial slices in the CT study: -62.85 cm, -60 cm, -58.3 cm. This procedure was performed for both the NinjaFlex and Agilus-60 bolus caps.

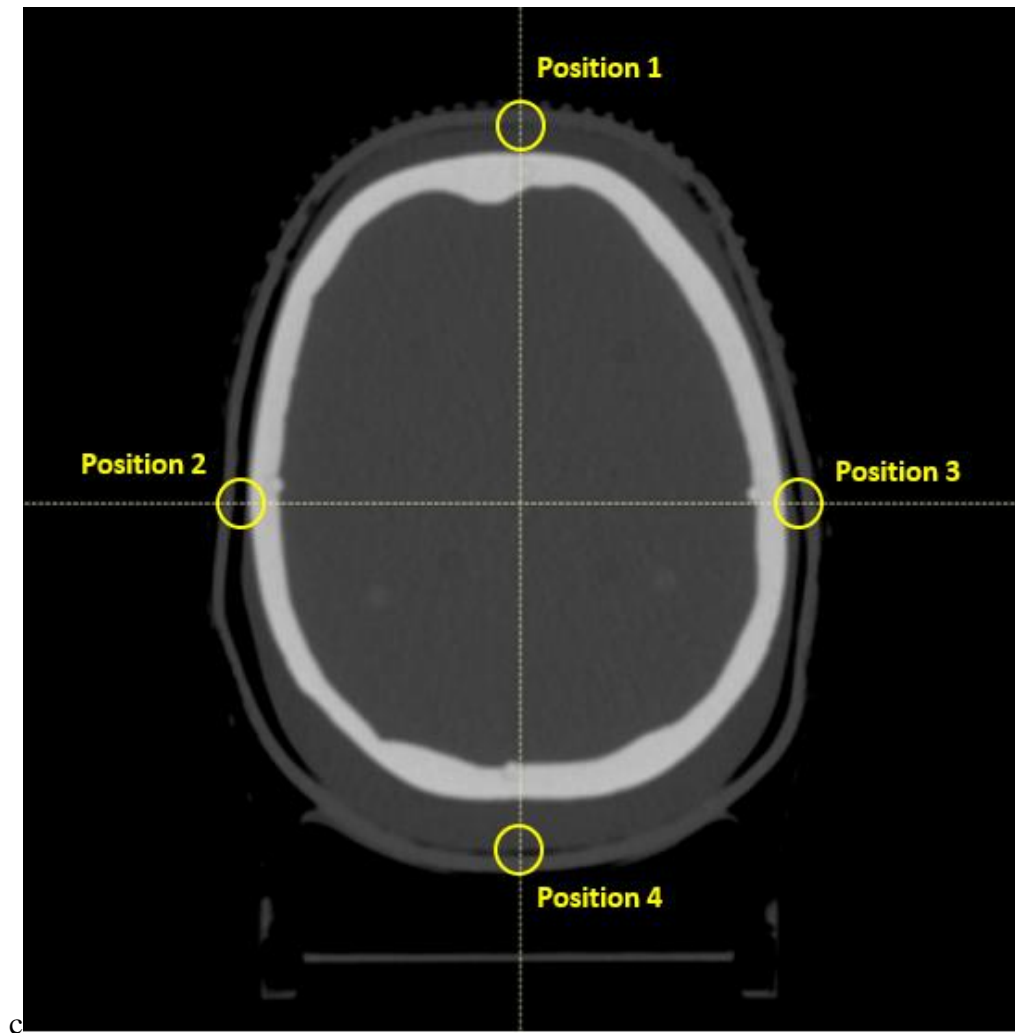


Figure 3-16: Picture showing the locations of the measurement positions for measuring the gap between the bolus and the scalp.

3.3 Results

3.3.1 3D-Printed Bolus Cap Designs

Sections 3.2.2 and 3.2.3 detailed the results of the different bolus cap design iterations and how the final designs for each material were chosen. Table 3-1 presents data on the time to generate the 3D-model, time to 3D-print, and cost for each design iteration tested.

Table 3-1: Fabrication related data for each tested bolus cap design

Design	Modeling Time (min)	Fabrication Time (hours)	Cost
NinjaFlex 1	60	38	\$37
NinjaFlex 2	75	38	\$37
NinjaFlex 3	35	40	\$37
Agilus-60 1	60	40	\$2,000
Agilus-60 2	15	40	\$2,300

Coincidentally, as the designs were iterated the time required to make the bolus cap 3D-model decreased. This was mainly due to making the designs simpler and easier to model. Not only did the simpler designs end up being superior, but simpler designs that take less time to model are also ideal for implementation into a clinical workflow.

In general, the time required to 3D-print the different designs was consistent at approximately 40 hours. All designs required essentially the same amount of material and support to be used meaning the print time did not significantly change.

One of the main differences of the two materials is the cost to print the bolus cap. Because the NinjaFlex bolus cap was printed in-house, the only cost was the cost of the

material. The cost of the Agilus-60 bolus cap printed by the commercial vendor included the material and labor costs.

3.3.2 CT Simulation Measurements

CT slices from the CT simulation of the NinjaFlex bolus cap are presented in Figure 3-17. The corresponding CT slices from the CT simulation of the Agilus-60 bolus cap are presented in Figure 3-18.

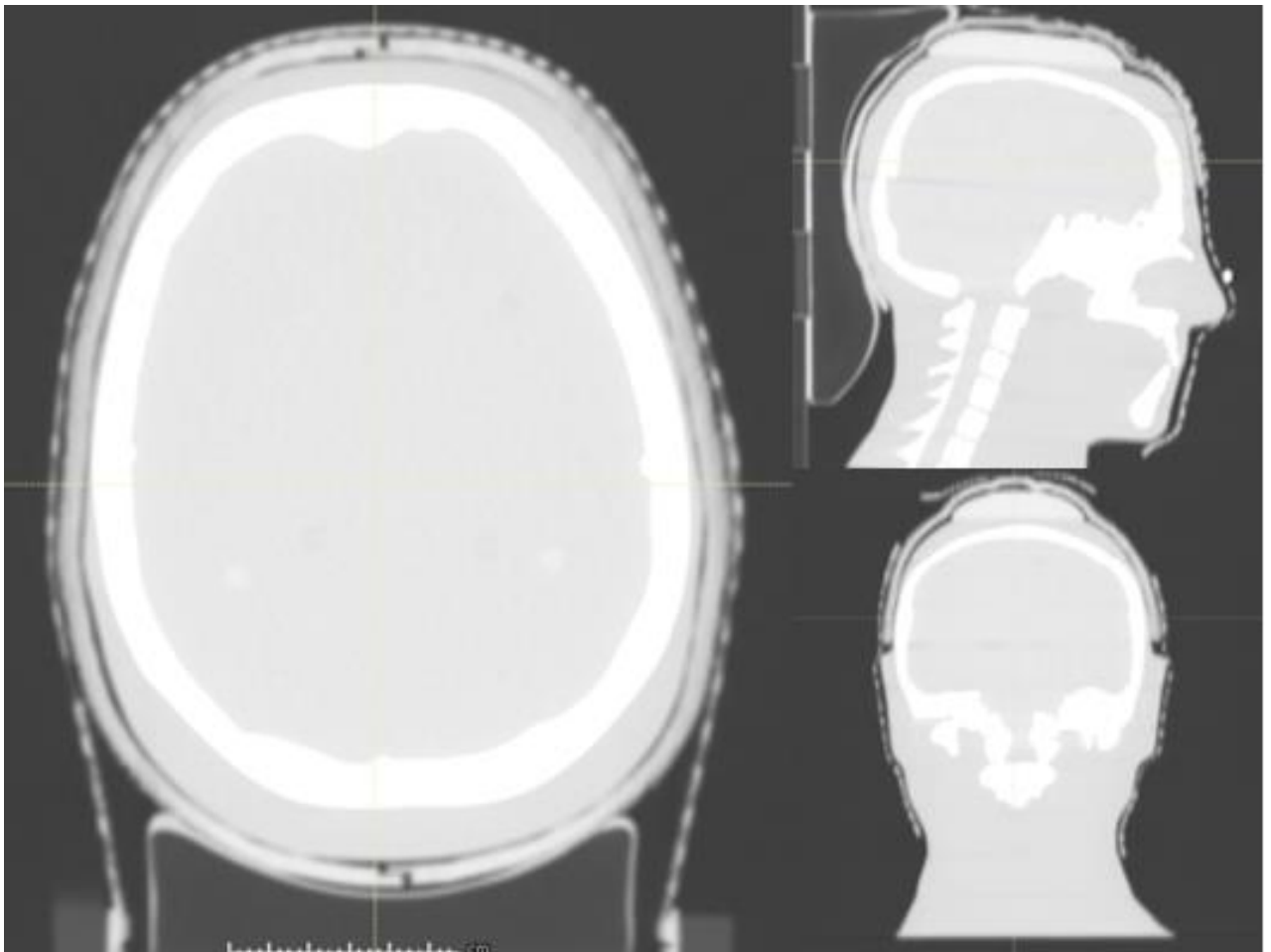


Figure 3-17: CT slices from the NinjaFlex bolus cap CT simulation.

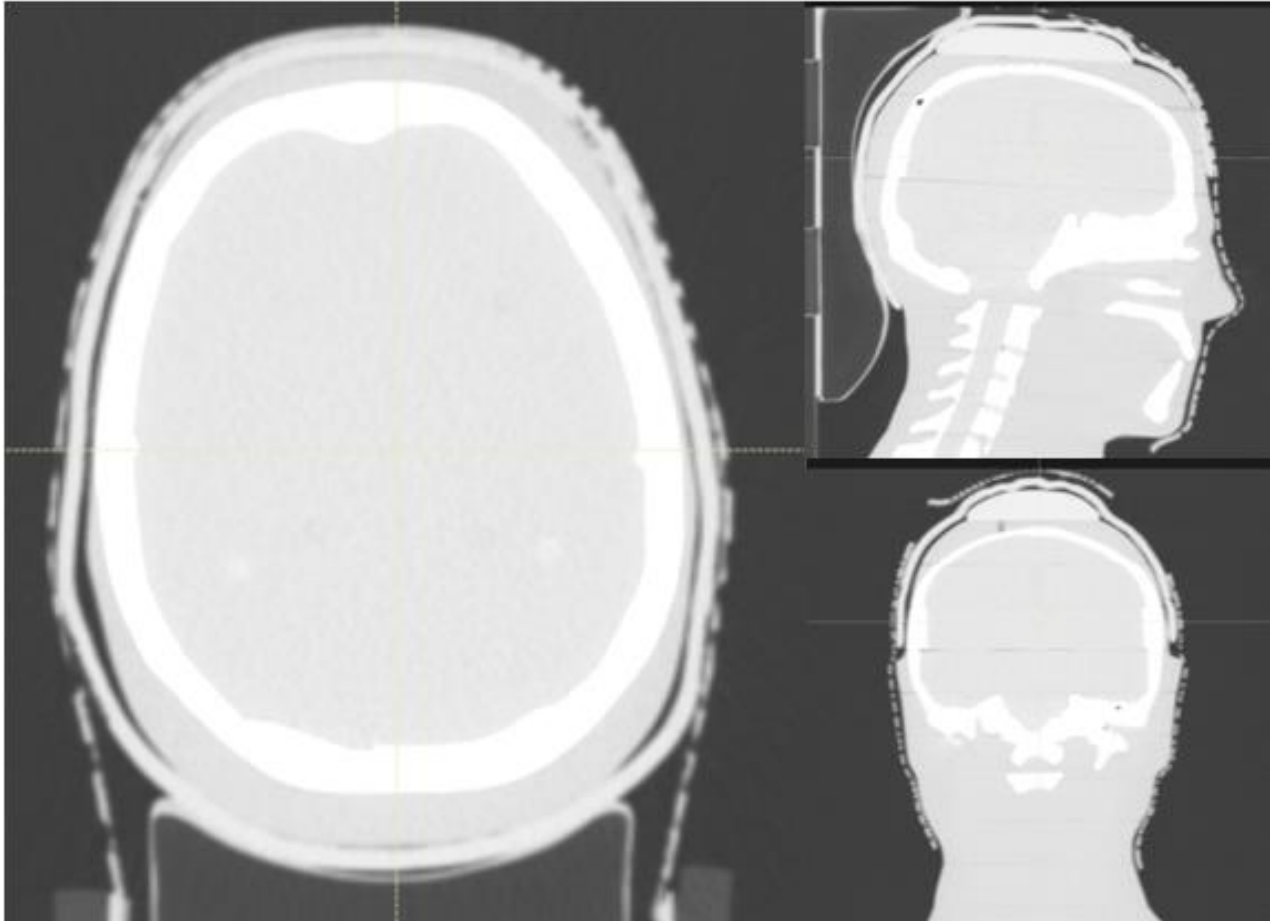


Figure 3-18: CT slices from the Agilus-60 bolus cap CT simulation.

In general, both bolus caps were very conformal to the phantom scalp. For most areas of the scalp, the bolus caps were flush to the scalp. This result confirmed that the method developed in Section 3.2.1 to generate the 3D-model for the phantom-specific bolus cap was accurate. Additionally this confirmed that the actual 3D-printed bolus caps were geometrically accurate to the 3D-model and did not shrink or expand significantly in the approximately month of time in between printing and CT simulation.

The results of the gap measurements are presented in Table 3-2.

Table 3-2: Gap measurements for both tested bolus caps

		Gap Distance (mm)	
Measurement Location		NinjaFlex Bolus	Agilus-60 Bolus
Slice 1 (-62.85 cm)	Pos. 1	0.9	0.0
	Pos. 2	0.9	1.9
	Pos. 3	1.4	1.0
	Pos. 4	1.4	1.0
	Max	2.0	4.0
Slice 2 (-60 cm)	Pos. 1	1.6	0.0
	Pos. 2	1.9	2.4
	Pos. 3	1.3	1.9
	Pos. 4	1.3	1.4
	Max	1.9	3.9
Slice 3 (-58.3 cm)	Pos. 1	2.8	2.4
	Pos. 2	2.4	3.8
	Pos. 3	2.2	1.9
	Pos. 4	1.8	1.9
	Max	2.5	3.8
Average		1.8	2.1

The average measured air gap was 1.8 mm for the NinjaFlex cap and 2.1 mm for the Agilus-60 cap. The increased rigidity of the NinjaFlex material results in the NinjaFlex bolus cap having slightly better average conformality than the Agilus bolus gap, but not significantly. In addition, for both bolus caps there was no measureable gap between the bolus and the scalp for most of the scalp treatment area. These results were in good agreement with a previous study in the literature, which measured air gaps for their bolus technique and found the average to be

1.0 mm.¹⁴ Where the technique developed in this study offers an advantage is in the maximum air gap. The maximum measured air gap over the entire scalp was 2.8 mm for the NinjaFlex cap and 4.0 mm for the Agilus-60 bolus cap. These gaps were much smaller than the maximum gap measured in the Lin *et al.* study, which measured a maximum air gap of 15.0 mm.

The results of the CT simulation study demonstrated both bolus caps were highly conformal to the phantom scalp, which was one of the primary issues with existing techniques that this project sought to solve.

4 Specific Aim 4: Demonstrate 3D-Printed Bolus Caps can Reproducibly Generate a Homogenous Dose to the Scalp

4.1 Introduction

The purpose of a bolus cap is to provide build-up to deliver adequate dose to the surface of the scalp. The previous chapters have been dedicated to finding suitable materials and designs for the 3D-printed bolus cap. Testing conducted in this chapter sought to demonstrate the 3D-printed bolus caps could reproducibly generate a homogenous dose to the scalp surface that is required for the clinical efficacy of total scalp irradiation.

Treatment planning was the first step in this process. The treatment plans would allow for an assessment of the dose distributions that can be achieved with the 3D-printed bolus caps and verify they can generate radiation treatment plans that meet clinical requirements. Treatment plans were also required to deliver a mock treatment to the head phantom to perform dosimetric verification.

Dosimetric verification measurements were the second step in the process. The treatment planning system is used to generate a radiation treatment plan, calculate dose to target and critical structures, and use this information to optimize the treatment plan. Professional guidelines state the dose calculated by the treatment planning system for a complex IMRT/VMAT treatment should be accurate to within 5% of the actual delivered dose.³⁵ Because the bolus caps were made of materials new to use in radiation oncology, it was important to verify the treatment planning system could accurately calculate dose in the 3D-printed bolus caps. Additionally, dose measurements on the surface of the scalp would allow for verification that 5 mm of the 3D-printed bolus material is sufficient to generate full dose to the scalp surface. Dosimetric verification was performed using thermoluminescent dosimeters (TLD).

Thermoluminescent dosimeters are a common detector used to measure dose in radiation oncology. TLD are classified as an integrating- passive type detector and are made of a solid state crystalline material, such as LiF.³⁶ These detectors work by leveraging the thermally-stimulated luminescence process that can occur due to the electronic band structure of electrons present in solid state materials, represented in Figure 4-1.

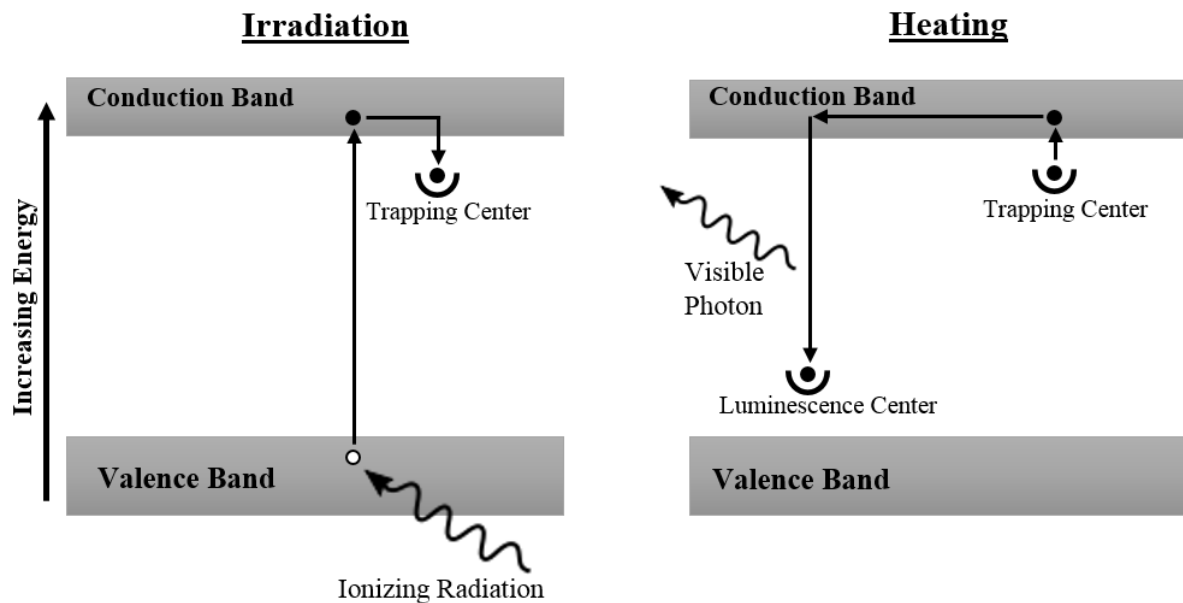


Figure 4-1: Diagram of the thermoluminescent process in TLD

Electrons in the ground state occupy the valence band of the material, and a higher energy conduction band exists that excited electrons can enter into. TLDs are doped with impurities, which create energy levels in between the conduction and valence band. Impurity materials create two main classes of energy levels in the band gap: trapping centers (created by Mg^{2+} ions) and luminescent centers (created by Ti^{4+} ions). Trapping centers are energy levels located closer to the conduction band that serve to trap electrons after they have been excited into the conduction band due to incident radiation. Luminescent centers are energy levels located closer to the valence band and have an energy difference with the conduction band such that energy

released by electrons getting trapped into the luminescent center results in a photon in the visual spectrum. When ionizing radiation is incident on the TLD, ionization causes an electron to be promoted into the conduction band and subsequently be captured into a trapping center. After irradiation, heating the material causes electrons to be thermally excited out of the trapping centers and back into the conduction band, where they can then fall into the luminescence centers and release visible light. The amount of light released is proportional to the total dose deposited in the TLD by radiation. This is the thermoluminescent process that allows TLD to be used to measure dose delivered by radiation.

The process to determine the dose delivered to a TLD begins by heating the material to a set temperature and using a photo multiplier tube to collect the thermoluminescent photons. TLD are typically heated at a linear rate of 2 °C/s up to 400 °C.³⁶ TLD are not absolute dosimeters due to the low efficiency of light production, and thus conversion factors must be used to convert the measured thermoluminescent signal into dose. Conversion factors are generated by irradiating standards TLD in a highly characterized radiation field and delivering a known dose. The known dose delivered to the standards is then used to generate a calibration from the light read out to dose, which can be used to convert measured thermoluminescence to dose for TLD irradiated to an unknown dose.

The most common commercial TLD used in radiation oncology is TLD-100, which is a LiF based material. This specific detector is chosen for measurements in radiation therapy for several reasons. The first is the effective atomic number of the material is 8.2,³⁶ which is very similar to the effective atomic number of tissue of 7.22,³⁷ which means photons will interact the same in the detector as in tissue, which is required for accurate dosimetry. Another reason is TLD-100 exhibits linearity in response for doses ranging from 1 to 10 Gy, which encompasses

the typical per fraction doses used in radiation therapy. TLD also exhibit a relatively flat energy response over most of the photon energies used in radiation therapy.³⁰ Additionally, the TLD signal decays very little meaning a detector can be read out immediately, or up to a couple months later. Finally, the TLD can be used in powdered form, which allows it to be fashioned into small capsules or flat-packages to be used in many special *in vivo* dose measurement applications, such as flush against the scalp under a bolus cap during total scalp irradiation.

In addition to verifying the bolus caps can deliver a homogenous dose to the scalp, verifying the reproducibility of the treatment setup was studied. VMAT based total scalp irradiation is generally delivered in 2 Gy fractions, with typical prescription doses ranging from 40 Gy to 70 Gy.³ This means that the patient has to be setup in the bolus and immobilization up to 35 times to deliver all fractions. Setup reproducibility is important to assure the treatment is delivered as planned. Limited reproducibility of the bolus technique currently used at MD Anderson was one of the main motivations for researching the use of 3D-printed bolus caps. Demonstrating the 3D-printed bolus caps are able to be reproducibly setup would further bolster the case that 3D-printed bolus caps are an improvement over current techniques.

4.2 Methods and Materials

4.2.1 Treatment Planning

VMAT treatment plans were created following current standard of care guidelines for the total scalp irradiation technique used at MD Anderson Cancer Center. The CT simulation scans acquired for both bolus caps in Section 3.2.4 were imported into the RayStation treatment planning system. The following procedure was used to create a VMAT treatment plan for each CT simulation.

The first step in the planning process was to contour the target and critical structures. The brain and brainstem were contoured using the head and neck AutoStructure script, which is an atlas based auto contouring program. The contours generated by the script were checked and edited if necessary. Two contracted brain contours were created, one using a uniform 1 cm contraction of the brain contour, and a second using a uniform 2 cm contraction of the brain contour. The contracted brain contours would be used in plan optimization to limit dose to normal tissue in the brain. A clinical target volume (CTV) contour that encompassed the scalp under the bolus cap to be treated was contoured by hand. To ensure full coverage to the CTV, a planning target volume (PTV) was created by uniform expansion of the CTV by 1 mm. The dose calculation grid was defined with an external contour of the patient and all treatment devices, including the head rest and immobilization mask, created using an HU threshold of -350. Finally, a contour of the bolus cap was contoured by hand. The density of the bolus cap contour was overridden to 1.05 g/cm^3 for the NinjaFlex plan and 1.14 g/cm^3 for the Agilus plan.

The second step in the planning process was to define the beams and fields that would be used to deliver radiation. Two arcs were created centered around the treatment isocenter, shown in Figure 4-2. This isocenter was selected to allow for adequate coverage of the entire CTV in one field. The first arc was set to start at 182° and end at 178° , and the second arc started at 179° and ended at 183° . Because RayStation calculates control points every 2 degrees in an arc, the offset of the starting and ending angles of the two arcs allowed for a control point to be defined at every angle between the two arcs.

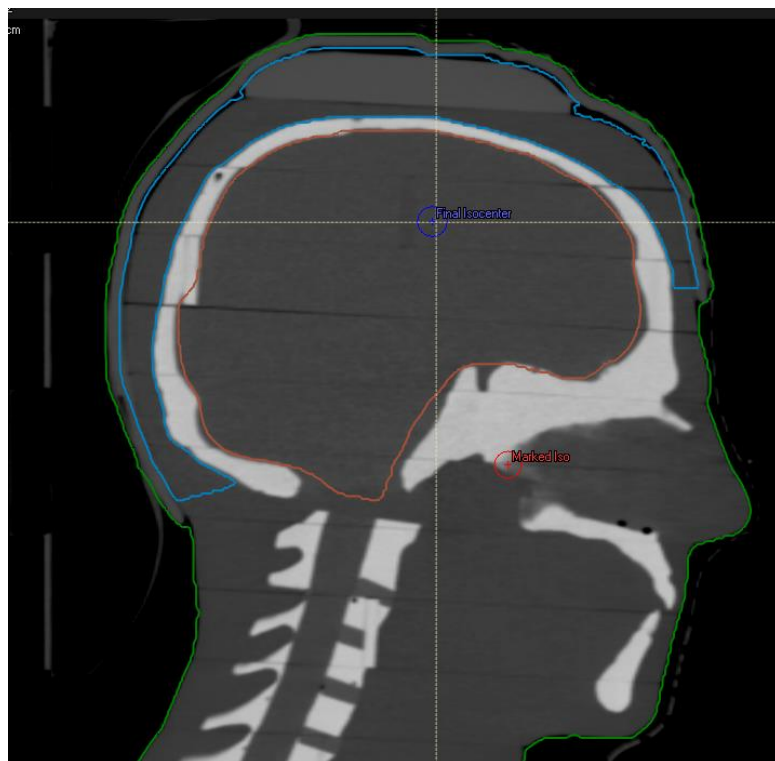


Figure 4-2: Picture showing the marked isocenter (red) and the defined treatment isocenter (blue).

The collimator angle for the first arc was set to 30° , and the second arc set to 90° . The collimator angles oriented the MLC to be perpendicular between the arcs, which allows the planning system to achieve better target coverage and minimize dose to normal tissue. Shown in Figure 4-3 are the collimator apertures for each arc. The field sizes were set to only be open enough to treat the scalp region. If the collimator is opened to cover the entire head, the TPS will attempt to block dose to the brain only using the MLC. Studies have shown that leaf end transmission between two opposite MLC leaves can transmit 5 – 20% of the primary beam, which would greatly increase the dose delivered to the brain.³⁸ For this reason, the standard technique used at MD Anderson uses the collimators to block the brain instead of the MLC to minimize dose to the brain.

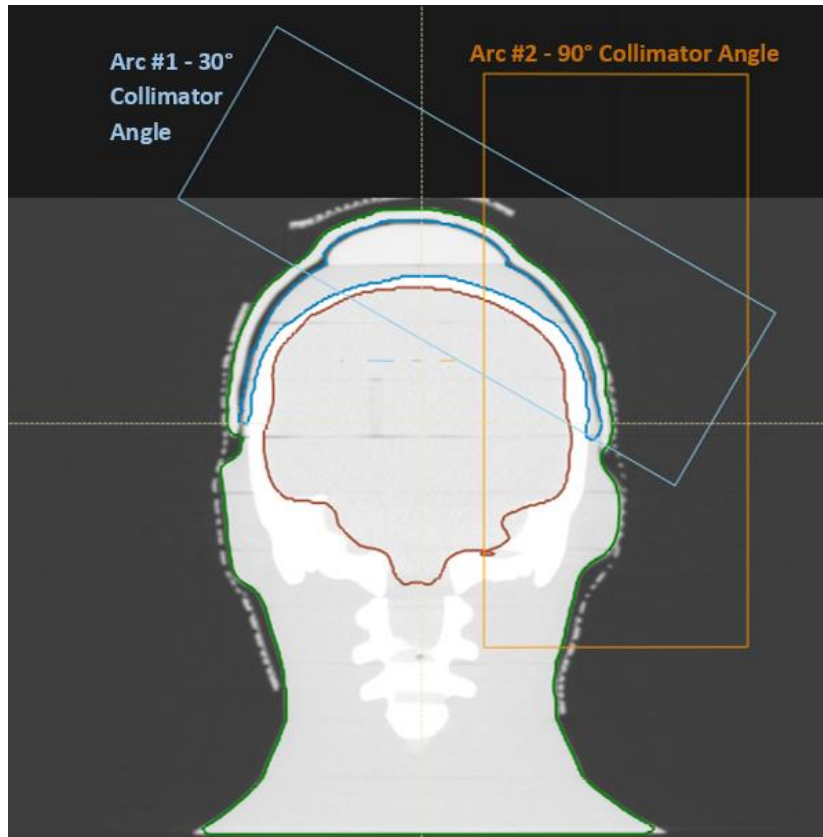


Figure 4-3: Picture of the collimator field sizes and angles used for both arcs. Also shown are the contours for the brain (brown), CTV (blue), and external contour (green).

After the contours and beams had been defined, the VMAT planning optimization process was started. The RayStation Multi-Criteria Optimization (MCO) tool was used to start this process. The MCO tool allows the planner to enter planning objectives and constraints, and the software generates a set of Pareto optimal plans based on the given parameters.³⁹ The set of Pareto optimal plans all satisfy the given constraints while offering many solutions for meeting individual objectives while trading off other objectives. The MCO tool is useful for generating initial beam parameters to be further optimized manually. The constraints and objectives that were used in the MCO tool are presented in Table 4-1.

Table 4-1: MCO planning objectives and constraints

ROI	Value	Objective or Constraint
PTV	Min DVH 6000 cGy to 99% volume	Constraint
PTV	Max DVH 6300 cGy to 5% volume	Constraint
PTV	Uniform Dose 6000 cGy	Objective
PTV	Min Dose 6000 cGy	Objective
Brain	Max EUD 0 cGy	Objective
Brain – 1 cm	Max EUD 0 cGy	Objective
Brain – 2 cm	Max EUD 0 cGy	Objective

The beam parameters generated by the MCO tool were further iterated and optimized manually to achieve a clinically optimal plan. The objectives and corresponding weights used for manual optimization are presented in Table 4-2. Plans were evaluated by scaling the dose to the prescription of 6000 cGy to dose at 97% volume in the scalp PTV. Approximately 50-100 iterations were performed to achieve clinically acceptable plans.

Table 4-2: Objectives used to manually optimize VMAT treatment plans

ROI	Function	Objective Weighting
-	Mimic Pareto Plan	30
PTV	Uniform Dose 6000 cGy	50
PTV	Max DVH 6050 cGy to 30% volume	20
Avoidance	Max Dose 720 cGy	1
Brain	Max Dose 5800 cGy	20
Brain – 2 cm	Max Dose 550 cGy	1

The dose volume histograms (DVH) for the final treatment plans for the NinjaFlex and Agilus bolus were compared. Additionally, the D1 (dose to 1% of volume) for the brain and D99 for the scalp CTV were compared against planning guidelines.

4.2.2 Dosimetric Validation

Dosimetric validation measurements were performed to assure the bolus cap generates adequate build up to deliver full dose to the scalp surface, and that the doses are in agreement with those calculated by the treatment plan generated for each bolus cap.

The detectors used to measure the dose delivered to the scalp surface were TLD. TLD-100 powder was packaged into small plastic sleeves called flat-packs. Shown in Figure 4-4 are flat-pack TLD taped to the phantom head demonstrating how the flat-pack TLD are able to be flush against the scalp.

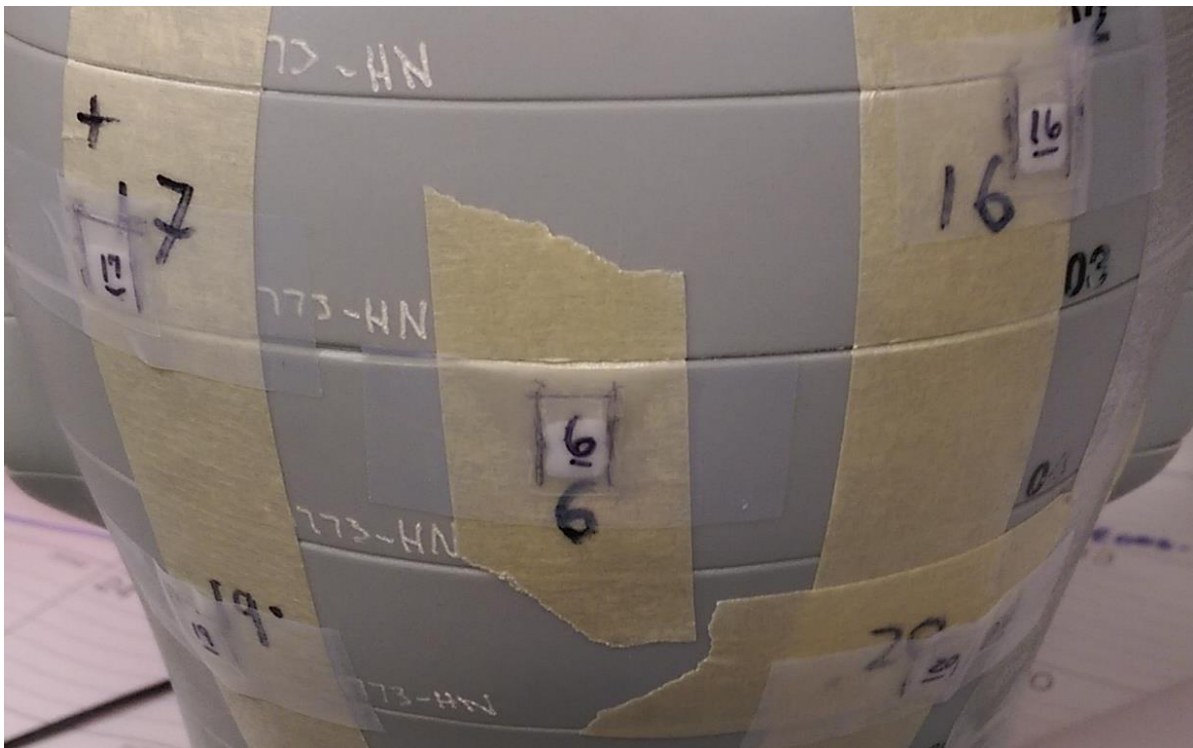


Figure 4-4: Picture of flat-pack TLD taped to the phantom scalp surface.

Twenty locations in the treatment area under the bolus cap were marked on the phantom scalp. Shown in Figure 4-5 are the locations marked with BBs. A CT scan was acquired of the phantom with the BBs, which was subsequently imported into RayStation. The BB scan was registered and fused with the CT simulation scans used for treatment planning, and the BBs were used to contour the location of the TLDs on the planning CT. The TLD contours were created using a brush radius of 0.25 cm, and extended on three slices where the BB could be seen. The average TPS calculated dose at all twenty TLD locations was recorded.

For the treatment delivery, twenty flat-pack TLD were taped to the marked locations on the phantom scalp. The bolus cap was fitted on the phantom and the phantom was placed in the planned treatment setup on the treatment couch of a Varian 21iX linear accelerator. The couch shifts required to move from the marked isocenter to the treatment isocenter were applied. Lateral and AP kV images were obtained with the onboard kV imager to verify the position of the phantom against reference digitally reconstructed radiographs produced by the TPS. One fraction of the planned treatment was delivered. This procedure was performed for both the NinjaFlex and Agilus bolus caps.

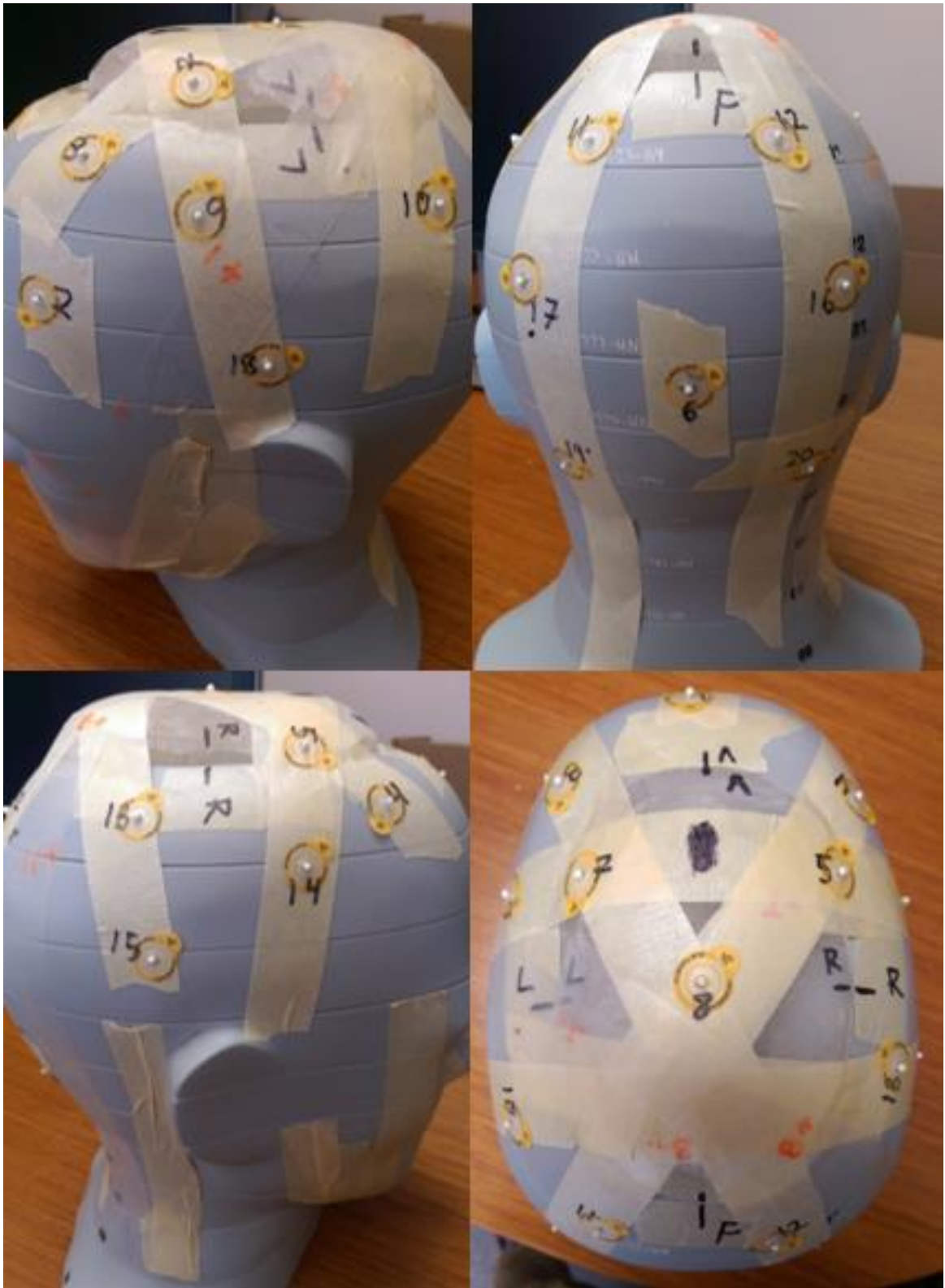


Figure 4-5: Pictures of the TLD locations on the phantom scalp marked with BBs

The TLD were read by Imaging and Radiation Oncology Core (IROC) Houston using their published technique.⁴⁰ The dose delivered to the TLD (D) was calculated using Equation 3:

Equation 3

$$D = TSK_LK_FK_E$$

The variables are as follows. T is the light reading from the TLD per unit mass. S is the system calibration factor that converts the light reading into dose based on the conversion factor generated from standards. Two standards TLD were irradiated to 283.5 cGy and read to generate the system calibration factor. K_L is the linearity correction, which corrects for the dose response of TLD. The linearity correction factor is calculated for each TLD based on a linear equation. K_F is the fading correction factor. The TLD were read 27 days after irradiation and the decay of the signal was corrected for with the fading correction. K_E is the energy correction factor, which IROC has defined for their system for 6 MV photons. The correction factors used to calculate dose with Equation 3 are presented in Table 4-3.

Table 4-3: Correction factors used to convert TLD reading to dose

Correction Factor	Value
S	0.078656
K_L	$-0.000341915(T * S * K_F * K_E) + 1.102573$
K_F	1.019939
K_E	1.03

4.2.3 Reproducibility Study

To assess reproducibility of the bolus placement on the phantom scalp, two radiation therapists independently setup the phantom with the Agilus bolus cap into the treatment setup.

CT scans of each therapist's setup were acquired. The CT scans were imported into RayStation, where they were registered with the planning CT using the phantom's bony anatomy. The procedure outlined in Section 3.2.4 was used to measure the gaps between the bolus and the scalp for both scans. Measured gaps were compared to those measured in the original CT simulation used for treatment planning.

4.3 Results

4.3.1 Treatment Planning

The isodose distributions for the NinjaFlex and Agilus bolus cap plans are presented in Figure 4-6 and Figure 4-7, respectively.

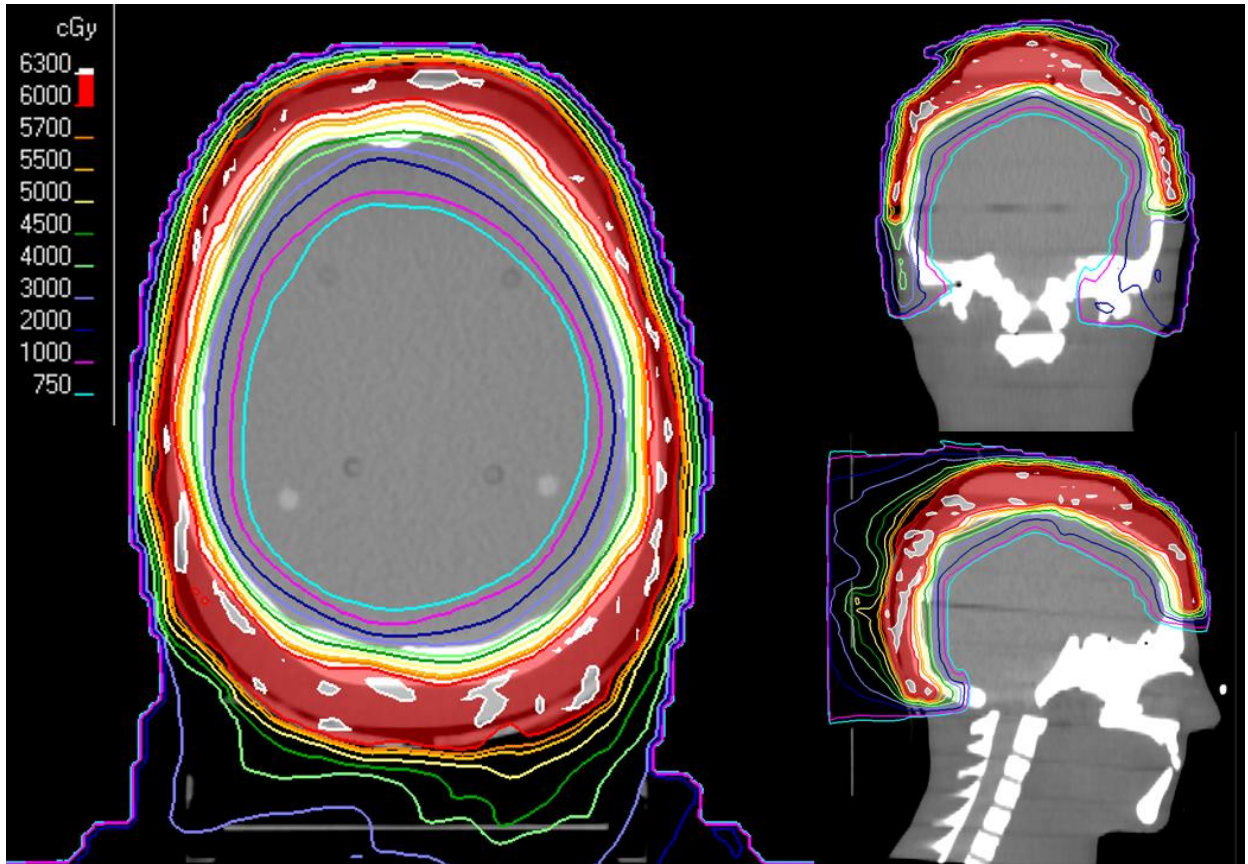


Figure 4-6: Isodose distributions for NinjaFlex bolus cap plan.

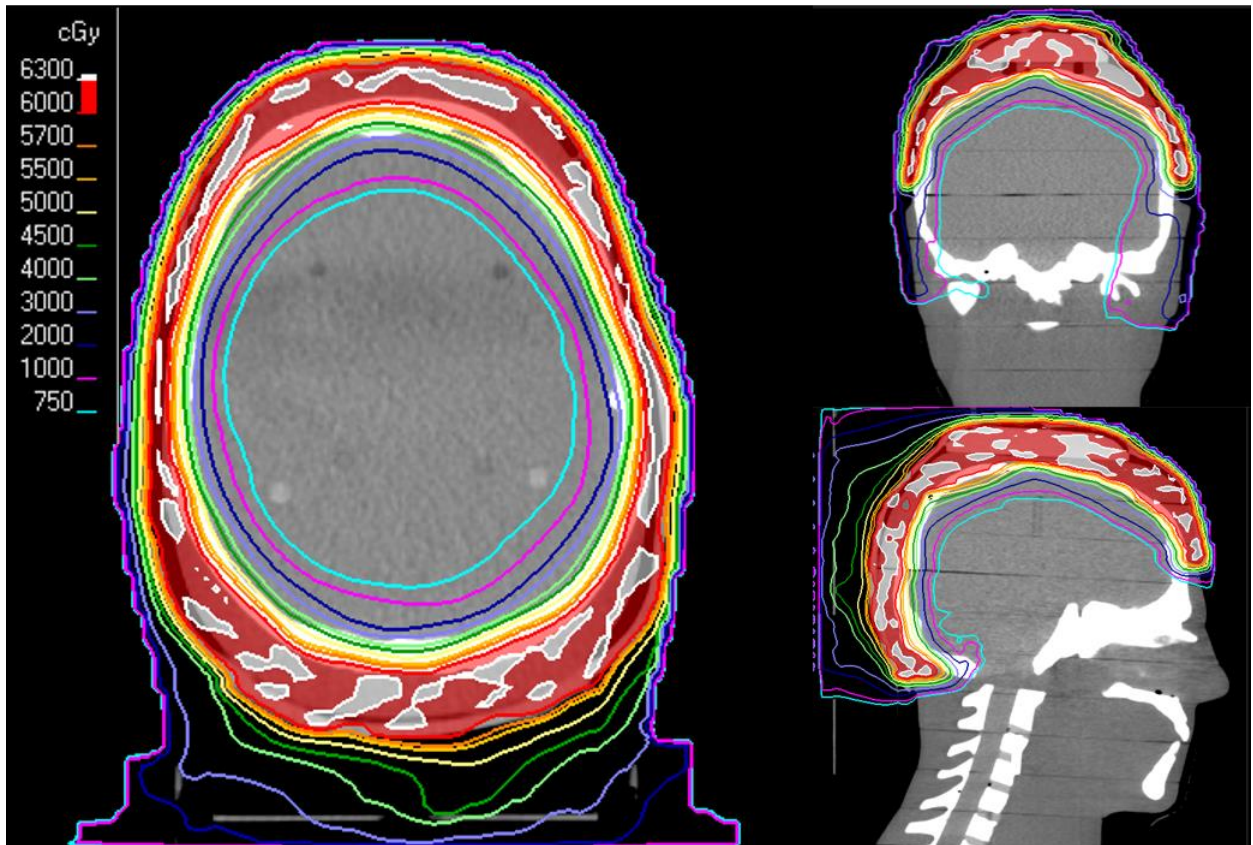


Figure 4-7: Isodose distributions for Agilus bolus cap plan.

The isodose distributions show that both bolus cap plans were essentially equivalent. Both show adequate coverage of the scalp CTV with the 100% isodose line, while the low dose lines are tight to the skull and minimize low dose coverage of most of the brain. The main difference between the plans is the Agilus plan had more 105% hot spots (6300 cGy line) compared to the NinjaFlex plan. This may be due to the slightly higher density of the Agilus cap, or differences in the optimization process leading to a slightly hotter plan. In general, 5% hot spots are acceptable to assure adequate coverage of the CTV. The DVH for both plans are presented in Figure 4-8. The DVH show the dose distributions for the two plans were comparable.

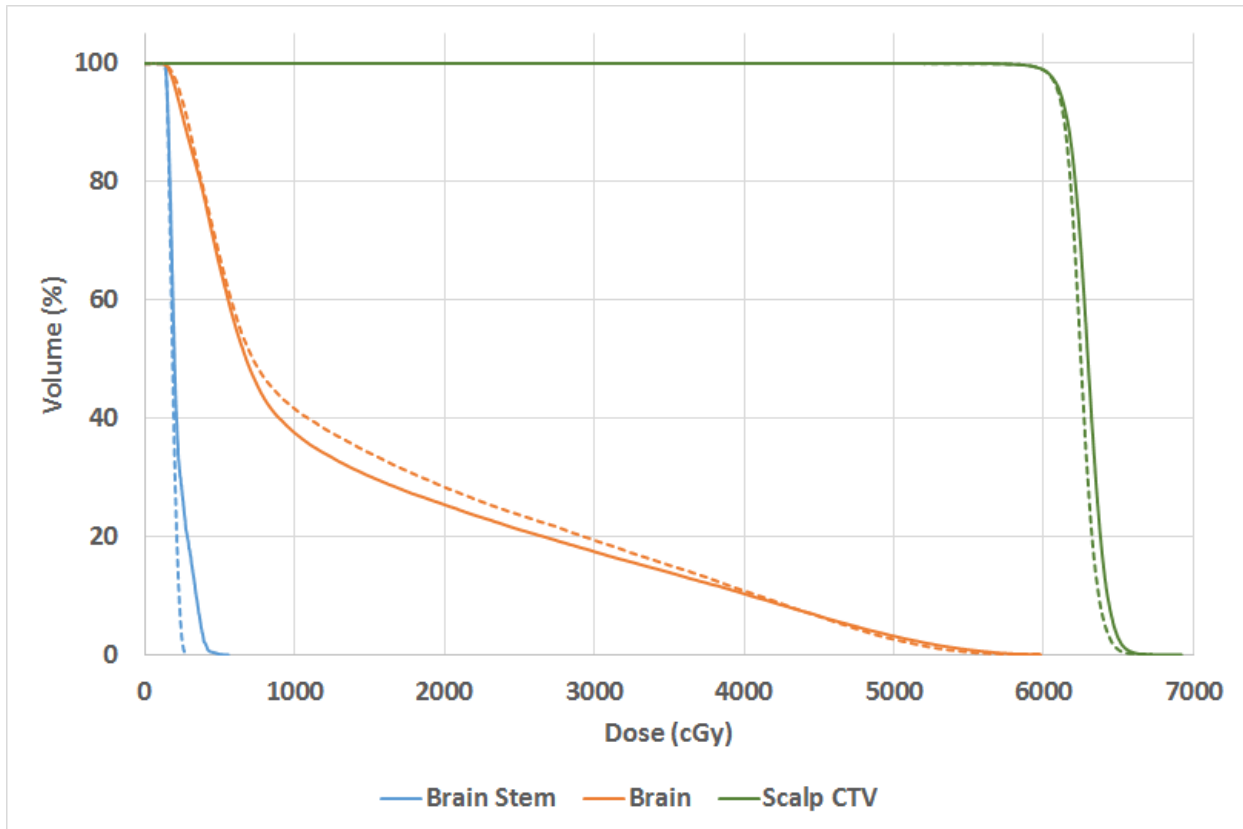


Figure 4-8: DVH for the NinjaFlex plan (dotted lines) and the Agilus plan (solid line).

The clinical acceptability of TSI plans is primarily determined by the CTV coverage and the maximum dose to the brain. The clinical goals and corresponding values for both plans are presented in Table 4-4.

Table 4-4: Dose statistics for bolus cap treatment plans

	Scalp CTV D99 (cGy)	Brain D1 (cGy)
Guideline	6000	< 5400
NinjaFlex Cap Plan	5994	5288
Agilus Cap Plan	5990	5454

To provide the highest probability the treatment achieves local control, the CTV should receive at least 99% – 100% coverage. Both plans achieved a D99 of at least 59.9 Gy, which meets clinical guidelines. To reduce the risk of cerebral radionecrosis, studies have established a guideline to not exceed 54 Gy maximum dose delivered to the brain.⁴¹ The NinjaFlex plan met this guideline with a brain D1 of 52.9 Gy. The Agilus plan had a brain D1 of 54.5 Gy, which is just above the guideline. Further plan optimization may have been able to reduce the D1 in the Agilus plan to less than 54 Gy, but for an actual patient treatment, this tradeoff would be acceptable if required to achieve 99% CTV coverage. Both plans were approved by a radiation oncologist specializing in head and neck treatments

4.3.2 Dosimetric Validation

The results of the TLD measurements are presented in Table 4-5. TLD results demonstrated that both bolus caps were able to generate adequate build up to deliver full dose to the scalp surface. TLD under the Agilus bolus cap measured an average surface dose (\pm coefficient of variation) of $205.9 \pm 2.7\%$ cGy, and the NinjaFlex bolus cap TLD measured an average surface dose of $206.3 \pm 2.2\%$ cGy. Furthermore, the TLD results show both bolus caps were able to generate a homogeneous dose to the scalp, with all TLD measurements being within 3% coefficient of variation.

The results also demonstrate that the measured doses were in good agreement with the doses calculated by the treatment planning system. All but one of the TLD measurements were within the 5% guideline for TPS dose calculation accuracy. The average percent error between the TPS dose and the TLD dose was 2.4% for the Agilus bolus cap and 1.4% for the NinjaFlex bolus cap. Although these statistics may suggest that the NinjaFlex bolus cap was better modeled by the TPS, it is important to note that the process used in this study to read the TLD

achieves an uncertainty of 2.3% in the measured dose.⁴⁰ This means all but one of the TLD measurements were within two standard deviations of the TPS predicted dose, which demonstrates good agreement. Another possibility of why the NinjaFlex cap demonstrated slightly better agreement could be due to an Order Effect, as the Agilus cap was first to be setup and irradiated, followed by the NinjaFlex cap. The setup of the NinjaFlex cap may have been better due to the experience gained from the first setup of the Agilus bolus cap, leading to better TPS and TLD agreement.

Table 4-5: TLD results compared to TPS

	Agilus Bolus Cap			NinjaFlex Bolus Cap		
TLD Location	TPS Dose (cGy)	TLD Dose (cGy)	Percent Difference	TPS Dose (cGy)	TLD Dose (cGy)	Percent Difference
1	206.6	213.9	3.4%	207.3	205.8	0.7%
2	209.6	214.0	2.1%	207.4	208.0	0.3%
3	209.4	205.4	2.0%	209.2	212.0	1.3%
4	210.3	216.9	3.1%	205.9	205.9	0.0%
5	210.0	207.0	1.5%	207.8	206.8	0.5%
6	208.8	205.2	1.7%	212.9	204.9	3.9%
7	211.6	206.7	2.4%	210.1	213.1	1.4%
8	210.0	206.5	1.7%	209.4	212.1	1.3%
9	207.9	204.0	1.9%	201.3	199.4	1.0%
10	212.7	203.4	4.6%	208.3	209.5	0.6%
11	205.3	198.2	3.6%	207.2	204.5	1.3%
12	209.4	207.2	1.0%	208.2	209.7	0.7%
13	206.8	194.5	6.3%	206.2	207.5	0.6%
14	213.1	209.0	1.9%	203.0	207.6	2.2%
15	205.8	198.5	3.7%	202.1	195.2	3.6%
16	211.0	209.0	1.0%	209.4	213.0	1.7%
17	207.0	206.8	0.1%	206.3	203.7	1.2%
18	210.0	206.2	1.8%	203.9	202.6	0.6%
19	210.4	209.4	0.5%	209.4	204.4	2.4%
20	205.1	197.1	4.1%	205.0	200.2	2.4%
Average	209.0	205.9	2.4%	207.0	206.3	1.4%
SD	2.3	5.6	1.4%	2.8	4.6	1.0%
% SD	1.1%	2.7%		1.4%	2.2%	

The primary limitation of the dosimetric validation measurements is that only one set of TLD measurements was able to be obtained. Repeated measurements would have allowed for less uncertainty in the measured dose and may have also elucidated if the outlier percent differences between the TPS and TLD were due to bolus positioning and setup related errors or just a disagreement in the TPS calculated dose.

4.3.3 Reproducibility Study

The results of the air gap measurements from the setup reproducibility scans are presented in Table 4-6. In general, the bolus positioning on the phantom was reproducible, with the average positioning difference between the original CT scan and the two reproducibility scans being 0.6 mm, and the maximum difference being 2.3 mm.

Table 4-6: Bolus and scalp gap measurements for therapist reproducibility setups

	Scan	Original CT Sim (mm)	Therapist Scan #1 (mm)	Therapist Scan #2 (mm)	Max Difference (mm)
Slice 1 (-62.85 cm)	Pos. 1	0.0	0.0	0.0	0.0
	Pos. 2	1.9	1.7	1.0	0.9
	Pos. 3	1.0	1.3	2.3	1.3
	Pos. 4	1.0	1.3	0.5	0.5
	Max	4.0	4.1	3.6	0.4
Slice 2 (-60 cm)	Pos. 1	0.0	1.3	2.3	2.3
	Pos. 2	2.4	2.7	2.3	0.3
	Pos. 3	1.9	2.0	2.3	0.4
	Pos. 4	1.4	1.3	2.3	0.9
	Max	3.9	5.6	3.6	1.7
Slice 3 (-58.3 cm)	Pos. 1	2.4	1.0	3.2	1.4
	Pos. 2	3.8	3.7	3.2	0.6
	Pos. 3	1.9	2.3	2.7	0.8
	Pos. 4	1.9	2.3	2.7	0.8
	Max	3.8	5.5	3.7	1.7

A fusion of the original CT simulation scan and therapist scan #1 is presented in Figure 4-9. The fusion image shows that the bolus cap was generally just as conformal to the scalp in the therapist's setup as in the original CT simulation scan.

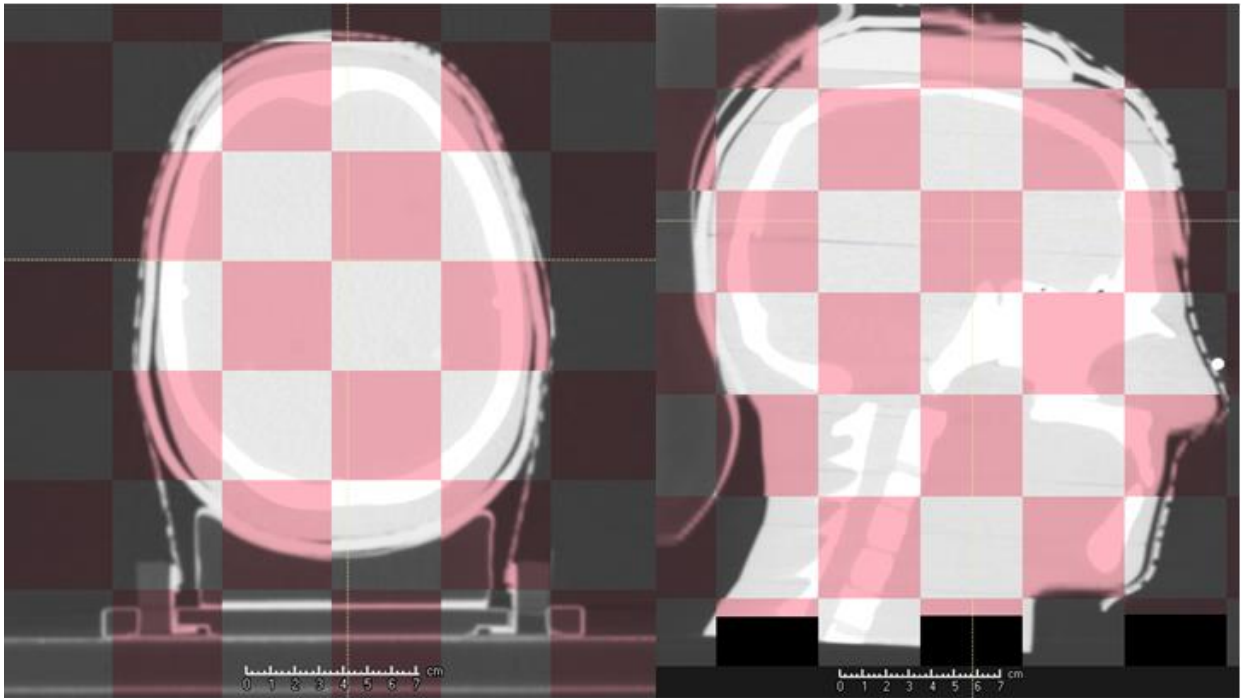


Figure 4-9: Fusion of the original CT simulation used for treatment planning (white) and the therapist scan 1 (pink)

The minimal bolus positioning differences observed between the therapist setups and the original CT scan should not significantly affect the dose delivered to the scalp. A previous study in the literature has shown that a 2 mm air gap between the surface of a water phantom and a 5 mm bolus, irradiated with a 6 MV beam with a field size of $6\text{ cm} \times 6\text{ cm}$ caused a reduction in the surface dose of only 1.5%.⁴² Another concern when discussing treatment reproducibility is patient positioning. Studies have shown that the average daily patient positioning uncertainty for head and neck treatments is 3 mm, and sometimes couch shifts of up to 5 mm are required.⁴³ This means uncertainty in patient positioning is more likely to be greater than the uncertainty in positioning of the 3D-printed bolus caps observed in this study, which suggests patient

positioning would be the limiting factor in the reproducibility of TSI treatment. All factors considered, the results showed the conformality of the 3D-printed bolus caps is within radiation treatment uncertainty limits to reproducibly generate a homogenous dose to the scalp surface for total scalp irradiation.

Although these measurements were only acquired for the Agilus bolus cap, the NinjaFlex bolus cap is more rigid than the Agilus, and should exhibit similar setup reproducibility.

5 Specific Aim 5: Development of a Clinical Workflow for Fabrication

5.1 Introduction

The goal of the final specific aim was to translate the 3D-printed bolus caps into clinical use for total scalp irradiation patients. Part of this process was to create a clinical workflow for the fabrication of the patient-specific bolus caps.

One of the initial motivations for this research was the time intensive nature of fabricating the bolus caps with the current MD Anderson technique. While the actual 3D-printing of the bolus cap does not require any user involvement, the 3D-modeling process can be time intensive, especially for users with limited CAD experience. Fortunately, many of the steps in the 3D-modeling process had the capability to be automated through scripting. Scripting would reduce the amount of user involved time needed to make the 3D-model for the patient-specific bolus caps. Automating the modeling process also assures the patient-specific bolus cap models are produced in the same manner as the design developed and validated in this work to assure quality and consistency of the 3D-printed bolus caps.

5.2 Methods and Materials

The process for creating the 3D-model of the bolus cap was presented in Section 3.2.1. The software used to create the 3D-model was RayStation and 3DSlicer, both of which are able to be scripted.

A RayStation script was developed that automates the workflow outlined in Section 3.2.1 to create the bolus cap contour. RayStation scripting is based on the open-source Python programming language. A majority of the script was developed using the RayStation built-in “record script” function, which converts a user’s interaction with the graphical user interface

into python commands. The RayStation scripting manual was also referenced for examples on how to access lists of contours and an example of adding a dialogue box to communicate with the user. The RayStation script developed is available in Appendix 7.1.

To use the script, the user must first manually create a sagittal contour of the desired extent of the bolus cap on the scalp. The contour needs to be exactly named “Bolus_Outline” for the script to work. Once the outline contour has been defined, the script can be executed and the remaining steps of creating the external contour, and doing the expansions, contractions, and ROI algebra are automatically performed by the script. The user must then manually export the CT DICOM and contour data for the next step in the model creation workflow.

A script for 3DSlicer 4.8.0 was created to convert the DICOM data into an .STL 3D-model file. Like RayStation, 3DSlicer scripting is based on the Python programming language. The 3DSlicer online documentation and forums were used for reference of what functions to call and the syntax to use for scripting in 3DSlicer.¹ To execute the script, a helper BAT file was created that automatically opens 3DSlicer and to execute the python script. The BAT file is available in Appendix 7.2. 3DSlicer will first prompt the user to navigate to the DICOM files that were exported from RayStation to import them into 3DSlicer. After the files are imported, the user resumes the script by typing ‘c’ into the interpreter console and the script will proceed. The process to convert the DICOM contour to an .STL file is an arcane multi-step process. First the DICOM contour must be converted into a binary label map within 3DSlicer. The binary label map must then be converted into a model object. Finally, the model object is exported as an .STL file. This entire process is automated by the 3DSlicer script. The script also automatically pulls the patient name and medical record number from the DICOM header and

¹ https://www.slicer.org/wiki/Documentation/Nightly/Developers/Python_scripting

puts this information in the .STL file name that is saved in the user's "My Documents" folder.

The 3DSlicer script developed is available in Appendix 7.3.

The complete automated workflow is presented in Figure 5-1.

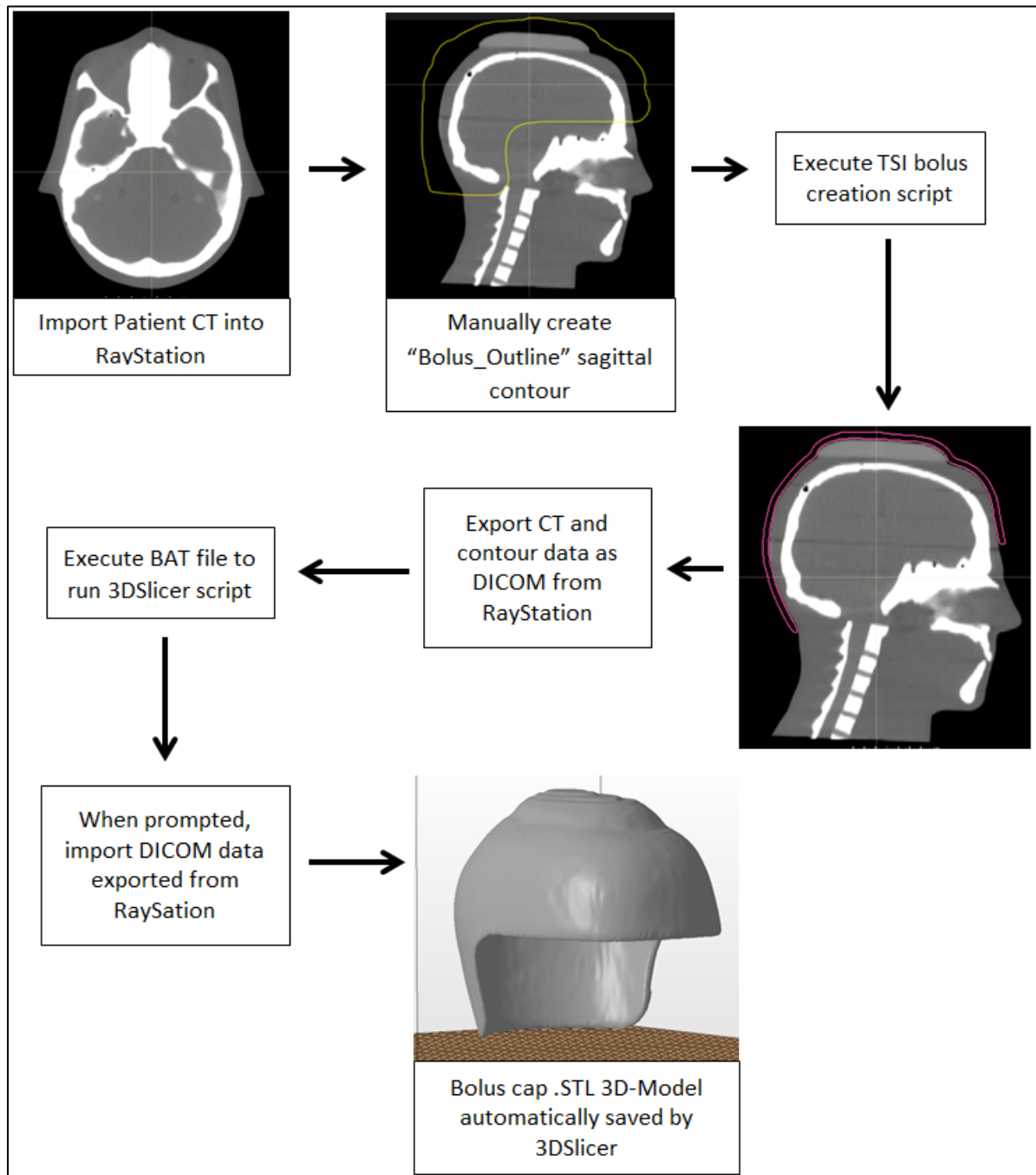


Figure 5-1: Automated workflow to create patient-specific bolus cap 3D-model

The final 3D-model produced by the automated workflow can be directly sent to a commercial 3D-printing company to be 3D-printed, as is the case for the Agilus-60 bolus cap.

If the in-house method is to be used to 3D-print a two piece NinjaFlex bolus cap, further manual manipulation of the 3D-model produced by the automated workflow is required to model the two halves that fit together with the overlapping lip in the middle, shown in Figure 3-12. The overlapping lip can be manually modeled in CAD software such as Netfabb. The process used for creating the lip was to first cut out a 1 cm thick strip centered on the sagittal midplane of the cap. A copy of the strip was created and scaled to 97%. Boolean functions were used to create a union of the original strip and the smaller scaled strip. The union operation forms the “lower lip”, and the “upper lip” is formed by subtraction of the scaled strip from the original strip. The “upper lip” is joined with one half of the cap and the “lower lip” is joined to the other half of the cap to create the final two models for each half of the bolus cap. For this work, there was no access to software that is capable of scripting these steps to automate the model creation.

5.3 Results

The scripts automated the creation of the patient-specific bolus cap 3D-model. The time to create the 3D-model from a patient’s CT scan using the automated scripts was approximately 15 minutes. A user who is very familiar with the automated workflow and the importing and exporting data steps may be able to create the 3D-model in as little as 5 minutes, as the scripts execute almost instantly.

The extra steps required to manually edit the one-piece 3D-model into two halves for the NinjaFlex cap added an additional 20 minutes to the model creation time.

6 Discussion

6.1 General Review

The hypothesis for this study was a 3D-printed bolus cap could reproducibly generate a homogeneous dose distribution over the scalp within $\pm 5\%$ of the prescribed dose. This study identified NinjaFlex and Agilus-60 as 3D-printing materials that are suitable for use in a bolus cap and demonstrated that 3D-printed bolus caps fabricated in both materials are conformal to the scalp and had air gaps of less than 4 mm. Total scalp irradiation treatment plans generated for an anthropomorphic head phantom fitted with the 3D-printed bolus caps met clinical requirements. Dosimetric validation conducted with TLD measurements demonstrated the 3D-printed bolus caps generated sufficient build up to deliver full dose to the scalp surface, and that the dose was uniform as evidenced by all measurements being within 2.7% standard deviation of the average. Furthermore, all 20 TLD measurements for the NinjaFlex bolus cap were within 5% agreement of the planned dose, and 95% of the TLD measurements for the Agilus bolus cap were within 5% agreement. Multiple independent setups of the bolus cap demonstrated that it can be reproducibly fitted on the phantom head to within 0.6 mm on average. This study has shown that 3D-printed bolus caps fulfilled all the conditions in the hypothesis, leading to the hypothesis being accepted.

6.2 Comparison of In-house and External Fabrication Methods

This work identified two methods for fabricating 3D-printed bolus caps, and both methods were researched and validated to be suitable for clinical use in total scalp irradiation. There are many factors when considering which method may work best for a certain clinic, including cost, patient comfort, and time and staffing requirements. These factors are presented in Table 6-1.

Table 6-1: Comparison of in-house and external fabrication methods

	In-House Fabrication: NinjaFlex	External Fabrication: Agilus-60
Type of 3D-Printer	Fused Deposition Modeling	PolyJet
3D-Modeling Time	35 minutes	15 minutes
3D-Printing Time	40 hours	40 hours
Material Cost	~ \$36	~ \$2,300 (inc. labor)
Printer Cost	~ \$11,000	~ \$200,000
Material Comfort	Non-Compressible, Semi-Flexible	Soft, Compressible, Flexible,

The main advantage of the in-house fabrication method is the reduced cost of the bolus compared to the external fabrication method. Another advantage is some radiation oncology departments are likely to already have an FDM 3D printer that, if large enough, would be able to 3D-print a NinjaFlex bolus cap, meaning this technique could be used immediately. However, if the department does not already have a 3D-printer, the main disadvantage of the in-house method is the department must have a staff member who can setup a 3D-printing program and can spend time to operate and maintain the 3D printer and troubleshoot any mechanical issues that arise. Another disadvantage of the method is the NinjaFlex bolus cap material is less soft and flexible compared to the Agilus material and may not be as comfortable to patients. Finally,

the NinjaFlex bolus cap needed to be printed in two pieces, which increased the amount of 3D-modeling time required.

In addition to the Agilus bolus cap being more comfortable for patients due to the soft and flexible material that can be 3D-printed by the external fabrication method, this method does not require a radiation oncology department to invest resources or time into the ownership and maintenance of a 3D-printer. The physics team can easily run the automated scripts to create the patient-specific bolus cap 3D-model and directly send the model to a commercial vendor to be printed. Out of the two fabrication methods, the external fabrication method would require the lowest time commitment from the staff to model and oversee the actual 3D-printing of the bolus cap. The main downside is the high price of the bolus cap, which is likely to exceed the cost of what can be charged to insurance for a treatment device. However, the reduced staff time required to fabricate the bolus that is enabled by the external fabrication may help to “offset” some of the cost of the Agilus bolus cap.

6.3 Clinical Implications

The main motivation for this research were the issues of non-conformality and limited reproducibility of the bolus cap fabricated using the current MD Anderson technique. The 3D-printed bolus caps that have been developed in this study have been shown to be highly conformal to scalp. Additionally, the bolus caps have been shown to be able to be reproducibly setup, which should reduce the incidence of air gaps and non-conformity shown in Figure 1-5 that is observed with the current bolus cap fabrication technique. The technique developed in this current study also offers better conformality than other techniques presented in the literature, which can have air gaps of up to 1.5 cm.¹⁴ The improved conformality and

reproducibility of patient-specific 3D-printed bolus caps can lead to more consistent treatment over all fractions and may improve clinical outcomes in total scalp irradiation.

Another limitation with the current MD Anderson technique is the extensive time required to manually fabricate the bolus during the patient's CT simulation. The current technique can take up to 40 minutes and requires the efforts of 2 therapists, a physicist, and a physician. The technique developed in the current study makes it possible to fabricate the bolus cap before a patient's CT simulation. Most patients that are referred to receive total scalp irradiation will have already had a diagnostic CT scan of their head for diagnosis purposes before CT simulation. The patient's prior diagnostic CT scan can be used to create a patient-specific bolus cap 3D-model, and a 3D-printed bolus cap made from the diagnostic scan should fit the patient at the time of CT simulation as the scalp does not significantly change. Being able to model and 3D-print a conformal bolus cap before CT simulation would significantly reduce the time required for TSI CT simulation. This in-turn reduces the time commitment of the staff and the patient, and increases the availability of the CT simulation suite. Reduced CT simulation time is one of the main advantages of the 3D-printed bolus cap technique over other techniques presented in the literature, as most require manual fabrication of the bolus or custom support devices during CT simulation.

Other possible clinical implications resulting from the current study are other uses of Agilus material and PolyJet 3D printers in radiation oncology. This study validated Agilus-60 as a 3D-printing material suitable for fabricating a bolus or tissue compensator for use in radiation therapy. There are other treatment sites that may benefit from the improved patient-comfort enabled by the softness and flexibility of the Agilus material, such as the ear or areas on the face. Additionally, the ability of PolyJet printers to dynamically print rigid and soft materials in

one object offers new possibilities for the fabrication of other custom treatment and immobilization devices used in radiation therapy. Some possible future applications to research include soft bite blocks, external brachytherapy applicators, and custom head rests made of a rigid material with a soft layer for the head.

This study also serves as a good reference for the general considerations that must be made when developing new 3D-printed radiation treatment devices, and provides procedures for the material analysis and validation tests that should be conducted when commissioning the use of a new 3D-printed treatment device for radiation therapy.

6.4 Limitations and Future Research

The primary limitation of this study was the majority of the development and validation tests for the 3D-printed bolus caps were done using an anthropomorphic head phantom rather than an actual patient. Although the head phantom serves as a good surrogate for testing the fabrication workflow and performing dosimetric measurements, it did not allow for an assessment on some of the issues that may arise when the 3D-printed bolus caps are used for actual patients. Some possible issues that could arise are limited conformality due to patient's hair, need to add margin if patients feel the bolus cap is too tight, or adjustments to the automated workflow based on differences in non-standard diagnostic CT scans.

Future research on this topic should focus on analyzing CT simulations of patients fitted with the 3D-printed bolus caps and *in vivo* dosimetry measurements to assess if the bolus cap designs or workflow could be altered to improve conformality, dosimetry, or reproducibility. Research can also be conducted on applying the workflow and scripts developed in this study to 3D-print bolus for other treatment sites.

6.5 Conclusion

This study has developed patient-specific 3D-printed bolus caps and validated them for clinical use in total scalp irradiation. Semi-automated workflows were developed to streamline the in-house or external fabrication of the 3D-printed bolus caps. The resulting 3D-printed bolus caps were highly conformal to the scalp and demonstrated improved setup reproducibility compared to existing techniques. Dosimetric measurements showed the bolus caps can generate full dose build up and deliver a uniform dose to the scalp. In conclusion, this study has developed a novel technique that offers a streamlined, minimally-labor intensive and reproducible technique to 3D-print highly conformal patient-specific bolus caps for total scalp irradiation.

7 Appendix

7.1 RayStation Bolus Contour Creation Script

```
# Script to create a patient-specific total scalp bolus contour using
patient's CT
# This script is under The MIT License (MIT) Copyright (c) 2018 Garrett
Baltz.

# INSTRUCTIONS:

# This script requires an ROI named "Bolus_Outline"
# Bolus Outline should be drawn along the sagittal plane and encompass the
desired extent of the scalp bolus
# The contour should first be drawn on the center sagittal slice of the CT.
# The contour should then be copied to a slice where the ears are visible so
they can be contoured out
# Copy this contour to replace the original center contour, and also paste
the contour on the opposite side of the patient
# Interpolate the contour so it extends across all sagittal slices of the
patient
# Once this contour is in place, the script can be run.

# Once the script is finished, export all DICOM information so it can be used
with the 3DSlicer script to convert
# the DICOM to .stl file ready for printing.

from connect import *
import sys

# Load current patient
case = get_current("Case")
examination = get_current("Examination")

# Load in names of all ROIs
roi_names = [r.Name for r in case.PatientModel.RegionsOfInterest]

# Check if Bolus Outline has been defined, if not tell user to create and
resume script
if 'Bolus_Outline' not in roi_names:
    await_user_input('Bolus_Outline ROI does not exist! Please create then
resume script')

# Generate External body contour
with CompositeAction('Create external (BodyROI)'):

    retval_0 = case.PatientModel.CreateRoi(Name="BodyROI", Color="0, 128, 64",
Type="External", TissueName="", RoiMaterial=None)

    retval_0.CreateExternalGeometry(Examination=examination, ThresholdLevel=-
250)

# prompt user to check that external ROI is correct and doesn't include
couch/headrest
```

```

await_user_input('Review the created external contour and edit if necessary')

# Create the expanded body contour
with CompositeAction('Expand (BodyROI)'):

    retval_1 = case.PatientModel.CreateRoi(Name="Bolus", Color="Yellow",
    Type="Bolus", TissueName=None, RoiMaterial=None)

    retval_1.SetMarginExpression(SourceRoiName="BodyROI", MarginSettings={
    'Type': "Expand", 'Superior': 0.5, 'Inferior': 0.5, 'Anterior': 0.5,
    'Posterior': 0.5, 'Right': 0.5, 'Left': 0.5 })

    retval_1.UpdateDerivedGeometry(Examination=examination, Algorithm="Auto")

# subtract contour
with CompositeAction('ROI Algebra (BolusOutline2)'):

    retval_2 = case.PatientModel.CreateRoi(Name="BolusOutline2", Color="Blue",
    Type="Organ", TissueName=None, RoiMaterial=None)

    retval_2.SetAlgebraExpression(ExpressionA={ 'Operation': "Intersection",
    'SourceRoiNames': ["Bolus"], 'MarginSettings': { 'Type': "Expand",
    'Superior': 0, 'Inferior': 0, 'Anterior': 0, 'Posterior': 0, 'Right': 0,
    'Left': 0 } }, ExpressionB={ 'Operation': "Intersection", 'SourceRoiNames':
    ["Bolus_Outline"], 'MarginSettings': { 'Type': "Expand", 'Superior': 0,
    'Inferior': 0, 'Anterior': 0, 'Posterior': 0, 'Right': 0, 'Left': 0 } },
    ResultOperation="Intersection", ResultMarginSettings={ 'Type': "Expand",
    'Superior': 0, 'Inferior': 0, 'Anterior': 0, 'Posterior': 0, 'Right': 0,
    'Left': 0 })

    retval_2.UpdateDerivedGeometry(Examination=examination, Algorithm="Auto")

# create final bolus contour
with CompositeAction('ROI Algebra (FinalBolus)'):

    retval_3 = case.PatientModel.CreateRoi(Name="FinalBolus", Color="White",
    Type="Organ", TissueName=None, RoiMaterial=None)

    retval_3.SetAlgebraExpression(ExpressionA={ 'Operation': "Union",
    'SourceRoiNames': ["BolusOutline2"], 'MarginSettings': { 'Type': "Expand",
    'Superior': 0, 'Inferior': 0, 'Anterior': 0, 'Posterior': 0, 'Right': 0,
    'Left': 0 } }, ExpressionB={ 'Operation': "Union", 'SourceRoiNames':
    ["BodyROI"], 'MarginSettings': { 'Type': "Expand", 'Superior': 0, 'Inferior':
    0, 'Anterior': 0, 'Posterior': 0, 'Right': 0, 'Left': 0 } },
    ResultOperation="Subtraction", ResultMarginSettings={ 'Type': "Expand",
    'Superior': 0, 'Inferior': 0, 'Anterior': 0, 'Posterior': 0, 'Right': 0,
    'Left': 0 })

    retval_3.UpdateDerivedGeometry(Examination=examination, Algorithm="Auto")

# Underive ROIs
if case.PatientModel.RegionsOfInterest['Bolus'].DerivedRoiExpression:
    case.PatientModel.RegionsOfInterest['Bolus'].DeleteExpression()

if case.PatientModel.RegionsOfInterest['BolusOutline2'].DerivedRoiExpression:

```

```
case.PatientModel.RegionsOfInterest['BolusOutline2'].DeleteExpression()  
  
if case.PatientModel.RegionsOfInterest['FinalBolus'].DerivedRoiExpression:  
    case.PatientModel.RegionsOfInterest['FinalBolus'].DeleteExpression()  
  
# Delete helper intermediary ROIs  
case.PatientModel.RegionsOfInterest['BolusOutline2'].DeleteRoi()  
case.PatientModel.RegionsOfInterest['Bolus'].DeleteRoi()
```

7.2 BAT Script to Open 3DSlicer

```
"C:\Program Files\Slicer 4.8.0\slicer.exe" --python-script
'%cd%\SlicerScript.py'
```

7.3 3DSlicer DICOM Contour to .STL Conversion Script

```
from __main__ import vtk, qt, ctk, slicer
import re, os

# Script to convert Exported RayStation Bolus ROI to final .stl file
# ready to be 3D-printed
# This script is under The MIT License (MIT) Copyright (c) 2018 Garrett
Baltz.

# Prompt to load DICOM dataset
m = slicer.util.mainWindow()
m.moduleSelector().selectModule('DICOM')

def MakeModel():
    # Generate Binary Label Map
    segmentations = slicer.util.getNodesByClass('vtkMRMLSegmentationNode')
    segmentations[0].CreateBinaryLabelmapRepresentation()
    segmentations[0].SetMasterRepresentationToBinaryLabelmap()

    # Subtract body contour from Bolus Contour
    seg = getNode('*RTSTRUCT*')
    segmentEditorWidget = slicer.qMRMLSegmentEditorWidget()
    segmentEditorWidget.setMRMLScene(slicer.mrmlScene)

    segmentEditorNode = slicer.vtkMRMLSegmentEditorNode()
    slicer.mrmlScene.AddNode(segmentEditorNode)
    segmentEditorWidget.setMRMLSegmentEditorNode(segmentEditorNode)
    segmentEditorWidget.setSegmentationNode(seg)

    segmentEditorWidget.setActiveEffectByName("Logical operators")
    effect = segmentEditorWidget.activeEffect()

    effect.parameterSetNode().SetSelectedSegmentID("FinalBolus")

    effect.setParameter("Operation", 'SUBTRACT')
    effect.setParameter("ModifierSegmentID", "BodyROI")
    effect.self().onApply()

    # export segmentation to a model

    modelHierarchyNodeNode =
slicer.mrmlScene.AddNewNodeByClass('vtkMRMLModelHierarchyNode')
    segmentIds = vtk.vtkStringArray()
    seg.GetSegmentation().GetSegmentIDs(segmentIds)
    slicer.modules.segmentations.logic().ExportSegmentsToModelHierarchy(seg,
segmentIds, modelHierarchyNodeNode)
```

```

    # this is code to get the patient's ID and name to include in the file
name
    shNode =
slicer.vtkMRMLSubjectHierarchyNode().GetSubjectHierarchyNode(slicer.mrmlScene
)
    shNode.GetAttribute('DICOM.instanceUIDs')
    rtStructNode = slicer.util.getNode("*RTSTRUCT*")
    rtStructShItemID = shNode.GetItemByDataNode(rtStructNode)
    ctSliceInstanceUids = shNode.GetItemAttribute(rtStructShItemID,
'DICOM.ReferencedInstanceUIDs').split()
    filename = slicer.dicomDatabase.fileForInstance(ctSliceInstanceUids[0])
    patientID = slicer.dicomDatabase.fileValue(filename, '0010,0020')
    patientName = slicer.dicomDatabase.fileValue(filename, '0010,0010')
    print("3D Model Created. Saving File...\n")

    # save model to a folder in user's documents
    models = slicer.util.getNodesByClass('vtkMRMLModelNode')
    modelsList = []

    for model in models:
        modelsList.append(model.GetName())

    pathToMyUserFolder = os.path.expanduser('~')
    saveFolder = pathToMyUserFolder + '/Documents/TSI-
Bolus_3D_Printer_Files/'

    # Check if a folder exists to save 3D print file to, if not create it
    if not os.path.exists(saveFolder):
        os.makedirs(saveFolder)

    savePath = saveFolder + patientID + '_' + patientName + '_Bolus-3D-Print-
File.stl'
    slicer.util.saveNode(models[modelsList.index("FinalBolus")], savePath)

    print("\n Script Finished\n3D .stl file has been saved to " + savePath +
"\n You can close this program")

# While loop to wait until user selects DICOM file and DICOM is loaded
while True:
    input = raw_input("Type 'c' and press Enter after CT has been loaded to
start script \n\n")
    if re.match('c', input):
        print("DICOM Loaded. Creating 3D Model...\n")
        MakeModel()
        break

```

8 Bibliography

1. Wojcicka JB, Lasher DE, McAfee SS, Fortier GA. Dosimetric comparison of three different treatment techniques in extensive scalp lesion irradiation. *Radiother Oncol.* 2009;91(2):255-260. doi:10.1016/j.radonc.2008.09.022.
2. Toro JR, Travis LB, Hongyu JW, Zhu K, Fletcher CDM, Devesa SS. Incidence patterns of soft tissue sarcomas, regardless of primary site, in the Surveillance, Epidemiology and End Results program, 1978-2001: An analysis of 26,758 cases. *Int J Cancer.* 2006;119(12):2922-2930. doi:10.1002/ijc.22239.
3. Patel SH, Hayden RE, Hinni ML, Wong WW, Foote RL, Milani S, Wu Q, Ko SJ, Halyard MY. Angiosarcoma of the scalp and face: The mayo clinic experience. *JAMA Otolaryngol - Head Neck Surg.* 2015;141(4):335-340. doi:10.1001/jamaoto.2014.3584.
4. Ogawa K, Takahashi K, Asato Y, Yamamoto Y, Taira K, Matori S, Iraha S, Yagi N, Yogi A, Haranaga S, Fujita J, Uezato H, Murayama S. Treatment and prognosis of angiosarcoma of the scalp and face: A retrospective analysis of 48 patients. *Br J Radiol.* 2012;85(1019):1127-1133. doi:10.1259/bjr/31655219.
5. Able CM, Mills MD, McNeese MD, Hogstrom KR. Evaluation of a total scalp electron irradiation technique. *Int J Radiat Oncol Biol Phys.* 1991;21(4):1063-1072. doi:10.1016/0360-3016(91)90751-O.
6. Mellenberg DE, Schoeppel SL. Total scalp treatment of mycosis fungoides: the 4 X 4 technique. *Int J Radiat Oncol Biol Phys.* 1993;27(4):953-958. doi:10.1016/0360-3016(93)90473-9.
7. Yaparpalvi R, Fontenla DP, Beitler JJ. Improved dose homogeneity in scalp irradiation

using a single set-up point and different energy electron beams. *Br J Radiol.* 2002;75(896):670-677.

8. Tung SS, Shiu AS, Starkschall G, Morrison WH, Hogstrom KR. Dosimetric evaluation of total scalp irradiation using a lateral electron-photon technique. *Int J Radiat Oncol Biol Phys.* 1993;27(1):153-160. doi:10.1016/0360-3016(93)90433-V.
9. Teoh M, Clark CH, Wood K, Whitaker S, Nisbet A. Volumetric modulated arc therapy: a review of current literature and clinical use in practice. *Br J Radiol.* 2011;84(1007):967-996. doi:10.1259/bjr/22373346.
10. Orton N, Jaradat H, Welsh J, Tomé W. Total scalp irradiation using helical tomotherapy. *Med Dosim.* 2005;30(3):162-168. doi:10.1016/j.meddos.2005.05.002.
11. Song JH, Jung JY, Park HW, Lee GW, Chae SM, Kay CS, Son SH. Dosimetric comparison of three different treatment modalities for total scalp irradiation: The conventional lateral photon-electron technique, helical tomotherapy, and volumetric-modulated arc therapy. *J Radiat Res.* 2015;56(4):717-726. doi:10.1093/jrr/rru049.
12. Vyas V, Palmer L, Mudge R, Jiang R, Fleck A, Schaly B, Osei E, Charland P. On bolus for megavoltage photon and electron radiation therapy. *Med Dosim.* 2013;38(3):268-273. doi:10.1016/j.meddos.2013.02.007.
13. Bedford JL, Childs PJ, Hansen VN, Warrington AP, Mendes RL, Glees JP. Treatment of extensive scalp lesions with segmental intensity-modulated photon therapy. *Int J Radiat Oncol Biol Phys.* 2005;62(5):1549-1558. doi:10.1016/j.ijrobp.2005.04.001.
14. Lin SH, Latronico D, Teslow T, Bajaj GK. A highly reproducible bolus immobilization

- technique for the treatment of scalp malignancies. *Med Dosim.* 2008;33(1):30-35.
doi:10.1016/j.meddos.2007.04.005.
15. Sponseller P, Paravathaneni U. A case study of radiotherapy planning for intensity modulation radiation therapy for the whole scalp with matching electron treatment. *Med Dosim.* 2013;38(2):122-124. doi:10.1016/j.meddos.2012.09.002.
 16. Schmid RK, Harker-Murray A, Niemczyk K, Robbins JR. Diffuse recurrent cutaneous melanoma of the scalp and neck successfully treated with volumetric modulated arc therapy and concurrent Ipilimumab. *Pract Radiat Oncol.* 2017.
doi:10.1016/j.prro.2017.09.006.
 17. Wong K V., Hernandez A. A Review of Additive Manufacturing. *ISRN Mech Eng.* 2012;2012:1-10. doi:10.5402/2012/208760.
 18. N. Turner B, Strong R, A. Gold S. A review of melt extrusion additive manufacturing processes: I. Process design and modeling. *Rapid Prototyp J.* 2014;20(3):192-204.
doi:10.1108/RPJ-01-2013-0012.
 19. Barclift MW, Williams CB. Examining Variability in the Mechanical Properties of Parts Manufactured Via Polyjet Direct 3D Printing. *Int Solid Free Fabr Symp.* 2012;(March):876-890. doi:10.1017/CBO9781107415324.004.
 20. Su S, Moran K, Robar JL. Design and production of 3D printed bolus for electron radiation therapy. *J Appl Clin Med Phys.* 2014;15(August):194-211.
doi:10.1120/jacmp.v15i4.4831.
 21. Burleson S, Baker J, Hsia AT, Xu Z. Use of 3D printers to create a patient-specific 3D

- bolus for external beam therapy. *J Appl Clin Med Phys*. 2015;16(3):166-178.
doi:10.1120/jacmp.v16i3.5247.
22. Łukowiak M, Jezierska K, Boehlke M, Wiecko M, Łukowiak A, Podraza W, Lewocki M, Masojć B, Falco M. Utilization of a 3D printer to fabricate boluses used for electron therapy of skin lesions of the eye canthi. *J Appl Clin Med Phys*. 2017;18(1):76-81.
doi:10.1002/acm2.12013.
 23. Park JW, Yea JW. Three-dimensional customized bolus for intensity-modulated radiotherapy in a patient with Kimura's disease involving the auricle. *Cancer/Radiotherapie*. 2016;20(3):205-209. doi:10.1016/j.canrad.2015.11.003.
 24. Park S-Y, Kim J, Joo YH, Lee JC, Park JM. Total body irradiation with a compensator fabricated using a 3D optical scanner and a 3D printer. *Phys Med Biol*. 2017;62(9):3735-3756. doi:10.1088/1361-6560/aa6866.
 25. Bushberg JT, Seibert JA, Leidholdt EM, Boone JM. *The Essential Physics of Medical Imaging*. Wolters Kluwer Health; 2011.
 26. Hadziahmetovic M, Weldon M, Pearson M, Werner P, Siddiqui F. Scalp uniform bolus application (SCUBA) technique for homogenous scalp and regional nodal irradiation. *Pract Radiat Oncol*. 2014;4(1):e95-e99. doi:10.1016/j.prro.2013.05.005.
 27. Craft DF, Kry SF, Balter P, Salehpour M, Woodward W, Howell RM. Material matters: Analysis of density uncertainty in 3D printing and its consequences for radiation oncology. *Med Phys*. 2018. doi:10.1002/mp.12839.
 28. Rubber Hardness. National Physical Laboratory. <http://www.npl.co.uk/science->

technology/mass-and-force/hardness/rubber-hardness.

29. Craft DF, Howell RM. Preparation and fabrication of a full-scale, sagittal-sliced, 3D-printed, patient-specific radiotherapy phantom. *J Appl Clin Med Phys*. 2017;18(5):285-292. doi:10.1002/acm2.12162.
30. Khan FM, Gibbons JP. *Khan's The Physics of Radiation Therapy*. Wolters Kluwer Health; 2014.
31. Agilus Specification Sheet. STRATASYS. http://www.stratasys.com/-/media/files/material-spec-sheets/mss_agilus30.pdf.
32. Fedorov A, Beichel R, Kalpathy-Cramer J, Finet J, Fillion-Robbin J-C, Pujol S, Bauer C, Jennings D, Fennessy F, Sonka M, Buatti J, Aylward S, Miller J V., Pieper S, Kikinis R. 3D slicer as an image computing platform for the quantitative imaging network. *Magn Reson Imaging*. 2012;30(9):1323-1341. doi:10.1016/j.mri.2012.05.001.3D.
33. Pinter C, Lasso A, Wang A, Jaffray D, Fichtinger G. SlicerRT: Radiation therapy research toolkit for 3D Slicer. *Med Phys*. 2012;39(10):6332-6338. doi:10.1118/1.4754659.
34. NinjaFlex 85A TPU Flexible 3D Printing Filament | NinjaTek. <https://ninjatek.com/products/filaments/ninjabflex/>. Accessed March 25, 2018.
35. Smilowitz JB, Das IJ, Feygelman V, Fraass BA, Kry SF, Marshall IR, Mihailidis DN, Ouhib Z, Ritter T, Snyder GM, Fairbrent L. AAPM Medical Physics Practice Guideline 5.a.: Commissioning and QA of Treatment Planning Dose Calculations — Megavoltage Photon and Electron Beams. 2015;16(5):14-34. doi:10.1120/jacmp.v16i5.5768.

36. Knoll GF. *Radiation Detection and Measurement*. John Wiley & Sons; 2010.
37. Jayachandran CA. Calculated effective atomic number and Kerma values for tissue-equivalent and dosimetry materials. *Phys Med Biol*. 1971;16(4):617-623.
doi:10.1088/0031-9155/16/4/005.
38. LoSasso T, Chui CS, Ling CC. Physical and dosimetric aspects of a multileaf collimation system used in the dynamic mode for implementing intensity modulated radiotherapy. *Med Phys*. 1998;25(10):1919-1927. doi:10.1118/1.598381.
39. Craft DL, Hong TS, Shih HA, Bortfeld TR. Improved planning time and plan quality through multicriteria optimization for intensity-modulated radiotherapy. *Int J Radiat Oncol Biol Phys*. 2012;82(1):83-90. doi:10.1016/j.ijrobp.2010.12.007.
40. Kirby TH, Hanson WF, Johnston DA. Uncertainty analysis of absorbed dose calculations from thermoluminescence dosimeters. *Med Phys*. 1992;19(6):1427-1433.
doi:10.1118/1.596797.
41. Marks JE, Baglan RJ, Prasad SC, Blank WF. Cerebral radionecrosis: Incidence and risk in relation to dose, time, fractionation and volume. *Int J Radiat Oncol Biol Phys*. 1981;7(2):243-252. doi:10.1016/0360-3016(81)90443-0.
42. Chung J-B, Kim J-S, Kim I-A, Lee J-W. Surface dose measurements from air gaps under a bolus by using a MOSFET dosimeter in clinical oblique photon beams. *J Korean Phys Soc*. 2012;61(7):1143-1147. doi:10.3938/jkps.61.1143.
43. Orisamolu A, Anderson N, Lin A. Setup Uncertainty as Determined by Daily Image Guided Radiation Therapy (IGRT) for Head-and-Neck Cancer (HNC): Evaluation of

Safety and Implications on Defining Planning Target Volume (PTV) Margins. *Int J Radiat Oncol Biol Phys.* 2018;87(2):S464-S465. doi:10.1016/j.ijrobp.2013.06.1229.

Vita

Garrett Christopher Baltz was born in Fresno, California, the son of Stuart Baltz and Phyllis Baltz. After completing his work at Yosemite High School, Oakhurst, California in 2012, he matriculated at University of California, Berkeley in Berkeley, California. In May 2016, he received the degree of Bachelor of Science with a major in Nuclear Engineering. In August of 2016, he entered The University of Texas MD Anderson Cancer Center UTHHealth Graduate School of Biomedical Sciences. In May 2018, he received the degree of Master of Science in Medical Physics. In September 2018, he went on to continue his clinical training as a resident in the Radiation Therapy Residency program at MD Anderson Cancer Center.

Permanent address:

524 Silvaner Ct.

El Dorado Hills, CA 95762